https://doi.org/10.1070/RCR5026

Micro- and mesoporous metal-organic frameworks for hydrocarbon separation

Konstantin A. Kovalenko, Andrei S. Potapov, Vladimir P. Fedin

Nikolaev Institute of Inorganic Chemistry, Siberian Branch of the Russian Academy of Sciences, prosp. Akademika Lavrentieva 3, 630090 Novosibirsk, Russian Federation

The review presents data on the use of porous metal-organic frameworks for the separation of some industrially important hydrocarbon mixtures, such as ethane and ethylene, propane and propylene, benzene and cyclohexane, and xylene isomers. It is shown that enhancing the efficiency of materials based on porous metal-organic frameworks relies on understanding the nature of adsorption sites in their structures, the specifics of interactions between the framework and a particular substrate, and the structural response of the framework (host) as it is filled with guest molecules. The achievements of fundamental studies and unresolved problems related to the use of porous metal-organic frameworks in industrial hydrocarbon separation processes are critically analyzed.
The bibliography includes 183 references.

Contents

1. Introduction 1
2. Separation of ethane and ethylene 2
3. Propane/propylene separation 11
   3.1. Thermodynamic separation 11
   3.2. Kinetic separation 12
   3.3. Separation based on the gate opening effect 14
4. Separation of benzene and cyclohexane 15
5. Separation of isomeric xylenes 20
6. The structural formulas of the organic compounds mentioned in the review 26
7. Conclusion 27
8. List of abbreviations and symbols 27
9. References 28

K.A.Kovalenko. Candidate of Chemical Sciences, Senior Researcher at the Institute of Inorganic Chemistry, Siberian Branch of the Russian Academy of Sciences.
E-mail: k.a.kovalenko@niic.nsc.ru
Current research interests: synthesis and functional properties of metal-organic frameworks, sorption processes on porous materials.
A.S.Potapov. Doctor of Chemical Sciences, Associate Professor, Leading Researcher at the same Institute.
E-mail: potapov@niic.nsc.ru
Current research interests: synthesis of nitrogen-containing heterocyclic ligands, coordination polymers.
V.P.Fedin. Corresponding Member of the Russian Academy of Sciences, Professor, Doctor of Chemical Sciences, Head of the Department of Chemistry of Coordination, Cluster and Supramolecular Compounds at the same Institute.
E-mail: cluster@niic.nsc.ru
Current research interests: synthesis and functional properties of metal-organic frameworks, supramolecular chemistry.

Translation: S.S.Veselyi

1. Introduction

The discovery of new classes of functional materials plays an important role in the development of both fundamental studies and advanced technologies. Studies on metal-organic frameworks (MOFs) began at the turn of the century.† This is a class of crystalline porous materials obtained by self-assembly from metal cations or clusters and organic linkers.[1,2] The growing interest in these compounds is primarily caused by the prospects of their wide practical application as components for the new generation of various types of functional materials with enhanced or unique properties.[3,4] For example, MOF demonstrate record-high sorption characteristics among all porous materials, while the pore sizes vary over a wide range from a few angstroms to tens of nanometers.[5] These structural features open up unique prospects for the use of MOF, in particular, in heterogeneous catalysis[6,7] and in processes for the separation of complex mixtures,[8] for purification and storage of industrially important gases such as hydrogen, methane, carbon dioxide, acetylene,[9–13] and in the development of new types of sensors,[14] materials with high proton conductivity,[15,16] supercapacitors[17] and for biomedical applications.[18] It is obvious that further studies on MOFs, especially the search for new functional properties and their unexpected and promising fields of application, studies on fundamental structure – properties relationships, and development of convenient scalable methods for the production of such materials are important from both fundamental and applied points of view.[1,4,9,11]

In the most developed economies, up to 15% of the total energy is consumed in the chemical separation and purification processes. The development of innovative materials for high-efficiency and high-selectivity adsorption and membrane-based separation technologies will make it pos-

† Abbreviations used in English-language literature: MOFs (metal-organic frameworks), PCP (porous coordination polymers).

Received 03 June 2021

© 2022 Uspekhi Khimii, ZIOC RAS, Russian Academy of Sciences and IOP Publishing Limited

sible to replace the traditional distillation processes and significantly reduce energy consumption, including that for large-scale products in the treatment of natural gas and oil. Separation processes based on porous materials can reduce energy consumption by ~70–90%.[19] Micro- and mesoporous MOFs are regarded as new promising materials for the separation of hydrocarbons.[20,21] The possibility to intentionally adjust the size and topology of MOF pores and the functional groups on their surface in a wide range, the easy post-synthesis modification and the frequently observed dynamic behaviour of the framework allow such polymers to be tuned for supramolecular recognition of a required substrate, which makes them promising sorbents for the separation of complex mixtures, including hydrocarbons produced on industrial scale.

Studies published in recent years have already demonstrated the impressive potential of MOFs that have been found to be efficient sorbents for the separation of industrially important mixtures of a number of hydrocarbons (Table 1).

It is known that two main separation mechanisms are implemented in the separation processes on solid porous sorbents.[8,23] The thermodynamic (equilibrium) separation is characteristic of materials with pores that are sufficiently large for the free passage of molecules from a mixture into the framework. In this case, the separation selectivity is determined by the difference in the interaction of the individual mixture components with the framework walls.

Table 1. Some physical characteristics of the hydrocarbons to be separated.[22]

Hydrocarbon	T_b, K	ΔH_{vap}, kJ mol^{-1}	d_k, Å	Polarizability, 10^{-25} cm^3	μ, D
Hydrocarbons to be separated: ethane and ethylene					
Ethane (C_2H_6)	184.55	14.7	4.443	44.3–44.7	0, 0.65 [a]
Ethylene (C_2H_4)	169.42	13.54	4.163	42.52	0, 1.50 [a]
Hydrocarbons to be separated: propane and propylene					
Propane (C_3H_8)	231.02	19.04	4.3–5.118	62.9–63.7	0.084
Propylene (C_3H_6)	225.46	18.42	4.678	62.6	0.366
Hydrocarbons to be separated: benzene and cyclohexane					
Benzene (C_6H_6)	353.3	33.9	5.6	103.7	0
Cyclohexane (C_6H_{12})	353.9	33.1	6.1	109.4	0
Hydrocarbons to be separated: xylene isomers					
o-Xylene (*o*-C_8H_{10})	417.6 225.2 [b]	42.7	7.4	14.9	0.62
m-Xylene (*m*-C_8H_{10})	412.3 248.2 [b]	43.4	7.1	14.2	0.36
p-Xylene (*p*-C_8H_{10})	411.5 286.4 [b]	42.4	6.7	13.7	0

Notes. The following designations are used: T_b is boiling point, ΔH_{vap} is enthalpy of vapourization, d_k is kinetic diameter, μ is dipole moment. [a] Quadrupole moment in Debye-Ångströms. [b] Melting point, K.

The selectivity of adsorption separation is understood as the preferential adsorption of one gas with respect to another. Mathematically, selectivity is expressed by the formula:

$$S = \frac{n_1/n_2}{p_1/p_2} \quad (1)$$

where S is the selectivity (selectivity factor); n_1 and n_2 are the amounts of adsorbed components 1 and 2; p_1 and p_2 are their partial pressures in the gas phase.

The chemical modification of MOFs by incorporation of selected substituents makes it possible to control the adsorption separation process and significantly change the interaction energy of the substrate with the pore or channel walls. Thermodynamic separation can be particularly efficient for mixtures that consist of compounds of different chemical nature whose molecules have approximately the same size, for example, in the separation of ethane and ethylene (an alkane and an alkene), or cyclohexane and benzene (a cycloalkane and an aromatic compound).

In contrast, kinetic (nonequilibrium) separation is based on a difference in the diffusion rates of the guest molecules inside a framework. The diffusion process can be controlled by directed adjustment of the size and shape of the channels in a porous MOF structure. However, it is rather difficult to implement this separation mechanism efficiently for molecules with similar kinetic diameters. Apart from these main separation mechanisms, separation is possible in a number of MOFs exhibiting framework breathing due to the gate-opening effect that results in different adsorption capacities for different compounds.

This review critically analyzes the progress made and the unresolved problems in the application of MOFs for the separation of a number of hydrocarbon mixtures, namely ethane and ethylene, propane and propylene, benzene and cyclohexane, and xylene isomers. These hydrocarbons are the most important products of petrochemical industry and they are produced in amounts of tens of millions tons. However, since the physical properties of the components in these mixtures are similar, it is very difficult to implement separation processes on industrial scale as this requires enormous amounts of energy. Therefore, the development of new materials based on MOFs for high-efficiency and high-selectivity technologies for the adsorption separation of hydrocarbon mixtures is a pressing task.

2. Separation of ethane and ethylene

At present, the world production of ethylene exceeds 140 million tons per year and is predicted to increase annually by ~5%.[24] High purity requirements are imposed on ethylene used for polymerization, namely, its content should be >99.9%, the content of acetylene should be <2 ppm, and that of ethane and methane should be <200 ppm. The main method of ethylene production involves ethane dehydrogenation, so the problem of separating ethane and ethylene is extremely important.

The majority of adsorbents based on MOF selectively adsorb ethylene from ethylene–ethane mixtures. This is explained by the possibility of interaction of its π-system with the framework walls. The strongest interactions occur between the π-system and open metal sites,[‡] as well as polar

[‡] They are also called coordinatively unsaturated sites.

Table 2. Adsorption characteristics of certain most important ethylene-selective MOF at a pressure of 1 bar.

MOF [a]	*T*, K	S_{IAST} for the $C_2H_4-C_2H_6$ mixture with 1 : 1 composition [b]	Adsorption capacity, mmol g^{-1}		Ref.
			C_2H_4	C_2H_6	
HKUST-1	273	3.6	7.20	6.03	28
Mg-MOF-74	318	4.44	6.24	4.70	29
Mn-MOF-74	318	8.13	6.33	5.11	29
Fe-MOF-74	318	13.6	6.30	5.11	29
Co-MOF-74	318	5.82	6.07	5.25	29
Ni-MOF-74	318	5.93	6.01	4.71	29
Zn-MOF-74	318	2.70	5.38	4.61	
NOTT-300	293	48.7	4.28	0.85	30
Cr-MIL-100-SO_3Ag	296	9.7	3.26	1.47	31, 32
UTSA-280	298	> 10 000	2.5	0.1	33
Cu(I)-MFU-4*l*	296	–	3.76	2.76	34
Cu^I@UiO-66-$(COOH)_2$	298	80.8	2.14	0.81	35
Cu(OPTz)	270	75	1.43	0.22	36

[a] For the nomenclature and origination of the names of metal-organic structures, see V.V.Butova, M.A.Soldatov, A.A.Guda, K.A.Lomachenko, C.Lamberti. *Russ. Chem. Rev.*, **85**, 307 (2016).
[b] Selectivity factor calculated by the ideal adsorption solution theory (IAST).

and electron-withdrawing groups. Significant progress has been reached both in terms of C_2H_4 and C_2H_6 selectivity factors and ethylene sorption capacity.[22,24–27] The adsorption characteristics of some ethylene-selective MOFs demonstrating a high efficiency of separation of ethylene–ethane mixtures are presented in Table 2.

However, the interest in the development of sorbents for trapping ethane from its mixtures with ethylene increased significantly in the past few years. Such adsorbents are more attractive for practical use, since industrial mixtures of these gases usually contain up to 10% ethane [37] whose content in the outgoing ethylene needs to be diminished. The use of adsorbents that are more specific to ethane than to ethylene would significantly reduce the energy consumption for the separation and adsorbent regeneration. Thus, it was reported [38] that ethylene-selective MOFs make it possible to obtain pure ethylene only in a complete adsorption–desorption cycle; the purity of ethylene amounted to 99% in some experiments. To achieve a higher purity (99.95%), at least four full adsorption–desorption cycles and significant amounts of energy would be required. A considerable reduction in energy consumption can be achieved using ethane-selective MOFs.

There are fewer ethane-selective adsorbents among MOFs than ethylene-selective ones, and the phenomenon of preferential ethane adsorption over ethylene adsorption is often described as unusual or inverse adsorption. Adsorbents exhibiting such properties show promise for the industry from the economic point of view for the following reasons:[39]

— the formation of chemical bonds with the π-systems of alkenes results in higher energy consumption for adsorbent regeneration compared to the physical sorption of ethane;

— ethylene-specific sorbents require an additional desorption stage to obtain pure ethylene, which makes the implementation of an industrial process using sorbents of this type more difficult;

— in order to reduce costs and use a smaller amount of the adsorbent in the adsorber in the purification of a mixture of gases formed upon oil cracking with a typical composition of $C_2H_6 : C_2H_4 = 1 : 15$, the use of an ethane-selective sorbent to capture ethane is certainly more preferable than the use of an ethylene-selective sorbent.

The general requirements for sorbents exhibiting selective adsorption of ethane over ethylene include: the absence of open metal sites in the structure, a low polarity or hydrophobicity of the inner surface of cavities and channels, and the presence of specific sites for ethane adsorption. These requirements can be met by optimizing the pore size and shape and electrostatic charge distribution on the framework surface. Since the polarizabilities of ethane and ethylene molecules have similar values (see Table 1) and the quadrupole moment of the ethylene molecule noticeably exceeds that of the ethane molecule, polar sorbents exhibit selective sorption for ethylene, whereas in most cases nonpolar sorbents only demonstrate low selectivity for ethane. Nevertheless, the selectivity factors obtained and the data on breakthrough experiments reported in a number of papers give hope that compounds of this class can be used in industrial applications.

In 2016, the results of the first theoretical screening study of 278 MOFs were published,[40] according to which 64% of them are promising for the separation of $C_2H_6-C_2H_4$ mixtures: the product of selectivity and working capacity of these MOFs [§] (in mmol g^{-1}) exceeds 3. Some MOFs have higher working capacities and higher selectivity factors than traditional zeolites. Calculations showed that the selectivity of MOFs decreases with an increase in pressure. The lack of a direct correlation between selectivity and pore size was noted. Nevertheless, as a rule, MOFs with pore sizes < 5 Å demonstrate higher selectivity values, while those with pore sizes > 10 Å usually have low selectivities since the molecules of both gases can freely diffuse into the cavities.

Thus, the adsorption selectivity of a material is determined by a number of factors (topology, volume, size, and shape of pores) and cannot be predicted on the basis of any of these factors alone. Subsequently, Altintas and Keskin [40] expanded their predictions on the basis of calculations of the selectivity of membrane separation of ethane and ethylene for 175 MOFs.[42] The results of those calculations showed that the majority of MOFs are selective to ethane while fewer of them are selective to ethylene, and also that MOFs membranes have higher gas permeability values than the well-known membrane materials based on zeolites and activated carbons. It was emphasized that the calculations were performed for membranes with ideal structure, so the real selectivity values may be smaller.

The results of an expanded screening study of 1747 MOFs undertaken to identify the most promising candidates for the separation of ethane and ethylene were reported by Tang and Jiang.[43] Sixteen MOFs were identified that are promising in terms of selectivity ($S > 2.16$) and working capacity for ethane ($N > 0.54$ mmol g^{-1}). The authors suggested estimating the efficiency of sorbents as a

[§] The value of this parameter was previously chosen arbitrarily as a reference value to estimate the zeolite efficiency.[41]

trade-off (TSN) between the selectivity and working capacity (ΔN)

$$\mathrm{TSN} = \Delta N_{C_2H_6} \log(S_{C_2H_6/C_2H_4}) \quad (2)$$

since separation efficiency is determined by a complex interplay of these factors. Topological analysis has shown that various topologies of coordination nets are possible in the most efficient MOFs: **pcu**, **dia**, **pts**, **ctn**, and **xmz**. The most significant factors in terms of MOF design include the shape and size of pores, the ligand geometry and electronic properties, and the absence of highly polar functional groups.[44] Moreover, the type and structure of inorganic building blocks affect the preferred adsorption of ethane much less strongly.

Thus, data of screening studies have shown that numerous MOFs can potentially possess high selectivity and efficiency in the separation of ethane–ethylene mixtures.

The first examples of MOFs that selectively adsorb ethane from an ethane–ethylene mixture (Table 3) were represented by zeolite-like imidazolate frameworks ZIF-7 (microporous zinc benzimidazolate) and ZIF-8 (microporous zinc 2-methylimidazolate).[45, 46] A similar behaviour was demonstrated by their cobalt analogue, ZIF-69 [microporous cobalt(II) 2-methylimidazolate].[54] The adsorption selectivity calculated according to the IAST theory for all

Table 3. Adsorption characteristics of ethane-selective MOFs at a pressure of 1 bar.

MOF	T, K	S_{IAST} for the $C_2H_4-C_2H_6$ mixture with 1 : 1 composition	Adsorption capacity, mmol g^{-1}		Ref.
			C_2H_6	C_2H_4	
ZIF-7	298	3	1.9	1.9	45
ZIF-8	293	1.85	2.5	1.3	46
IRMOF-8	298	2.8	3.6	2.4	47, 48
	318	2.1	1.6	1.1	47, 48
ZIF-4	293	2.2	2.3	2.2	49
MAF-49	316	9	1.7	1.7	38
[Ni(bdc)(dabco)$_{0.5}$]	273	2	6.9	5.6	50
	298	2	5.0	3.4	50
[Ni(tmbdc)(dabco)$_{0.5}$]	298	2	5.4	4.9	51
[Zn(bdc)(dabco)$_{0.5}$]	298	1.75	4.45	3.16	52
[Co(bdc)(dabco)$_{0.5}$]	298	1.85	4.13	2.77	52
[Cu(bdc)(dabco)$_{0.5}$]	298	1.85	3.68	2.53	52
PCN-245	298	1.8	3.3	2.4	53
ZIF-69	298	1.64	2.2	1.8	54
ZJU-30	298	1.7	2.0	1.8	55
JNU-2	298	1.3	4.1	3.6	37
[$Fe_2(O_2)$(dobdc)]	298	4.4	3.4	2.6	56
PCN-250	298	1.9	5.2	4.2	57
MUF-15	293	1.96	4.7	4.1	58
[Cu(Qc)$_2$]	298	3.45	2.7	1.2	59, 60
MIL-142A	298	1.51	3.8	2.9	30
UiO-66-2CF_3	298	2.5	1.8	1.6	61
Ni-4PyC	298	1.7	3.8	3.5	62
MIL-53(Al)-FA	308	1.9 [a]	3.7	3.5	63
In-soc-MOF-1	298	1.4 [a]	4.04	3.72	64
	308	1.4 [a]	3.47	3.18	64
NUM-7a	273	–	3.1	3.1	65
	298	1.76	2.9	2.6	65
	313	–	2.6	2.3	65
M-PNMI	298	1.27–1.42	2.76 (Mn)	2.02 (Mn)	66
(M = Mn, Zn, Cd)					
[Ln(btc)(H_2O)]	298	1.92 (Y)	3.46 (Y)	3.13 (Y)	67
(Ln = Y, Sm, Eu, Dy)	298	1.80 (Sm)	1.64 (Sm)	1.56 (Sm)	67
	298	1.87 (Eu)	2.85 (Eu)	2.85 (Eu)	67
	298	1.37 (Dy)	1.90 (Dy)	1.90 (Dy)	67
ZJU-120a	296	2.74	4.91	3.93	68
CPM-233	273	–	8.31	8.48	69
	298	1.64	7.45	6.52	69
CPM-733	273	–	7.97	8.43	69
	298	1.75	7.12	6.37	69
CPM-81-Co	298	1.80	5.49	5.04	70
DUT-8(Cu)	303	1.43	3.45	1.92	71
	293	–	4.74	2.44	71
	283	–	6.41	3.46	71
	273	–	7.59	4.78	71

Table 3 (continued)

MOF	T, K	S_{IAST} for the $C_2H_4-C_2H_6$ mixture with 1 : 1 composition	Adsorption capacity, mmol g^{-1}		Ref.
			C_2H_6	C_2H_4	
DUT-8(Ni)	303	1.65	3.96	2.27	71
	293	–	5.30	2.97	71
	283	–	6.41	4.08	71
	273	–	8.09	5.30	71
Azole-Th-1	273	–	5.4	5.0	72
	298	1.46	4.5	3.6	72
NIIC-10-Pr	273	1.5	3.0	2.8	73
	298	1.1	2.5	2.1	73
NIIC-10-Bu	273	2.6	2.6	2.6	73
	298	1.1	2.3	2.0	73
NIIC-20-Et	273	7.7	4.0	3.0	74
	298	3.5	2.4	1.8	74
NIIC-20-Pr	273	5.5	4.5	3.6	74
	298	4	2.4	1.9	74
NIIC-20-Bu	273	18.8	3.2	2.0	74
	298	15.4	2.5	1.4	74
NIIC-20-Pe	273	7.8	2.8	2.2	74
	298	8.4	2.2	1.6	74
NIIC-20-Gl	273	7.3	3.7	3.0	74
	298	8.7	2.1	1.7	74

Note. Here and in other tables, see the text for the explanation of organic ligand names; the structural formulas of these ligands are available in Section 6 (pp. 26, 27 of this review). [a] A mixture with 1 : 15 composition.

these MOFs was found to be relatively small (1.6–3). Later studies showed[75] that 3D-printed ZIF-7 monoliths showed completely different trends of separation selectivity *versus* mixture composition dependences than powdered materials. The maximum selectivity values can reach 11.0 and 11.8, respectively, for 1 : 1 $C_2H_6-C_2H_4$ mixtures (at $P/P_0 = 0.55$, where P_0 is the saturated vapour pressure at a given temperature) and 1 : 9 (at $P/P_0 = 0.3$) due to the gate-opening effect. As the fraction of ethane increases, the selectivity of both powdered samples and monoliths decreases. For example, no increase in the selectivity factor above 2 was observed in the separation of a 9 : 1 $C_2H_6-C_2H_4$ mixture by ZIF-7 monoliths.[75]

The activation energy of diffusion inside ZIF-8 cavities increases from ethylene (7.2 kJ mol^{-1}) to ethane (11.5 kJ mol^{-1}), while the diffusion coefficients of ethylene and ethane at 273 K differ 5.8-fold.[76] On the one hand, these values make it possible to expect that the practical use of ZIF-8 for the separation of ethane and ethylene would be feasible. However, though the breakthrough curves[45,46] confirm the preferential adsorption of ethane over ethylene, they still do not give grounds for the practical use of ZIF-8 for the separation of these compounds. Nevertheless, the results presented above stimulated the development of studies on the search for new ethane-selective MOFs, and in the past five years, considerable progress was made in this area in terms of increasing both selectivity factors and sorbent capacity.

The selective adsorption of ethane over ethylene was demonstrated for the well-known metal-organic framework IRMOF-8[¶] based on zinc and naphthalene-2,6-dicarboxylic acid (H_2ndc).[47] The selectivity factors are low (in the range from 1.5 to ~3). The calculated adsorption heats of both gases proved to be almost equal, though it was noted that the adsorption heat of ethane exceeded somewhat that of ethylene at low degrees of surface coverage. To identify the differences in the interaction of gases with the surface based on the density functional theory (DFT), calculations of the surface electrostatic potential were performed. The results identified three different adsorption sites (Fig. 1). The energy of ethane interaction with sites 1 and 3 is approximately 3–4 kJ mol^{-1} higher than that of ethylene interaction with these sites, which agrees with the experimental data on the adsorption heats at low coverages and determines the selectivity for ethane. Later studies showed that gas molecule–framework van der Waals interactions deter-

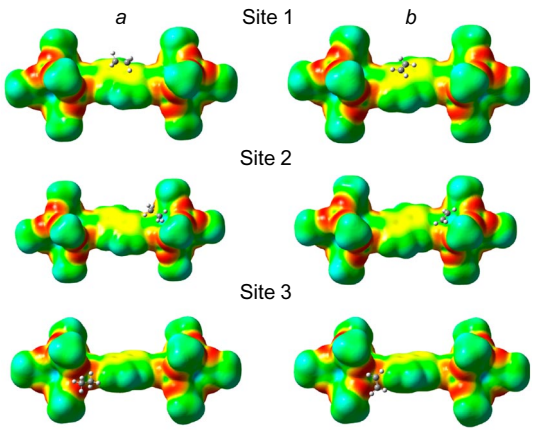


Figure 1. Adsorption sites of ethane (*a*) and ethylene (*b*) in the IRMOF-8 framework.[47] Carbon atoms are shown in grey and hydrogen atoms are in white. Green, blue, yellow and red colours indicate zero, minor positive, minor negative, and strongly negative electrostatic surface potentials, respectively. The image is published with permission from the American Chemical Society.

[¶] Representative of the IRMOF isoreticular family.

mine the selectivity of separation of ethane–ethylene mixtures, while interpenetrated IRMOF-8 demonstrates higher selectivity than the non-interpenetrated †† sample due to the higher density of organic linkers.[48]

Lv *et al.*[53] came to a similar conclusion and showed by calculations that ethane is stabilized inside an interpenetrated PCN-245 framework based on biphenyl-4,4′-dicarboxylic acid and trinuclear iron clusters $[Fe_3O(H_2O)_3(OOC)_6]^+$ with the shortest distances to the four nearest organic ligands in the range of 2.8–3.6 Å. The corresponding distances for ethylene to the three nearest organic ligands are in the range of 3.6–3.7 Å. It is interesting that yet another MOF based on the same inorganic building block but with a non-interpenetrated structure (PCN-285) exhibits preferential adsorption of ethylene compared to ethane.[53] However, the effect of interpenetrated is not so unambiguous, and PCN-250 built of the same trinuclear iron clusters and azobenzene-3,3′,5,5′-tetracarboxylate anions has a non-interpenetrated structure and shows preferential adsorption of ethane compared to ethylene, though the selectivity factor does not exceed 2.

Liao *et al.*[38] reported on an efficient adsorption process of ethylene and ethane separation from a 15 : 1 mixture that made it possible to obtain 56 L of ethylene with purity no less than 99.95% using 1 L of MAF-49 sorbent based on zinc and bis(5-amino-1*H*-1,2,4-triazol-3-yl)methane in one adsorption cycle. These undoubtedly high values are achieved due to the significantly different interaction of C_2H_6 and C_2H_4 molecules with the framework and, as a consequence, different shapes of the gas adsorption isotherms, despite the similar values of adsorption capacity for ethane and ethylene at 1 bar. The calculated heats of adsorption for ethane and ethylene were 60 and 48 kJ mol^{-1}, respectively. Monte Carlo calculations followed by DFT optimization made it possible to identify adsorption sites with high energies (Fig. 2), as well as small different structural distortions of the framework upon adsorption of ethylene and ethane, which contribute to their adsorption. It is important to note that the calculated data were supported by X-ray diffraction analysis (XRD) of MAF-49 single crystals filled with gases. Gas molecules could not be unambiguously localized in the structure because of their disordering and low content. Nevertheless, in all the structures, the residual electron density could be localized unambiguously within a narrow gate of the structure channel, which well agreed with the results of theoretical calculations.

Despite its low adsorption capacity, MAF-49 has long been the leader in the selectivity for ethane and ethylene separation: its selectivity factor is 9. Breakthrough experiments proved the high selectivity of separation on the MAF-49 framework; the purity of ethylene thus obtained was 99.984–99.986%. Liao *et al.*[38] also suggested a new molecular design strategy for the development of next-generation adsorbents involving the preparation of MOF in which the organic linkers can form a larger number of hydrogen bonds with ethane molecules and, accordingly, the interaction energy of C_2H_6 with the framework is greater than that of C_2H_4.

The energies of CH···O- and CH···π-interactions between the guest molecules and the framework are the key factor that determines the adsorption selectivity of C_2-hydrocarbons. It was found by Monte Carlo calculations[65] (Fig. 3) that the ethane molecule can be involved in the largest number of such interactions with the walls of the NUM-7a framework owing to the larger number of C–H-bonds and larger size compared to the planar ethylene molecule or the linear acetylene molecule. This framework is built of manganese(II) cations and 1,1,2,2-tetrakis(4-carboxyphenyl)ethylene anions and has one-dimensional channels with a cross section of 4.7 × 4.8 Å. The results of simulations of breakthrough curves showed the high potential of this compound for the separation of ethane–ethylene mixtures with compositions of 1 : 1 and 1 : 9.

Using Monte Carlo calculations, short CH···O host–guest interactions were identified in a series of M-PNMI frameworks based on the corresponding cations (M = Mn, Zn, Cd) and *N*,*N*′-di(4-pyridyl)naphthalene-1,4,5,8-tetra-

†† The terms interpenetrated and non-interpenetrated mean that the frameworks can be (or can be not, accordingly) inserted into each other, like, *e.g.*, catenanes.

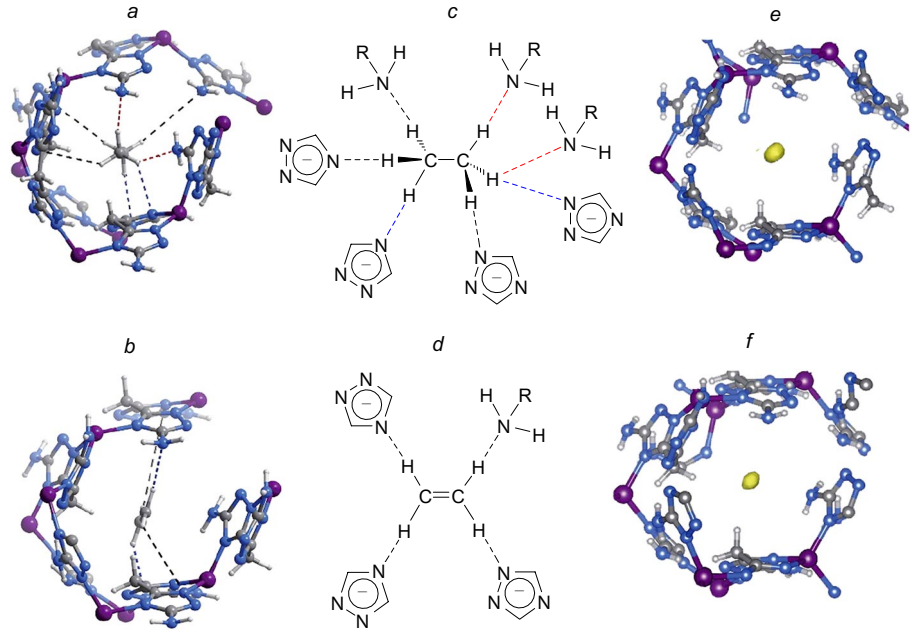


Figure 2. Preferred adsorption sites for ethane (*a*), ethylene (*b*) inside the MAF-49 framework obtained by computer simulation; schemes of the corresponding interactions for ethane (*c*) and ethylene (*d*), electron density distribution maps (indicated in yellow) in this framework filled with trace amounts of ethane (*e*) and ethylene (*f*). Strong interactions (hydrogen bond length < 2.3 Å) are indicated by red lines, weak interactions (hydrogen bond length 2.3–2.8 Å) by blue lines, and minor ones (bond length > 2.8 Å) by black lines.[38] Carbon atoms are shown in grey, hydrogen atoms in white, nitrogen atoms in blue, and zinc atoms in purple. The image is published with permission from the American Chemical Society.

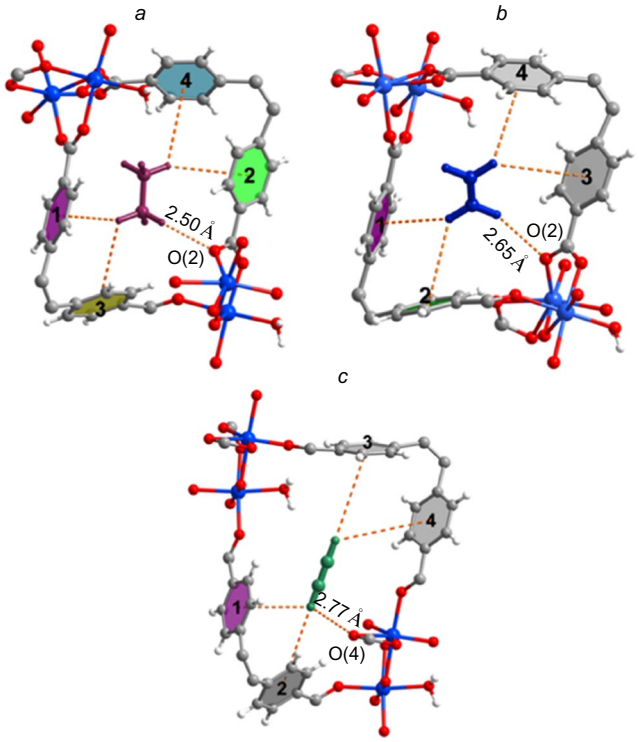


Figure 3. Interactions of ethane (purple) (*a*), ethylene (dark blue) (*b*) and acetylene (green) (*c*) molecules with the walls of NUM-7a framework based on Monte Carlo calculations. The CH···O distances are the smallest for ethane, which determines a higher energy of its interactions with the framework.[65] Carbon atoms are shown in grey, hydrogen atoms in white, oxygen atoms in red, and manganese atoms in blue. The numbers in the benzene rings are arranged in order of increasing distances from the benzene ring to the hydrogen atoms of the guest molecules. The benzene rings with distances greater than 4.00 Å are shown in dark grey. The figure is published with permission from the American Chemical Society.

carboxydiimide.[66] The bond lengths are in the range of 2.56–2.72 Å for ethane and 2.63–2.87 Å for ethylene. The selectivity factors calculated according to IAST do not exceed 1.5, but, according to breakthrough experiments, the separation efficiency of ethane–ethylene 1 : 9 and 1 : 15 mixtures on these sorbents is sufficiently high, which allows high-purity ethylene (> 99.99%) to be obtained.

Relatively short CH···O distances according to Monte Carlo and DFT calculations (Fig. 4) were also found for a series of frameworks Ln(btc) [Ln = Y, Sm, Eu, Dy; H_3btc is benzene-1,3,5-tricarboxylic (trimesic) acid]. Experimental breakthrough curves also confirm that it is possible to use these sorbents for efficient separation of ethylene and ethane mixtures with a low content of the latter.

A neutron diffraction study of a metal-organic framework $[Cu(Qc)_2]$ (where HQc is quinoline-5-carboxylic acid) saturated with deuterated ethylene or ethane was performed.[59] The molecules of both gases form multiple CH···π-interactions with aromatic rings of the ligand inside a rhombic framework cavity (Fig. 5). A greater number of such interactions are realized for ethane. They involve five of the six hydrogen atoms of its molecule. All four hydrogen atoms are involved in ethylene, but the interaction energy is lower than that for ethane. Thus, the shape of the cavity in $[Cu(Qc)_2]$ well matches ethane molecules, therefore a relatively high selectivity of C_2H_6/C_2H_4 separation is observed,

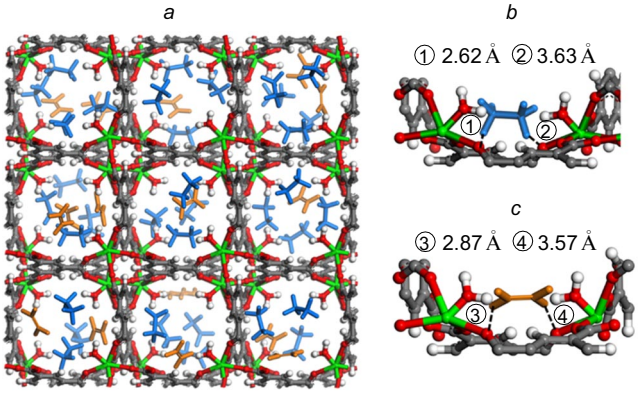


Figure 4. Results of Monte Carlo calculations for Y(btc) saturated with an equimolar $C_2H_6-C_2H_4$ mixture at 298 K and 1 bar (*a*); interactions of ethane (*b*) and ethylene (*c*) with the framework determined by DFT calculations.[67] Carbon atoms are shown in grey, hydrogen atoms in white, oxygen atoms in red, and yttrium atoms in green; ethane molecules are shown in blue, and ethylene molecules are shown in orange. The image is published with permission from the American Chemical Society.

which is also confirmed by breakthrough curves. The selectivity factor > 3 and the relatively high adsorption capacity for ethane (2.7 mmol g^{-1}) make $[Cu(Qc)_2]$ comparable with the most promising MOFs for the separation of ethane–ethylene mixtures.

The selectivity factor and adsorption capacity were further increased by oxidation of MOF with one-dimensional hexagonal channels Fe-CPO-27 (or Fe-MOF-74)

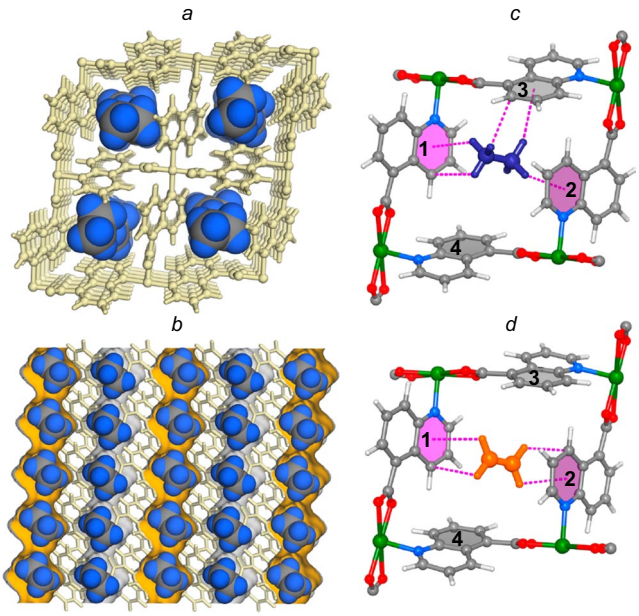


Figure 5. Crystal structures of $[Cu(Qc)_2]\cdot 0.41\,C_2D_6$ (*a*–*c*) and $[Cu(Qc)_2]\cdot 0.41\,C_2D_4$ (*d*) obtained by the neutron diffraction method; preferred adsorption sites of ethane (*c*) and ethylene (*d*). The purple lines indicate CH···π-interactions.[59] Carbon atoms are shown in grey, hydrogen atoms in white, oxygen atoms in red, deuterium atoms (*a*, *b*) or nitrogen atoms (*c*, *d*) in dark blue, and copper atoms in green; ethane molecules are shown in dark blue, and ethylene molecules in orange. The image is published with permission from the American Chemical Society.

based on 2,5-dihydroxyterephthalic acid (H_4dobdc).[56] Due to oxidation, the iron atoms inside the framework cavities are coordinated by peroxide groups that form rather strong hydrogen bonds with ethane molecules. According to neutron diffraction data, the D···O distances in a [$Fe_2(O_2)$(dobdc)] sample saturated with C_2D_6 amount to 2.17–2.22 Å, which is considerably smaller than the sum of the van der Waals radii of oxygen (1.52 Å) and hydrogen (1.20 Å). The hydrogen bonds with the ethylene molecule are much longer, *i.e.*, 2.20–2.41 Å. Experiments on the separation of a gas mixture showed that ethylene with a purity >99.99% can be obtained in just one cycle. The sorbent is stable and the separation rates do not decrease for at least five successive cycles. It is interesting that a non-oxidized sample of [Fe_2(dobdc)] shows preferential adsorption of ethylene rather than ethane, which seems to be due to the presence of an open site on iron cations.

Modifying the UiO-66 framework based on Zr_6 clusters and terephthalic acid by incorporation of two trifluoromethyl groups into the aromatic ring gave the UiO-66-2CF_3 framework.[61] This framework demonstrated selectivity of separation of ethane–ethylene mixtures with $S = 2.5$ in a wide range of pressures and one of the highest values of working capacity for ethane adsorption determined as the difference of the adsorption capacities at pressures of 10 and 1 bar. Thus, a relatively high selectivity and working capacity are successfully combined in the UiO-66-2CF_3 framework, which makes it promising for cyclic separations with adsorbent regeneration by pressure reduction. The good selectivity of this framework for ethane is provided by ligand rotations with changes in the gas pressure: at low pressure, the linkers have large rotation angles, and the small tetragonal cavities in the structure are not available for adsorption, but the rotation angles decrease with an increase in pressure, thus opening access to the tetrahedral cavities, while access to the octahedral cavities in the structure is made considerably easier. It is interesting that a similar effect was observed only for the framework with bulky CF_3 groups and was not observed in other isoreticular UiO-66 frameworks, such as UiO-Fum (based on fumaric acid) and UiO-66-Br (based on bromoterephthalic acid).

Using Th^{4+} and tetrazolobenzoic acid anions, an analogue of UiO-66 designated as Azole-Th-1 was obtained, which also showed selective adsorption of ethane and ethylene.[72] This MOF manifests high chemical stability (it is stable for 30 days in solutions of organic solvents and in aqueous solutions with pH 1–12), relatively high adsorption capacity for ethane and ethylene (4.5 and 3.6 mmol g^{-1}, respectively, at a temperature of 298 K and a pressure of 1 bar), moderate selectivity ($S = 1.46$) and good recoverability (no decrease in adsorption and separation parameters occurs for at least five consecutive separation–regeneration cycles). Azole-Th-1 can be used to obtain high purity (99.9%) ethylene both from binary ($C_2H_6-C_2H_4$) and ternary mixtures ($C_2H_6-C_2H_4-C_2H_2$). Monte Carlo and DFT calculations (Fig. 6) showed that the energy of framework interaction with an ethane molecule (43.1 kJ mol^{-1}) is significantly higher than with an ethylene molecule (33.5 kJ mol^{-1}). The tetrazole moieties inside the framework pores create a more stable adsorption site for C_2H_6 due to CH···π-interactions compared to adsorption sites without interaction with tetrazole.

The [Ni(bdc)(dabco)$_{0.5}$] framework with **pcu** topology based on nickel terephthalate layers bound *via* 1,4-diazabicyclo[2.2.2]octane (dabco) showed one of the highest

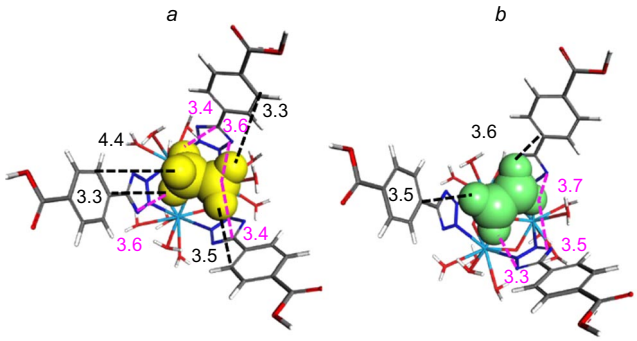


Figure 6. Assumed arrangement of adsorbed ethane (*a*) and ethylene (*b*) molecules near metal clusters inside the cavities of the Azole-Th-1 framework. Because of the high ligand disordering, the calculations were performed for four different models, but only one of them is shown in the figure.[72] Carbon atoms are shown in grey, hydrogen atoms in white, oxygen atoms in red, nitrogen atoms in blue, and thorium atoms in light blue; ethane molecules are shown in yellow and ethylene molecules, in green. Distances are in angstroms. The image is published with permission from Springer Nature.

adsorption capacities for ethane and ethylene.[50] Replacement of terephthalates with tetramethylterephthalates ($tmbdc^{2-}$) decreases the pore volume significantly (from 0.8 to 0.39 cm^3 g^{-1}) but increases the adsorption capacity for ethane from 5.0 to 5.4 mmol g^{-1} at 1 bar and 298 K.[51] Moreover, in [Ni(tmbdc)(dabco)$_{0.5}$] the selectivity of separation of ethane and ethylene increases from 1.62 to 1.985 according to IAST calculations, which is attributed to stronger guest–host interactions in smaller pores.

Replacement of terephthalic acid with naphthalene-1,4-dicarboxylic acid allows the adsorption of ethane by the ZJU-120a framework at 1 bar to be increased, despite the decrease in the pore aperture (from 5.8 to 4.4 Å), specific surface area (from 2791 to 1597 m^2 g^{-1}) and total pore volume (the adsorption capacity for N_2 at saturation decreases from 626 to 389 cm^3 g^{-1}).[68] The increase in ethane adsorption and the improved selectivity of ethane and ethylene separation compared to [Ni(bdc)(dabco)$_{0.5}$] are due to the formation of six relatively short CH···π interactions of the ethane molecule with two aromatic ligand rings located opposite each other, and only four longer interactions of ethylene with three aromatic rings of the ligands (Fig. 7).

The separation efficiency of the $C_2H_6-C_2H_4$ mixture on ZJU-120a reaches 8.39 L kg^{-1}. Further addition of new aromatic rings by replacing the ligand with anthracene-9,10-dicarboxylate anions (ZJU-121a framework) does not improve the properties due to too strong narrowing of the channel aperture. The adsorption isotherms of ethane and ethylene on the ZJU-121a framework are nearly the same, which makes separation of these gases almost impossible.

In the MUF-15 framework based on hexametallic building blocks {$Co_6(\mu_3\text{-}OH)_2(OOC)_{10}$} and isophthalate anions, the narrow and zigzag pores are decorated with benzene rings of isophthalate.[51] Along with the geometric size of the pores, such a surface favours a better binding of ethane molecules that are more polarizable than ethylene. Despite the low selectivity factors (1.9–2.0), MUF-15 demonstrated in a breakthrough experiment that it is possible to obtain ethylene with a purity acceptable for polymerization processes in one separation cycle, and the framework itself did not lose performance within at least 12 consecutive separa-

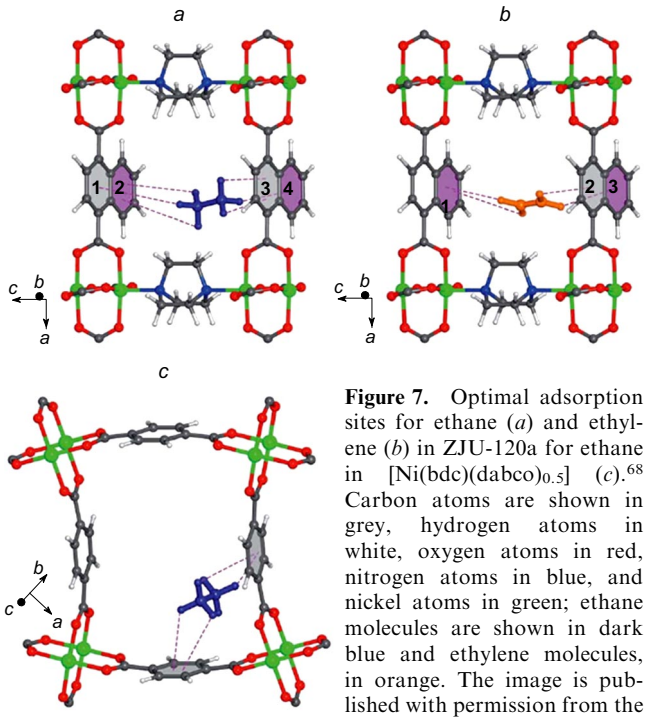


Figure 7. Optimal adsorption sites for ethane (*a*) and ethylene (*b*) in ZJU-120a for ethane in [Ni(bdc)(dabco)$_{0.5}$] (*c*).[68] Carbon atoms are shown in grey, hydrogen atoms in white, oxygen atoms in red, nitrogen atoms in blue, and nickel atoms in green; ethane molecules are shown in dark blue and ethylene molecules, in orange. The image is published with permission from the Royal Society of Chemistry.

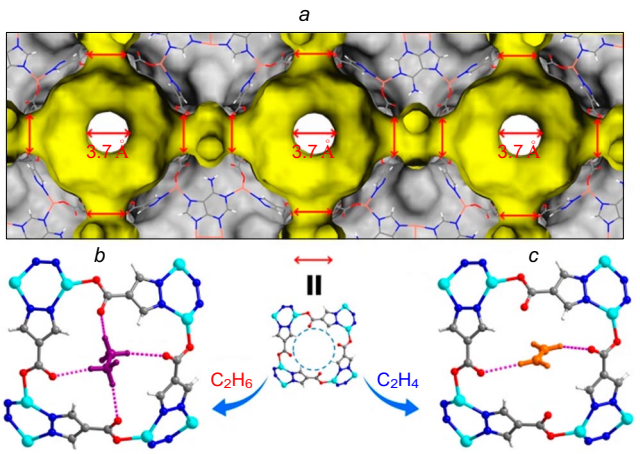


Figure 8. Schematic image of the channel structure in JNU-2 (*a*) and comparison of host–guest interactions for ethane and ethylene in this MOF according to DFT calculations (*b*, *c*). Fig. *a*, the inner surface of the channels is shown in yellow and the frame walls, in grey; in Fig. *b*, *c* the short hydrogen bonds (2.3 < H···O < 2.8 Å) are shown as dashed purple lines.[37] Carbon atoms are shown in grey, hydrogen atoms in white, oxygen atoms in red, nitrogen atoms in blue, and zinc atoms in turquoise; ethane molecules are shown in purple and ethylene molecules, in orange. The image is published with permission from the American Chemical Society.

tion–regeneration cycles. Incorporation of functional groups using substituted isophthalic acids ipa-X (X = F, NO_2, Br, Me) did not improve the selectivity of separation of the $C_2H_6-C_2H_4$ mixture.[77] What is more, MUF-15-NO_2 demonstrated inverse $C_2H_4-C_2H_6$ selectivity since strongly polar nitro groups can more efficiently interact with ethylene molecules whose quadrupole moment is larger than that of ethane molecules.

As a rule, kinetic (nonequilibrium) separation is difficult to implement for molecules that have similar kinetic diameters. In the JNU-2 framework based on pyrazole-4-carboxylic acid (H_2PyC) anions, adenine (Ade) and two types of metal clusters — $Cu^I_4(Ade)_4$ and $Zn_2(PyC)_2(\eta^1\text{-COO})_2(\eta^1\text{-Ade})_2$ — the gate aperture is ~3.7 Å, which is comparable to the kinetic diameters of ethane and ethylene molecules.[37] According to DFT calculations, the ethane molecule participates in a greater number of interactions with the oxygen atoms of the carboxyl group while passing through such gates, which affects the adsorption kinetics. Despite the low selectivity factor (1.3) calculated according to IAST, JNU-2 demonstrates a high efficiency of ethane/ethylene separation in a flow mode owing to the kinetic differences in their diffusion. It is possible to obtain >10 L of C_2H_4 with a purity >99.99% from a 1 : 1 gas mixture using 1 kg of JNU-2. Moreover, the stability of JNU-2 was confirmed in at least three consecutive separation–regeneration cycles. The high chemical stability of JNU-2 is also noteworthy: it maintained its structure and porosity for 30 days when kept at pH 2 and for >15 days when kept at pH 12 (Fig. 8).

Dividing channels with a large cross-section by an auxiliary ligand into channels with a smaller cross-section provides yet another efficient approach for increasing both the C_2H_6 adsorption capacity at 1 bar and the selectivity of separating ethane–ethylene mixtures.[69] This approach was demonstrated for MIL-88–MOF-235, a series of MOFs with general formula $[(M^1_2M^2)(O/OH)L^1_3]L^2$, where M^1 and M^2 are metals in the trinuclear building block, L^1 is a ligand forming a framework with **acs** topology, and L^2 is a ligand dividing a wide hexagonal channel into 6 narrow triangular channels. A total of 9 MOFs were synthesized. They were designated as CPM with various indices and differed in the metallocluster composition and the L^1 and L^2 ligands. The highest sorption capacity for ethane (7.45 mmol g^{-1}) was achieved on the metal-organic framework CPM-233 with the composition $[Mg_2V(OH)(bdc)_3]$tpt [where tpt is 2,4,6-tri(4-pyridyl)-1,3,5-triazine], while CPM-733 with the composition $[Co_2V(OH)(bdc)_3$tpt] showed the best selectivity (1.75) calculated according to IAST.

The effect of structure flexibility on the ethane and ethylene separation was demonstrated for a number of MOFs of the DUT-8 family based on bidentate carboxylate complexes with a paddle-wheel structure, naphthalene-2,6-dicarboxylic acid, and dabco.[71] Depending on the metal cation or the synthesis method, structurally rigid (Ni^{2+}, Cu^{2+}) or flexible (Ni^{2+}, Co^{2+}, Zn^{2+}) MOF were obtained. Flexible frameworks proved to be substantially limited in terms of use as C_2H_6 adsorbents since they had low adsorption capacity and their structure collapsed upon activation. In contrast, rigid DUT-8 frameworks showed record-high adsorption capacities up to 11.2 mmol g^{-1} in the temperature range of 283–303 K and at a pressure of 10 bar. The adsorption selectivity calculated according to IAST for DUT-8(Cu) is 1.8. The results of separation of ethane–ethylene mixtures in breakthrough experiment showed that the productivity of extraction of high-purity ethylene (>99.95%) with DUT-8(Cu) reached 20.8 L kg^{-1} at 1 bar and 45.0 L kg^{-1} at 5 bar.

The separation of ethane and ethylene on a commercially available metal-organic adsorbent MIL-53(Al)-FA based on aluminium and fumaric acid was studied.[63] Despite the low selectivity factor calculated according to IAST, the measured breakthrough curves showed that

99.95% ethylene purity with 1.28 mmol g^{-1} productivity could be achieved in one cycle.

The concept of angular bend modulation for the design of MOF without open metal sites based on an 8-linked secondary building block and a combination of pyridine-4-carboxylate anions with terephthalic or thiophene-2,5-dicarboxylic acids was suggested.[70] Cooperation of the two types of ligands (linear and bent ones) makes it possible to assemble the well-known trinuclear fragments $\{M_3O(OOC)_6L_3\}$ into a new type of an 8-linked secondary building block. The resulting metal-organic frameworks CPM-80–82 demonstrated high adsorption capacity for ethane and ethane-selective separation of an ethane–ethylene mixture. According to Monte–Carlo calculations, the difference in the adsorption energies of ethane and ethylene on CPM-81 framework is 1 kJ mol^{-1}, which is enough to reach a selectivity of ~1.8 (calculation according to IAST). The difference in the energies is due to the different number of CH···π-interactions that ethane (6) and ethylene (4) can form with the aromatic rings in the framework.

Using 12-nuclear carboxylate building blocks with the composition $\{Zn_{12}(OOC)_{12}(glycol)_6\}$ (where glycol is a deprotonated diol), MOF families (Fig. 9) based on isophthalate (NIIC-10 series of microporous polymers) and thiophene-2,5-dicarboxylate anions (NIIC-20 series of mesoporous polymers) were obtained.[73,74] Compounds of both families showed selective adsorption for ethane because the inner surfaces of the cavities were decorated with aliphatic groups of alcohols and contained no specific adsorption sites for ethylene.

The most impressive results for the selectivity of ethane and ethylene adsorption were demonstrated for the NIIC-20-Bu framework.[74] The selectivity factors calculated according to IAST reached 18.8 for the 1 : 1 mixture and 28.1 for the 1 : 15 mixture. It is interesting that the heats of ethane adsorption at zero coverage were systematically smaller for all the adsorbents of NIIC-20 series than the heats of ethylene adsorption. This means that high selectivity can only be due to the entropy factor. DFT calculations show that three adsorption sites making a significant contribution to the total adsorption capacity can be distinguished in the NIIC-20-Bu structure (Fig. 10). Adsorption site **B** showed the highest binding energies for both ethane (34.5 kJ mol^{-1}) and ethylene (37.3 kJ mol^{-1}) due to multiple CH···π- and CH···O-interactions with phenyl rings and carboxylate moieties. The interaction energies of gas molecules with similar groups in site **A** are markedly lower, whereas these energies are even lower in site **C** since it contains no polar groups. The energy of ethane interaction with adsorption site **A** is greater by 2.1 kJ mol^{-1} than that of ethylene, whereas for sites **B** and **C** stronger binding of ethylene than that of ethane by 2.8 and 1.5 kJ mol^{-1}, respectively, is observed. However, analysis of the structure of NIIC-20-Bu showed the ratio of the number of adsorption sites **A** : **B** : **C** to be 4 : 1 : 2. Consequently, sites **A** play

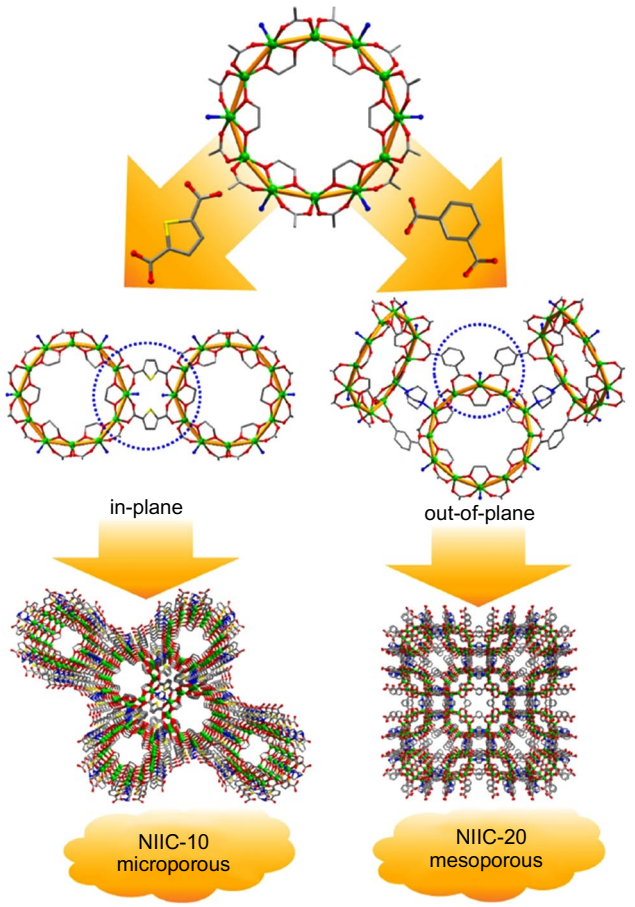


Figure 9. Local coordination environment and orientation of dicarboxylate bridging ligands in NIIC-10 and NIIC-20 leading to the formation of micro- and mesoporous frameworks.[74] Carbon atoms are shown in grey, oxygen atoms in red, sulfur atoms in yellow, nitrogen atoms in blue, and zinc atoms in green; orange rods demonstrate the formation of Zn_{12} 'wheels'. The image is published with permission from John Wiley and Sons.

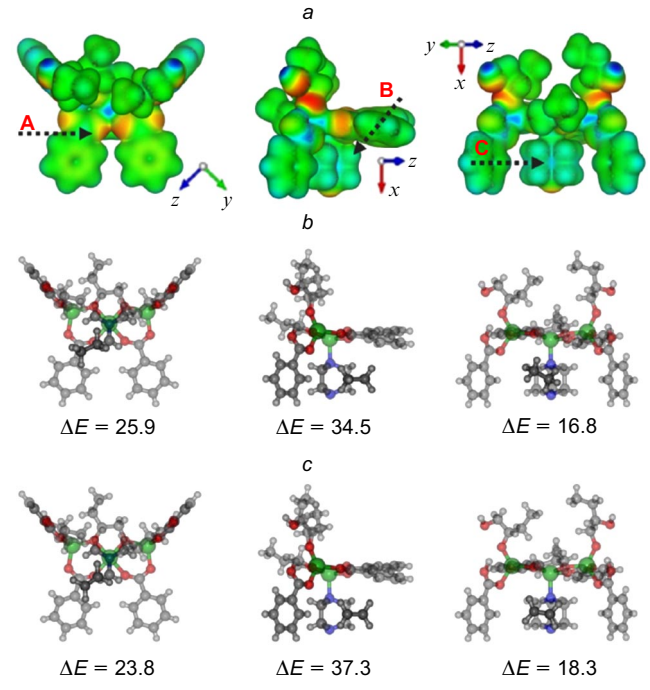


Figure 10. Calculated molecular electrostatic potential in a NIIC-20-Bu model (*a*); structures and bonding energies (ΔE in kJ mol^{-1}) for ethane (*b*) and ethylene (*c*) in adsorption sites **A**, **B**, **C**.[74] Carbon atoms are shown in grey, oxygen atoms in red, nitrogen atoms in blue, and zinc atoms in green; in Fig. *a*, zero electrostatic potential is shown in green, minor positive in blue, minor negative in yellow, and strongly negative in red. The image is published with permission from John Wiley and Sons.

the key role in the selective adsorption of ethane because they are more numerous in the framework. Thus, frameworks of the NIIC-20 family present the first example of MOFs in which the separation selectivity of ethane—ethylene mixtures is achieved due to the entropy contribution to adsorption on different adsorption sites.

3. Propane/propylene separation

Propylene is an important industrial gas that is used to produce polypropylene, a material with high resistance to fatigue, heat, organic solvents and moisture. Polypropylene is widely used in the production of films, fibres, containers, packaging, and personal protective equipment in laboratories and in medicine. The global propylene production exceeds 114 million tons per year.[78] The problem of propylene/propane separation is primarily relevant for polypropylene production.[79] The characteristics of some MOFs for propane and propylene adsorption are presented in Table 4. The purity of propylene must be >99.5% in most applications.[79] The propane fraction can be reused for dehydrogenation and propylene production or used separately, for example, in the production of liquefied gas for domestic applications or for the transport. However, the physical characteristics of propylene and propane are even more alike than those of ethane and ethylene: the boiling points differ by only 5.5 K, and there are nearly no differences in the kinetic diameters and polarizability of their molecules (see Table 1).

The method for propane/propylene separation involves a repetitive distillation—compression cycle in huge columns ~100 m high. The energy consumption of this process is estimated as ~12.9 GJ per ton of propylene, which is much higher than that in ethylene/ethane separation (~7.3 GJ per 1 ton of ethylene). Thus, the development of alternative energy-efficient technologies for propane/propylene separation, including adsorption separation on porous materials, is obviously very important.[79]

There are three main mechanisms for propane/propylene separation using MOFs (see Table 4):

— thermodynamic separation based on stronger binding of propylene to open metal sites and/or other 'strong' adsorption sites;

— kinetic separation based on the difference in the rate constants of propylene and propane diffusion;

— separation due to the gate opening effect that results in very different adsorption capacities of two gases in a certain pressure range.

3.1. Thermodynamic separation

HKUST-1 (Cu-BTC, MOF-199) based on inorganic copper(II) bidentate carboxylate blocks with a paddle-wheel type structure and trimesic (benzene-1,3,5-tricarboxylic) acid anions was the first MOF to demonstrate the thermodynamic separation of propane and propylene. This polymer is commercially available under the Basolite© C300 brand. The selectivity of propylene adsorption over propane that it demonstrated is due to the presence of coordinatively unsaturated copper atoms in activated HKUST-1, which can interact rather strongly with the π-system of propylene.[99] At low pressures, both gases are preferably adsorbed in small octahedral framework cavities. Numerous theoretical and experimental studies, including that of HKUST-1 moulded as pellets, extrudates, spheres, *etc*., were conducted and confirmed the efficiency of this sorbent for propylene/propane separation.[80, 81, 99–104] However, it was noted that the coordinatively unsaturated Cu^{2+} sites and small cavities have a mixed effect on the selectivity for propylene and propane. Perhaps, materials with larger pores would be more efficient than HKUST-1 if they comprise open metal sites.[105] The aforementioned MOF-74 (another common designation is CPO-27) may serve as an example of such a MOF.

Table 4. Adsorption characteristics of MOF at a pressure of 1 bar for propane and propylene.

MOF	*T*, K	S_{IAST} for the $C_3H_6-C_3H_8$ mixture with 1 : 1 composition	Adsorption capacity, mmol g^{-1}		Ref.
			C_3H_6	C_3H_8	
Thermodynamic separation [a]					
HKUST-1	323	3.3—5.5 [b]	7.9	6.5	80, 81
Mg-MOF-74	318	5.55	7.49	5.98	29
	298	4.7—10.1	7.8	6.9	82
	295	1.7	7.8	6.2	46
Mn-MOF-74	318	16.6	7.23	6.02	29
Fe-MOF-74	318	14.7	6.90	6.11	29
Ni-MOF-74	318	10.4	6.96	5.60	29
	298	10	4.7	3.9	83
Cu-MOF-74	303	12.7	7.6	6.4	84
Co-MOF-74	318	8.63	6.84	5.87	29
	303	9.3	7.0	6.0	84
	295	2.9	4.7	3.6	46
Zn-MOF-74	318	3.89	6.31	5.44	29
MIL-101(Cr)	303	1.2	7.9	6.2	85
MIL-101(Cr)_DAA	303	2.2	7.60	6.55	85
See [c]	298	—	2.30	2.46	86
$[Zn_2(5\text{-aip})_2(bpy)]$	298	19.8	1.91	0.76	87
AGTU-3a	298	7	1.2	0.4	88
Kinetic separation [d]					
ELM-12	298	15 [a] 204 [d]	1.48	1.36	89
	298	971	1.48	1.36	89
$[Zn(ox)_{0.5}(trz)]$	303	860	2.33	2.33	90
$[Zn(ox)_{0.5}(atrz)]$	303	175	1.64	—	90
KAUST-7	298	12 [b]	1.43	~0	91, 92
MAF-23	298	1.2	1.23	0.85	93
MAF23-O	298	15 [a] 204 [d]	1.30	0.09	93
GeFSIX-3-Ni	298	19 [b]	1.30	0.09	93
Y-abtc	298	—	2.0	~0	94
Frameworks demonstrating the open gate effect					
ZIF-7	303	1.25	2.4	2.3	95
	373	0.37	1.8	2.0	95
CPL-1	273	—	1.82	0.29	96
NJU-Bai8	298	4.6 [a]	2.89	2.89	97
	338	—	2.74	<0.3	97
$[Zn_2(bdc\text{-}Cl)_2(tpt)]$	273	5.2 [b]	3.32	1.62	98

[a] The selectivity factors were calculated according to IAST, unless specified otherwise. [b] The selectivity factor was determined from breakthrough curves. [c] Composition: $[Me_2NH_2]_2[Tb_6(\mu_3\text{-}OH)_8.(abtc)_3(dmf)_{1.5}(H_2O)_{1.5}]\cdot 1.75\,H_2O$. [d] The selectivity factors were determined as the ratios of diffusion coefficients, unless specified otherwise.

Metal-organic coordination polymers of the MOF-74 family are formed by 2,5-dihydroxyterephthalate anions and divalent metal cations. Their structure contains wide one-dimensional hexagonal channels with a characteristic size of ~11 Å. The channels are decorated with aqua-ligands that coordinate metal cations. The aqua-ligands can be removed by slight heating to give open metal sites.[82] The adsorption of propylene and propane on a series of frameworks differing in metal cations[29, 46, 83, 84] and pore sizes[106] was studied. The results showed that the formation of a π-bond favour a higher adsorption capacity for propylene at low pressures due to strong interactions with open metal sites. In fact, according to the neutron diffraction method, the Co—C(sp^2) distances in a sample of C_3H_6@Co-MOF-74 range within 2.66–2.73 Å.[29] The considerably larger dipole moment of the propylene molecule compared to the propane molecule results in strong dipole–dipole interactions between the adsorbed propylene molecules, which increase the adsorption capacity for propylene at a pressure of 1 bar by ~1/6 compared to propane (Fig. 11), even though the kinetic diameter of the propylene molecule is larger than that of propane (see Table 1).[82]

The propylene/propane separation efficiency on MOFs of the MOF-74 family increases in the following series of metal cations:[29, 83, 84] Zn ≈ Mg < Co ≈ Ni < Cu < Fe ≈ Mn. It has been shown that frameworks comprising cobalt and copper do not lose separation efficiency for at least 10 consecutive separation–regeneration cycles.[84]

Using the isoreticular approach, a number of MOF-74 family MOFs differing in the length of the organic ligand can be obtained. Monte Carlo simulation was used to compare the adsorption properties of the MOF-74-(I–IV) isoreticular series, where the Roman number indicates the number of benzene rings in the ligand [I is 2,5-dihydroxyterephthalic acid, II — bis(3-hydroxy-4-carboxyphenyl)benzene, III is bis(3-hydroxy-4-carboxyphenyl)-4,4′-biphenyl, IV is bis(3-hydroxy-4-carboxyphenyl)-4,4″-*p*-terphenyl].[106] As the ligand length increases, the following values increase markedly and monotonically: pore diameter (from ~10 to ~28 Å), specific surface area (from 1350 to 2480 $m^2\ g^{-1}$) and pore volume (from 0.60 to 1.60 $cm^3\ g^{-1}$), but the predicted propane and propylene adsorption capacities do not follow this simple pattern. The maximum adsorption capacities for propylene (14.1 mmol g^{-1}) and propane (11.9 mmol g^{-1}) were found for MOF-74-II, whereas the same values for MOF-74-I are as small as 8.6 and 7.1 mmol g^{-1}, respectively. The calculations confirmed once again the earlier findings[82] that at low pressures, propylene is predominantly adsorbed on open metal sites, whereas at ~1 bar it fills the pore centre. The best selectivity is expected for the parent of this series, namely, MOF-74-I.

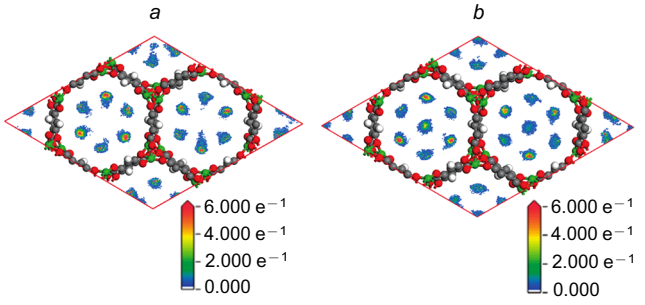


Figure 11. Equilibrium arrangement of propane (*a*) and propylene (*b*) molecules in Mg-MOF-74 channels at 1 bar and 298 K. An additional adsorption site in the middle of the channel was observed in the case of propylene sorption.[82] Carbon atoms are shown in grey, hydrogen atoms in white, oxygen atoms in red, and zinc atoms in green; the equilibrium arrangement of molecules is shown in different colours according to the probability scale presented in the figure. The image is published with permission from the American Chemical Society.

Coordination of 4,4′-diaminoazobenzene to open metal sites of mesoporous chromium(III) terephthalate $[Cr_3O(H_2O)_2X(bdc)_3]\cdot n\,H_2O$ (X = F, OH) designated as MIL-101(Cr) gave the modified polymer MIL-101(Cr)_DAA.[85] The difference in the isosteric adsorption heats of propylene and propane on MIL-101(Cr)_DAA and MIL-101(Cr) amounts to 13.4 and 0.6 kJ mol^{-1}, respectively. Moreover, a slight increase in the adsorption capacity for propylene is observed at pressures <60 kPa. According to IAST calculations, the selectivity factor for an equimolar $C_3H_6-C_3H_8$ mixture at 1 bar is 2.2 while that at 30 kPa is 4.6. A high stability of the sorbent was demonstrated in 20 separation—regeneration cycles. It should be noted that regeneration is easily performed by evacuation or by nitrogen purging of the column with the sorbent.

The open metal sites formed by group 11 metal cations (Cu, Ag, Au) exhibit elevated affinity to form π-complexes compared to 3d-metal cations that are commonly used to build MOF due to their 'softer' nature.[31, 32] This conclusion is also confirmed by theoretical calculations performed for MOF containing the C≡C—Cu or C≡C—Ag moieties.[107] Such groups within the porous structure are preferable propylene binding sites due to M—π-interactions. The metal-organic framework AGTU-3a based on Ag^+ cations and deprotonated thiourea derivative Py—CH=N—NHC(S)NH_2 demonstrated a relatively high selectivity factor of 7 at 1 bar and a moderate adsorption capacity.[88] Moreover, the high heat of adsorption at zero coverage (68 kJ mol^{-1}) unambiguously hints at strong Ag—π interaction. The approach based on the inclusion of Cu^I or Ag^I cations into the framework cavities can be very efficient for increasing the selectivity of separation of not only propylene—propane mixtures but also of other alkene–alkane mixtures.

3.2. Kinetic separation

Metal-organic coordination polymers with suitable pore sizes and shapes are considered as promising candidates for kinetic propane/propylene separation.[90] ZIF-8 was the first example of an MOF where the kinetic separation of a mixture of these hydrocarbons was demonstrated.[108] The adsorption isotherms of propylene and propane on ZIF-8 nearly coincide, nevertheless propane adsorption was found to be slightly more preferable (2.82 mmol g^{-1}) than that of propylene (2.62 mmol g^{-1}).[13] The selectivity factor of adsorption separation of a propylene—propane mixture calculated from the analysis of breakthrough curves amounted to 0.7. This value is insufficient for efficient separation. Nevertheless, numerous modern studies deal with the creation of membranes for separation based on ZIF-8 and comparison of their efficiency.[109–113]

Metal-organic coordination polymers $[Zn(ox)_{0.5}(trz)]$ and $[Zn(ox)_{0.5}(atrz)]$ (ox is oxalate, Htrz is 1,2,4-triazole, Hatrz is 3-amino-1*H*-1,2,4-triazole) contain narrow one-dimensional channels comprising zigzag moieties

8.4–8.9 Å long that are separated from each other by narrow 'bottlenecks' with diameters of ~2.9 and ~2.6 Å, respectively.[90] Though the sorption capacities for propane and propylene are nearly identical, the adsorption rate of propylene is much higher than that of propane. The kinetic selectivity factors calculated as the ratio of diffusion coefficients of propylene and propane at 323 K were 1565 and 220 for $[Zn(ox)_{0.5}(trz)]$ and $[Zn(ox)_{0.5}(atrz)]$, respectively.

Complete separation of propane and propylene that allows the individual components with high purity to be isolated was demonstrated for the first time for the KAUST-7 framework with the composition $[NiNbOFS(pyr)_2]\cdot 2H_2O$ (pyr is pyrazine).[91] For this purpose, the aperture of channels was fine-tuned by replacing $[SiF_6]^{2-}$ anionic ligands with $[NbOF_5]^{2-}$ in SIFSIX-3, a known family of coordination polymers. As a result, the distances between the adjacent fluorine atoms decreased and, accordingly, the aperture of channels decreased by ~0.4 Å. The original compound SIFSIX-3-Ni showed no selective adsorption of propane and propylene. Replacement of the ligand resulted in a dramatic decrease in propane adsorption capacity almost to zero (0.1 mmol g^{-1} at 1.5 bar and 298 K), *i.e.* molecular sieve-like highly efficient separation of propylene and propane was implemented. A column filled with ~1.4 g of KAUST-7 can retain propylene, allowing only pure propane through, for ~480 s at 4 mL min^{-1} flow rate of the equimolar mixture. It is also important to note that, in addition to thermal stability, KAUST-7 is highly resistant to water vapour and hydrogen sulfide. The column can be easily regenerated by pressure reduction to 0.01 bar or by purging with an inert gas (helium) at 1.2 bar.

The effect of small changes in the channel size was also demonstrated for compounds GeFSIX-3-Ni (4.42 × 4.42 Å) and GeFSIX-3-Co (4.72 × 4.72 Å) with the composition $[M(pyr)_2GeF_6]$ (M = Ni, Co) as examples.[92] Electron-withdrawing fluorine atoms in GeF_6^{2-} anions can act as efficient binding sites for hydrocarbon molecules with various acidity and polarity values. According to DFT calculations, the C_3H_6 molecule is located at the centre of a GeFSIX-3-Ni pore and forms four F···HC hydrogen bonds 2.03, 2.17, 2.24 and 2.60 Å long (Fig. 12).

A similar effect of the size of the structure gates was demonstrated for two coordination polymers based on hexanuclear complexes $\{(RE)_6(\mu_3\text{-}OH)_8(OOC)_{12}\}$ (where RE is a rare-earth element) and biphenyl-3,3′,5,5′-tetracarboxylic acid (H_4abtc), biphenyl-3,3′,5,5′-tetracarboxylic acid (H_4bptc) or azobenzene-3,3′,5,5′-tetracarboxylic acid anions (H_4abtc) and designated as RE-ftw/kle-MOF.[86] The compound based on yttrium and H_4bptc contains cavities with ~9.5 Å diameter accessible through very narrow windows with 2.6–2.9 Å diameter. A minimum pressure of 5 bar is required (for N_2, CH_4, C_2H_4) to reach an adsorption capacity of ~0.2 mmol g^{-1}, while the adsorption capacity for C_2H_6, C_3H_6 and C_3H_8 does not reach even 0.15 mmol g^{-1} at 8 bar pressure and a temperature of 298 K. The cavity size (9.6 Å) in the compound based on terbium and H_4abtc is nearly identical to that in Y-ftw/kle-MOF, but the aperture of the gates is considerably larger, *i.e.*, 4.44 × 2.35 Å. Though the adsorption capacities for propylene (2.30 mmol g^{-1}) and propane (2.46 mmol g^{-1}) are similar, the adsorption of propylene occurs much more quickly than that of propane. In a breakthrough experiment at a flow rate of 6 mL min^{-1} of an equimolar mixture, the propylene retention time was

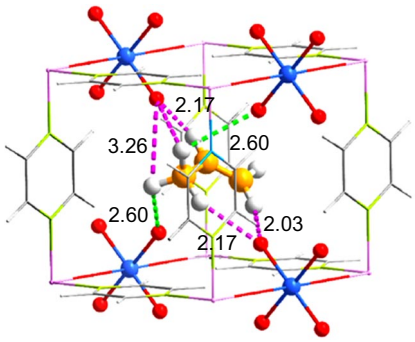


Figure 12. Adsorption site for the C_3H_6 molecule inside GeFSIX-3-Ni cavities according to DFT calculations.[92] Carbon is yellow, fluorine is red, hydrogen is white, germanium is blue; nitrogen is light green, nickel is pink. The distances are given in angstroms. The image is published with permission from the American Chemical Society.

10 min (1.49 g MOF), which is equivalent to an adsorption capacity of 0.9 mmol g^{-1}. It is interesting that the adsorption capacity for n-butane on Tb-ftw/kle-MOF reached a value of 2.7 mmol g^{-1} (at 1 bar and 298 K), whereas adsorption of isobutane was not observed.

In the structure of the Y-abtc coordination polymer with the composition $[Y_6(OH)_8(abtc)_3(H_2O)_6(DMA)_2]$ (where DMA is dimethylacetamide), access to relatively large cavities is opened through gates with a size of 4.72 Å.[94] This size is suitable for complete kinetic separation of propane (molecule diameter 5.1 Å) and propylene (molecule diameter 4.68 Å) whose adsorption capacities at 298 K amount to ~2 and 0.1 mmol g^{-1}, respectively. Measurement of breakthrough curves confirmed that Y-abtc can be used to obtain propylene with a purity of at least 99.5%, while the retention time of propylene with Y-abtc was 12.9 min g^{-1}, which is about two times larger than the value obtained with KAUST-7 (5.7 min g^{-1}).

A good combination of thermodynamic and kinetic factors was demonstrated for the MAF-23 framework with the composition $[Zn_2(btm)_2]$ [where H_2btm is bis(5-methyl-1*H*-1,2,4-triazol-3-yl)methane] and its oxidized analogue MAF-23-O with the composition $[Zn_2(btm)(btk)]$ [where H_2btk is bis(5-methyl-1*H*-1,2,4-triazol-3-yl)methanone] obtained by selective oxidation of half of methylene groups in MAF-23 into carbonyl groups.[93] This oxidation results in a considerable increase in the selectivity of $C_3H_6-C_3H_8$ adsorption. As expected, the difference in the heats of propylene and propane adsorption increases from 2.3 to 31.1 kJ mol^{-1} (thermodynamic factor) and the diffusion coefficients of these gases (kinetic factor) change considerably: $(3.3:2.8)\times 10^{-10}$ for MAF-23 and $(0.82:0.0073)\times 10^{-10}$ m^2 s^{-1} for MAF-23-O, *i.e.* the kinetic selectivity increases by two orders of magnitude.

An example of a MOF that provides efficient kinetic separation of propylene and propane with a kinetic selectivity factor of 204 at 298 K and 971 at 308 K is given by ELM-12 with the composition $[Cu(bpy)_2(OTf)_2]$ (where bpy is 4,4′-bipyridine and OTf^- is trifluoromethylsulfonate).[89] The structure of ELM-12 contains zigzag 2D channels with a gate size of ~4.0 Å. The adsorption capacities for propane and propylene are very similar, the selectivity factor calculated according to IAST is as small as 1.5, so kinetic effects serve as the main driving force. DFT calculations have shown that C_3H_6 and C_3H_8 molecules predominantly interact with triflate groups. Moreover, the

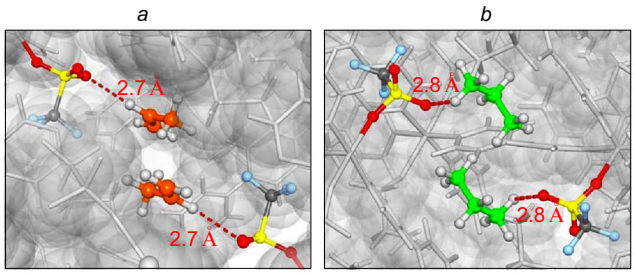


Figure 13. Interactions of C_3H_6 (*a*) and C_3H_8 (*b*) molecules with the ELM-12 framework.[89] The grey rods represent the framework; the carbon atoms in C_3H_6 and C_3H_8 are shown in orange and green, respectively; the white balls correspond to hydrogen atoms, red to oxygen atoms, yellow to sulfur atoms, and blue to fluorine atoms. The image is published with permission from Elsevier.

relatively large H···O distances (2.7–2.8 Å) indicate that the interactions with the framework are weak (Fig. 13). According to calculations, both molecules have similar thermodynamic affinity to the framework, in good agreement with the observed adsorption equilibria.

The possibility of using ELM-12 for industrial separation of propylene and propane was demonstrated in a series of breakthrough experiments using this MOF obtained in gram and kilogram amounts. The efficiency of a kilogram-scale sample is not inferior to a laboratory-made sample. Moreover, the results of studies on the adsorption properties and X-ray diffraction analysis confirmed the stability of the structure for at least three years in storage under ordinary conditions.

3.3. Separation based on the gate opening effect

The separation of propylene and propane on MOFs such as ZIF-7,[95] CPL-1[96] and NJU-Bai[8,89,97] is achieved due to the gate opening effect. In this case, the adsorption isotherms have a stepped shape due to the fact that gate opening occurs at a certain pressure and the adsorption capacity increases stepwise (Fig. 14). Separation becomes possible in a pressure range between the steps for various gases. This is rather a strong technological limitation, since sorbents whose operation in based on this effect are efficient only within certain, usually narrow, pressure and temperature ranges. On the other hand, regeneration of adsorbents of this type usually requires the smallest power consumption.

In the case of ZIF-7 at 373 K, the 'gate opening' pressures for propylene and propane are 95 and 28 kPa, respectively, hence the difference in these values is 67 kPa.[95] With a temperature decrease to 298 K, the difference decreases to 2 kPa, *i.e.* the separation of propylene and propane is possible only at elevated temperatures. The separation efficiency is also adversely affected by a pressure increase; the yield of pure propylene decreases even at a total pressure of 200 kPa.

For CPL-1 based on copper(II), pyrazine and pyrazine-2,3-dicarboxylate anions, an increase in the 'gate opening' pressure was observed in the case of C_3H_6 adsorption in the temperature range of 273–288 K; this effect was not observed at temperatures >293 K and pressures <1 bar.[96] Thus, the adsorption separation of propylene and propane on CPL-1 at 273 K with adsorbent regeneration at room temperature is possible. The regeneration efficiency is high enough both under static conditions (evacuation at a pressure of 90 kPa and a temperature of 298 K) and under

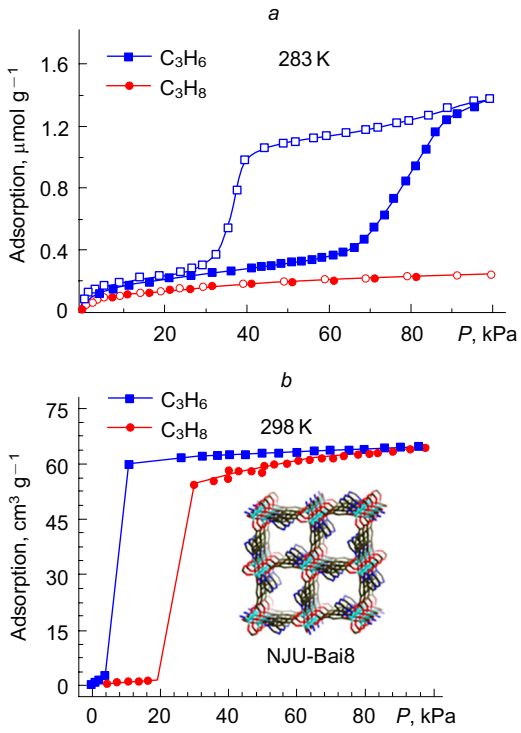


Figure 14. Typical shape of adsorption isotherms of the MOF exhibiting the gate opening effect: CPL-1 (*a*) and NJU-Bai8 (*b*).[96,97] In Fig. *a*, shaded symbols correspond to the adsorption branch of the isotherm, whereas the unshaded ones, to the desorption branch. In the structure in Fig. *b*, black indicates carbon atoms, red indicates oxygen atoms, dark blue indicates nitrogen atoms, and blue indicates copper atoms. The image is published with permission from Elsevier.

dynamic regeneration conditions (helium purging at a flow rate of 20 mL min^{-1} at 298 K) due to the low activation energy of desorption that equals 22.8 kJ mol^{-1}. According to molecular dynamic calculations, the propylene molecule is preferably adsorbed with formation of hydrogen bonds with the pyrazine molecule and causes its rotation, while propane is preferably adsorbed near the structurally rigid pyrazine-2,3-dicarboxylic acid molecule (Fig. 15).

The NJU-Bai8 framework also exhibits a strong temperature dependence of the gate opening pressure, moreover, this pressure for propane is ~5 times higher than that for propylene (see Fig. 14).[97] At temperatures >338 K it

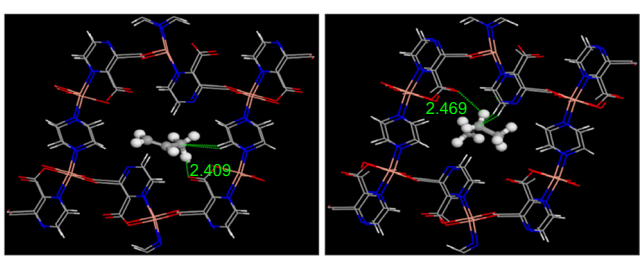


Figure 15. Adsorption sites of C_3H_6 (*a*) and C_3H_8 (*b*) in the CPL-1 structure.[96] Carbon atoms are shown in grey, hydrogen atoms in white, oxygen atoms in red, nitrogen atoms in blue, and copper atoms in orange. The distances are given in angstroms. The image is published with permission from Elsevier.

exceeds 1 bar for propane, so the adsorption capacity for propane under these conditions is low (<0.5 mmol g^{-1}). The adsorption capacity for propylene remains at 2.7 mmol g^{-1} in the temperature range of 298–348 K, which is somewhat unusual because, as a rule, the sorption capacity decreases with an increase in temperature. This phenomenon is related to the presence of pores in the flexible framework of NJU-Bai8 that perfectly fit the shape of the adsorbed C_3H_6 molecule, and hence, its strong interactions with the framework. The high separation efficiency of $C_3H_6-C_3H_8$ mixtures on the NJU-Bai8 framework was supported by calculations of the selectivity factor according to IAST, calculations and measurement of breakthrough curves, and measurement of desorption curves upon helium purging after saturation with the mixture to be separated. The retention time of propylene does not decrease for at least 10 consecutive separation–regeneration cycles, while the sorption capacity remains unchanged for at least 20 consecutive adsorption–desorption cycles.

4. Separation of benzene and cyclohexane

Cyclohexane is a raw material in the production of cyclohexanol, cyclohexanone, and eventually caprolactam required for making polyamide fibers and filaments. Cyclohexane is formed by catalytic hydrogenation of benzene, and small amounts of unreacted benzene should be separated to obtain the pure product. Simple distillation is not suitable for this because an azeotrope is formed and the boiling points of benzene (80.1 °C) and cyclohexane (80.7 °C) are close, so extractive or azeotropic distillation is used, which increases the separation costs.[114] Alternative methods that have not yet been put into production are based on adsorption separation on active carbons,[115,116] silica gel,[117] nanotubes[118] and cavitands.[119]

The selective sorption on MOFs of benzene compared to cyclohexane was first demonstrated by Shimomura *et al.*,[120] who studied a polymer with the composition [Zn(μ_4-TCNQ-TCNQ)bpy]$\cdot 1.5\,C_6H_6$ based on Zn^{2+} ions, 4,4′-bipyridine and a ligand with an extended π-system, namely, 7,7,8,8-tetracyano-quinodimethane dimer (TCNQ-TCNQ). The size of channels in the structure of this MOF matches benzene molecules almost perfectly; moreover, the benzene molecules incorporated in the framework channels are stabilized by CH–π-interactions with the quinodimethane moieties. Though the aperture of the gates in the channels is smaller than necessary for the free exit of benzene molecules, sorption is reversible, which is evidence of the framework flexibility. The adsorption isotherm of benzene demonstrates the gate opening effect, such that the capacity for benzene remains insignificant up to a certain pressure, and once a sufficient concentration of molecules on the surface of framework has been reached, the pores open and the capacity increases abruptly. In the case of cyclohexane, the capacity remains low even at high relative pressures and no gate opening effect is observed. After sorption from vapours of a mixture of benzene and cyclohexane in 1 : 1 ratio, the selectivity factor was 96 : 4 (Table 5).

In a later paper,[124] the same MOF demonstrated selective benzene sorption with a factor of 32 even with a thousandfold excess of cyclohexane in the original mixture. It is interesting that for a metal-organic framework based on Mn^{2+} nearly isostructural to compound Zn(μ_4-TCNQ-TCNQ)(bpy)]$\cdot 1.5\,C_6H_6$ with the same capabilities for CH–π-contacts of the framework with benzene molecules, no 'gate opening' effect was observed on the adsorption isotherm of benzene, and the sorption selectivity for cyclohexane became smaller. This indicates that a strong sorbate–framework interaction alone is insufficient to achieve high selectivity, pore-blocking effects or gate opening.

The importance of framework flexibility for the selective sorption of only one of the guests was demonstrated[121] for MAF-2 with the composition [Cu(etz)] (where Hetz is 3,5-diethyl-1*H*-1,2,4-triazole) as an example. A study of the structure of this framework showed that its rather large cavities (9 Å in diameter) are closed in static state; the pore aperture that amounts to ~1.5 Å is too small for any molecule to penetrate. At the same time, the conformational mobility of ethyl groups that close the entrance to the cavities ensures that molecules <4.2 Å in diameter along the smaller dimension can penetrate through them. As a result, MAF-2 has a high (206 mg g^{-1}) sorption capacity for benzene (molecule size $3.3\times6.6\times7.3$ Å) but a negligible capacity (9 mg g^{-1}) for cyclohexane (molecule size $5.0\times6.6\times7.2$ Å).

Size-selective incorporation of benzene was also observed in a MOF with the composition [Zn(salen)], where H_2salen is *trans*-*N*,*N*′-bis[3-*tert*-butyl-5-(4-pyridyl ethynyl)salicylidene]cyclohexane-1,2-diamine.[122] Benzene molecules in the framework channels were stabilized by CH–π-interactions involving cyclohexane moieties of the ligand. Though the size of the framework gates allowed cyclohexane molecules to penetrate into the cavities, too, this did not occur because these molecules cannot participate in the interactions specified.

A structural confirmation of π–π-interactions of sorbed benzene molecules with the pyridine rings in the structure of the Cu_2I_2(bttp)] C_6H_6 framework [where bttp is benzene-1,3,5-tri(isonicotinate) or 1,3,5-tris(4-pyridylacetoxy)benzene] was obtained.[125] The framework is a polycatenate network of two-dimensional layers with hexagonal channels that have an effective aperture of 9–12 Å. When the activated framework is saturated with benzene from the liquid phase, one benzene molecule per formula unit is sorbed. These molecules are arranged parallel to the pyridine rings of the ligand to form π–π-contacts (Fig. 16). Cyclohexane cannot participate in contacts of this kind, so its sorption is insignificant in the entire pressure range studied.

The 'gate opening' effect in the MOF with the composition [Zn_2(todp)$_2$(dmf)$_2$] based on Zn^{2+} ions and a flexible π-electron deficient ligand, pyromellitic acid *N*,*N*′-bis(1-carboxyethyl)diimide (H_2todp), under the impact of sorbate molecules was studied.[128] To activate this MOF, coordinated solvent molecules were removed and one-dimensional channels in the framework structure were freed. The stabilization of benzene molecules due to π–π-interactions with the pore surface resulted in high benzene sorption capacity (up to one C_6H_6 molecule per formula unit). Cyclohexane did not interact with the surface of the framework and could not enter its channels.

The sorption of benzene and cyclohexane by two isoreticular frameworks [Zn(bcbpy)(pma)$_{0.5}$]$\cdot 7\,H_2O\cdot$DMF and [Zn(bcbpe)(pma)$_{0.5}$]$\cdot 8\,H_2O\cdot$DMF [where Hbcbpy is 1-(4-carboxybenzyl)-4,4′-bipyridinium; Hbcbpe is 1-(4-carboxybenzyl)-4-[2-(4-pyridyl)vinyl]pyridinium; H_4pma is benzene-1,2,4,5-tetracarboxylic acid (pyromellitic acid)] was studied.[129] Both frameworks showed high capacity for benzene (52 and 108 mg g^{-1}, respectively) and the volume

Table 5. Sorption properties of MOFs that manifest selectivity to benzene and cyclohexane.

MOF	Adsorption capacity, mmol g^{-1}		P/P_0	S	Ref.
	C_6H_6	C_6H_{12}			
Selective to benzene					
Zn(μ_4-TCNQ-TCNQ)bpy	3.6	0.9	1	96 : 4, l	120
MAF-2	10.5	0.5	1	21, v	121
Zn(salen)	5.6	1.1	~0.9	5, v	122
MAF-24 β	10.24	0.95	~0.88	10.8, v	123
[Mn(μ_4-TCNQ-TCNQ)bpy]	3.7	1.7	1	95 : 5, l	124
$[Cu_2I_2(bttp)]\cdot C_6H_6$	2.6	1.2	1	2.2, v	125
$[Ni_3(OH)(ina)_3(bdc)_{1.5}]$	2.9	0.02	1	16, v	126
CID-23	1.2	0.09	See [a]	96 : 4, l	127
$[Zn_2(todp)_2(dmf)_2]$	1.47	0.45	1	–	128
$[Zn(bcbpe)(pma)_{0.5}]\cdot 8\,H_2O\cdot DMF$	5.5	~0	~0.9	–	129
$[Zn(bcbpy)(pma)_{0.5}]\cdot 7\,H_2O\cdot DMF$	2.32	~0	~0.9	–	129
DAT-MOF-1	1.51	0.18	~0.9	200 (IAST)	130
$[Cu_2(dpipha)_2(NO_3)_2]\cdot o\text{-xyl}\cdot DMF$	1.7	0.09	~0.95	19, v	131
Mn-MOF-74	9.38	0.25	See [b]	10^5 (IAST)	132
MFOF-1	20.38	13.18	1	1.5, v	133
IPM-MOF-110	4.57	~0	1	–	134
$[CuI(atpy)]\cdot DMF\cdot H_2O$	2.77	~0	~ 0.9	–	135
$[Cu(bpp)_2(BF_4)_2]$	11	~0	1	–	136
$[Cd(ataia)]\cdot 4H_2O$	2.36	0.35	1	6.5, v	137
CUB-5	7.6	6	~0.11	1.3, v	138
NIIC-30-NO_2	2.89	0.23	~ 0.78	10^4 (IAST)	139
$(Me_2NH_2)[Cd(dtztp)_{0.5}(HCOO)]\cdot 1.5\,DMF\cdot H_2O$	6.52	1.09	1	7000 (IAST)	140
NIIC-10-Et	0.86	0.01	1	92, l	73
$[Zn_2(chdc)_2(dabco)]\cdot 2\,NMP$	5.3	2.82	1	1.88, v	141
$(Me_2NH_2)_2[Dy_6(\mu_3\text{-}OH)_8(ftzb)_6(H_2O)_6]$	4.42	2.42	1	2.8 (IAST)	142
NIIC-30(Ph)	2.38	0.60	1	4, v	143
Selective to cyclohexame					
MOF-5	183.2	73.7	See [c]	1 : 3, v	138
CUB-30	1.25	0.42	See [d]	1 : 3, v	138
MUF-77	6.53	8.71	See [d]	1 : 5, v	144
NIIC-10-Pe	0.40	2.33	1	1 : 5, l	73

Notes. According to IUPAC recommendations, coordinated dimethylformamide molecules are designated as dmf in the formulas, while solvate and solvent molecules are designated as DMF. The S values are given for sorption from the liquid phase (designated by letter 'l'), from vapour phase, or for vapour phase with calculation according to IAST (designated by letter 'v'). Pressure, kPa: ~10 (see [a]), ~12.5 (see [b]), ~0.1 (see [c]), ~1 (see [d]).

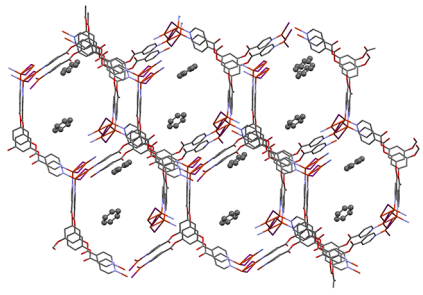


Figure 16. A fragment of the crystal structure of $[Cu_2I_2(bttp)]\,C_6H_6$ with benzene molecules included in its pores. Carbon is grey, oxygen is red, nitrogen is blue, copper is orange. The figure was created by the authors based on published data.[125]

of the framework pores differed by only 12.5%, whereas the difference in capacity values exceeded 200%. This effect was attributed to the denser packing of the sorbed benzene molecules due to stacking interactions with the more planar conjugated ligand, bcbpe, compared to bcbpy. Cyclohexane was almost not sorbed by these frameworks.

The role of π–π-stacking is the key in the selective benzene sorption by the DAT-MOF-1 framework with the composition $[Cu(dat)_2]$ [where Hdat is 4,6-diamino-2-(4-carboxyphenyl)triazine]. In a study of the sorption of vapours of benzene and cyclohexane alone, the selectivity factor calculated for the equimolar mixture according to IAST was 200.[130]

The sorption of benzene and cyclohexane vapours by MOF with the composition $[\{Cu_2(dpipha)_2(NO_3)_2\}\cdot\cdot o\text{-xyl}\cdot DMF]$ [where dipha is 5-*tert*-butyl-*N*,*N*′-di(4-pyridyl)isophthaldiamide; *o*-xyl is *o*-xylene] was studied.[131] The selectivity factor in the separation of the benzene–cyclohexane mixture was ~19. This value was attributed to the stronger interaction of benzene molecules with higher CH-acidity in comparison with the interaction of cyclohexane molecules with basic amido groups, as well as π–π- and

CH – π-interactions of benzene with the rings of the aromatic ligand.

A different type of interaction with the framework resulting in a high selectivity of benzene sorption in comparison with cyclohexane was found in another work.[132] A series of seven compounds of the M-MOF-74 family with the composition $[M_2(dobdc)]$ ($M = Mg^{2+}$, Mn^{2+}, Fe^{2+}, Co^{2+}, Ni^{2+}, Cu^{2+}, Zn^{2+}) containing open metal sites was studied. All of them showed a higher selectivity of benzene–cyclohexane mixture separation, with the highest values of capacity (9.38 mmol g^{-1}) and selectivity (10^5 according to IAST) demonstrated by Mn-MOF-74. The practical feasibility of benzene/cyclohexane separation was confirmed by NMR spectroscopy that showed that only benzene was incorporated in the framework upon sorption from a 1 : 1 mixture of vapors of these compounds. Molecular dynamics and DFT simulations showed that benzene molecules were localized near the metal ions (Fig. 17), with the highest charge transfer from the metal to benzene observed in Mn-MOF-74, *i.e.*, the adsorbent with the highest experimental adsorption factors.

It should be noted that Mukherjee *et al.*[132] were the first to perform a simulation of dynamic sorption separation of benzene and cyclohexane and to plot the breakthrough curves. The results of this simulation are important for demonstrating the practical feasibility of separation. They showed that when a mixture of benzene and cyclohexane flows through a tentative sorbent bed, pure cyclohexane appears almost immediately at the outlet, while benzene begins to escape much later.

A record-high sorption capacity for benzene (408 mg g^{-1}) was achieved by the MOF with the composition $[Co_4(\mu_3\text{-}F_3)(\mu_3\text{-}SO_4)(btb)(tpt)_2]\cdot 4.5\,DMA\cdot 5\,H_2O$ [MFOF-1, where H_3btb is 1,3,5-tris(4-carboxyphenyl)benzene; tpt is 2,4,6-tri(4-pyridyl)-1,3,5-triazine], which also manifested selectivity of benzene sorption over cyclohexane with a factor of 1.5 (see Table 5). The high capacity for benzene was explained[133] by π – π-stacking of its molecules with π-electron-deficient triazine rings. Significant hysteresis of adsorption–desorption isotherms indicates a strong interaction of the sorbate with the sorbent and the effect of pore 'locking' with sorbed molecules.

Nearly absolute selectivity of benzene sorption over cyclohexane was observed in the MOF with the composition [Zn(pbda)(dpni)] [IPM-MOF-110, where H_2pbda is 2-*tert*-butyl-1,4-bis(4-carboxyphenoxy)benzene; dpni is *N*,*N*′-di(4-pyridyl)naphthalene-1,4,5,8-tetracarboxydiimide].[134] This polymer is an ultramicroporous material whose pore aperture provides the effect of screening-out cyclohexane molecules, so the sorption capacity for this compound becomes negligibly small. Unfortunately, the results of sorption studies from benzene–cyclohexane mixtures were not presented in the article,[134] so we cannot estimate whether the separation is feasible in practice.

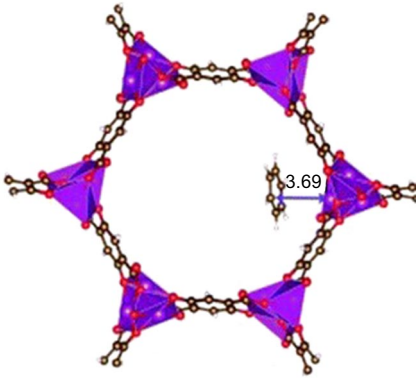


Figure 17. Interaction of the benzene molecule with Mn^{2+} open metal sites in the structure of Mn-MOF-74 according to DFT calculations.[132] Hydrogen is light grey, carbon is brown, oxygen is red, manganese polyhedra are purple.. The distances are given in angstroms. The image is published with permission from the Royal Society of Chemistry.

Specific sorption of benzene from a ternary benzene–cyclohexane–cyclohexene mixture, both in liquid and vapour phase, was observed on the MOF with the composition $[Ag_3(bcdaod)_2](SbF_6)_3\cdot CHCl_3\cdot H_2O$ [where bcdaod is 3,6-bis(quinoxaline-1-oxido-3-yl)-4,5-diazaocta-3,5-diene] with fairly wide channels (10 × 10 Å).[145] NMR spectroscopy showed that after removal of the guest water and chloroform molecules, the framework sorbed only benzene, while its desorption was only possible at 200 °C.

The MOF with the composition $[CuI(atpy)]\cdot DMF\cdot H_2O$ [where atpy is 4′-(9-anthryl)-4,2′:6′,4″-terpyridine] in which the two-dimensional layers form a supramolecular three-dimensional framework with rectangular channels of 10.56 × 7.32 Å was synthesized.[135] Though the dimensions of the channels allow the framework to sorb both benzene and cyclohexane, the capacity for cyclohexane is negligible. This is due to the fact that the inner surface of the channels is modified with anthracene residues that provide CH – π- and π – π-interactions of benzene molecules with the framework, while the sorption capacity for benzene is rather high, *i.e.*, up to 211 mg g^{-1}. This example shows that host–guest interactions play a more important role in determining the sorption selectivity than the geometry of channels in the framework cavities.

The synthesis of a three-dimensional coordination polymer $[Cu(bpp)_2(BF_4)_2]$ [where bpp is 1,3-di(4-pyridyl)propane] with a tightly packed, almost non-porous structure and a specific surface area as small as 14 $m^2\ g^{-1}$ according to BET ‡‡ was reported.[136] Treatment of the coordination polymer with an ethanol–water mixture (1 : 1) results in reversible structural rearrangement giving one-dimensional chains with the same composition. The coordination polymer obtained in this way exhibits sorption properties for some gases and vapours due to dynamic gate opening in the framework. The sorption capacity for benzene reaches 248 mg g^{-1}, which corresponds to two molecules per copper atom. At the same time, the capacity for cyclohexane and even toluene is negligibly small, and up to 1.9 benzene molecules per copper atom are sorbed from a benzene–cyclohexane vapour mixture.

The $[Cd(ataia)]\cdot 4\,H_2O$ coordination polymer [where H_2ataia is 5-[(4,6-diamino-1,3,5-triazine-2-yl)amino]isophthalic acid] with channels of three types oriented along the crystallographic axes *a*, *b* and *c* was reported.[137] The benzene adsorption isotherm on this MOF has a characteristic jump at $P/P_0 \approx 0.1$ indicating the gate opening effect in the sorption process. The selectivity factor of benzene sorption over cyclohexane is 6.5 at $P/P_0 = 1$. The sorption selectivity of benzene is due to the interaction of its molecules with the electron-deficient triazine rings.

In all the publications discussed above, metal-organic frameworks with enhanced sorption capacity for benzene were designed from ligands with aromatic rings that pro-

‡‡ Brunauer–Emmett–Teller method.

vided a π–π-interaction of the sorbate with the framework pore surfaces. A hitherto unknown three-dimensional material CUB-5 with the composition $[Zn_4O(cdc)_3]$ based on a rigid aliphatic linker, cubane-1,4-dicarboxylic acid (H_2cdc), was synthesized.[138] The size of the cubane-1,4-dicarboxylic acid molecule is close to the size of the terephthalic acid molecule (H_2bdc), so CUB-5 is an isoreticular analog of the well studied MOF-5, *i.e.*, zinc terephthalate $[Zn_4O(bdc)_3]$. A comparative study of benzene vapour sorption on CUB-5 and MOF-5 showed that CUB-5 sorbed significant amounts of benzene even at low partial pressures (7.6 mmol g^{-1} at $P/P_0 \approx 0.11$). Moreover, it was found using DFT calculations that the energy gain upon binding a benzene molecule is 6–7 kJ mol^{-1} larger in CUB-5 than in MOF-5. Obviously, the stabilization of the benzene molecule in CUB-5 pores is associated with their multiple CH–π-interactions with the methyl carbon atoms of the cubane linkers (Fig. 18).

Aliphatic linkers were used to build the MOF with the composition $\{[Zn_2(chdc)_2(dabco)]\cdot 2\,NMP\}$ (where H_2chdc is cyclohexane-1,4-dicarboxylic acid, dabco is *trans*-1,4-diaza[2.2.2]bicyclooctane, NMP is *N*-methylpyrrolidone) that has a primitive cubic structure with a gate aperture from 3.5 × 4 to 5 × 5 Å.[141] The multistep adsorption isotherms of benzene and cyclohexane vapours after activation of the framework indicate its dynamic ('breathing') behaviour in the presence of the sorbate. The sorption capacity for benzene at saturation is rather high and reaches 5.3 mmol g^{-1} (see Table 5).

A series of isostructural heterometallic coordination polymers NIIC-30-R with the composition $[Li_2Zn_2(R\text{-}bdc)_3(bpy)]$ (where H_2R-bdc represents terephthalic acid derivatives; R = H, Br, NH_2, NO_2) were studied.[139] These MOF comprise large cavities with a diameter of ~7 Å, while the aperture of the gates between them depends on the volume of substituent R and varies from 7 (R = H) to 3 Å (R = NO_2). A study of the adsorption of benzene vapour on the MOF of this series showed that the sorption capacity for benzene also depends on the nature of the substituent and expectedly decreases with an increase in its volume from 3.9 mmol g^{-1} for R = H to 2.9 mmol g^{-1} for R = NO_2. The best separation selectivity of the benzene–cyclohexane mixture was achieved for the MOF based on 2-nitroterephthalic acid (R = 2-NO_2) which showed the lowest sorption capacity for cyclohexane (0.2 mmol g^{-1}) while the ratio of the sorption capacities for benzene and cyclohexane was 15 at $P/P_0 \approx 1$. The selectivity factor calculated according to IAST was around 10^4 and was inferior only to that of Mn-MOF-74.[132] To explain the nature of the selectivity of benzene sorption by the

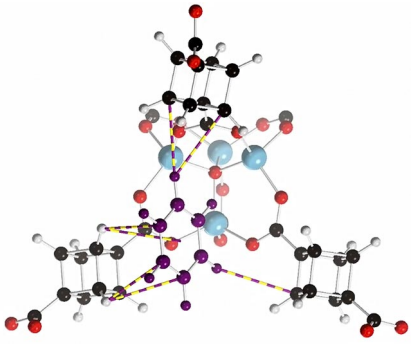


Figure 18. Interaction of a benzene molecule with CUB-5 according to DFT calculations.[138] Carbon is black, oxygen is red, zinc is blue; the bound benzene molecule is shown in purple. The image is published with permission from the American Chemical Society.

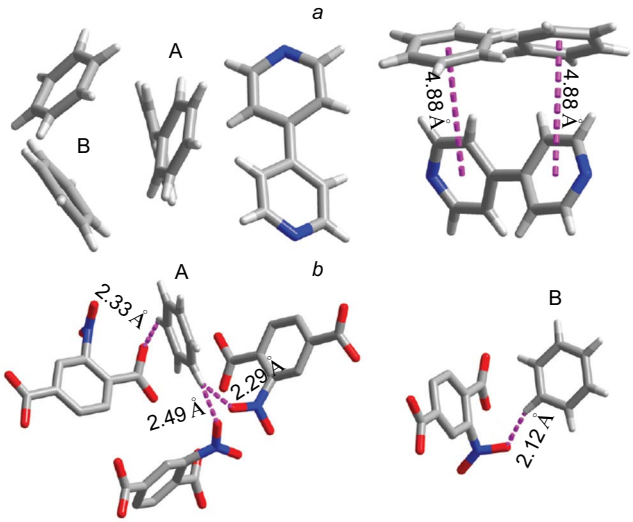


Figure 19. Localization of benzene molecules in the crystal structure of NIIC-30-NO_2 and their CH···π-contacts with 4,4′-bipyridine moieties (*a*); H···O-contacts of benzene molecules with nitro and carboxylate groups (*b*) according to XRD data.[139] Carbon is grey, oxygen is red, nitrogen is blue. The image is published with permission from the Royal Society of Chemistry.

NIIC-30-NO_2 framework, its crystal structure with incorporated benzene molecules was studied. Two types of benzene molecules designated as A and B can be distinguished in the structure (Fig. 19 *a*). Type A molecules are located near the 4,4′-bipyridyl linker and are oriented perpendicular to the pyridine ring planes to form CH···π-contacts. Moreover, these molecules are also involved in H···O-contacts with nitro and carboxy groups (Fig. 19 *b*). Type B molecules occupy the remaining free space in a pore and are bound to type A molecules by π–π-stacking. Cyclohexane molecules cannot participate in interactions of these types and penetrate into the pores more slowly due to their larger size. Thus, the selectivity of benzene sorption is determined by both thermodynamic and kinetic factors.

The studies on Li,Zn-heterometallic MOFs were continued by Sapianik *et al.*[143] Due to the presence of a phenylene substituent in the carboxylate linker, the system of channels in the coordination polymer NIIC-30(Ph) with the composition $[Li_2Zn_2(bpy)(ndc)_3]$ (where H_2ndc is naphthalene-1,4-dicarboxylic acid) differed significantly from the channel system in the MOF with terephthalic acid derivatives studied previously. In fact, the side channels were found to be blocked, and only one type of winding diagonal channels with cavity sizes of ~3 × 9 Å remained. The NIIC-30(Ph) polymer demonstrated a moderate sorption capacity for benzene (59 cm^3 g^{-1}) and selectivity of its sorption (~4) in comparison with cyclohexane. In the separation of a benzene–cyclohexane liquid mixture (10 : 90), a benzene content of 78% in the adsorbed phase was achieved, which indicates that this MOF is promising for further studies on the separation of benzene from cyclohexane if the content of the former is low. Based on single-crystal X-ray diffraction analysis of NIIC-30(Ph) with incorporated benzene molecules, 4 sites of localization of these molecules in the framework channels were identified (Fig. 20). In all these positions, benzene molecules form short contacts with naphthalene-1,4-dicarboxylic acid and 4,4′-bipyridine moieties with an average C···C interatomic distance of 3.73 Å.

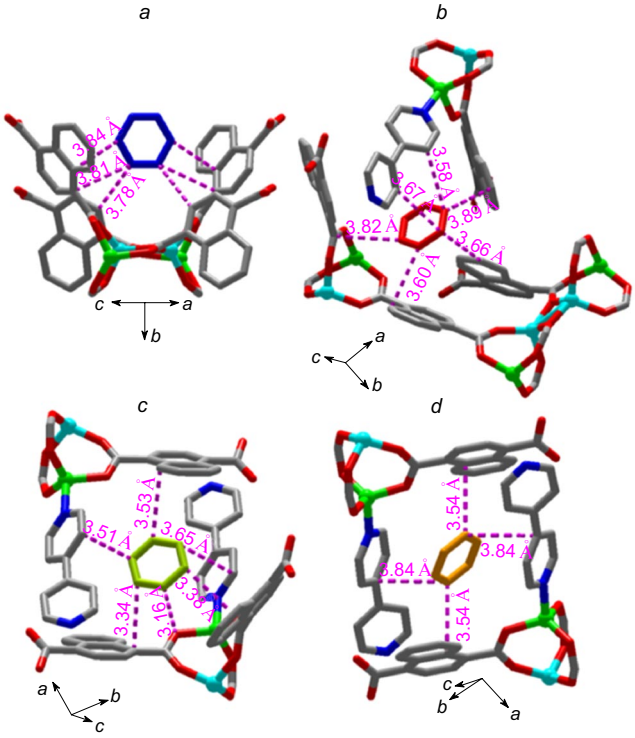


Figure 20. Interaction of sorbed benzene molecules in four different binding sites in the NIIC-30(Ph) framework according to XRD data.[143] Carbon atoms are shown in grey, oxygen atoms in red, nitrogen atoms in blue, zinc atoms in green, and lithium atoms in blue; different types of sorbed benzene molecules are shown in dark blue, red, green, and orange. The image is published with permission from the American Chemical Society.

This distance is shorter than the C···C contacts in crystalline benzene (3.81 Å), indicating a strong interaction between the benzene molecules and the framework.

A ligand with two types of donor groups, carboxyl and azole, was suggested [140] and the MOF with the composition $(Me_2NH_2)[Cd(dtztp)_{0.5}(HCOO)]\cdot 1.5\,DMF\cdot H_2O$ [where H_4dtztp is 2,5-di-(2*H*-tetrazol-5-yl)terephthalic acid] was synthesized using this ligand. The isotherm of benzene adsorption by this MOF demonstrated a sharp jump at low pressures, indicating strong interaction of the sorbate with the framework. The selectivity factor according to IAST was 7000 at 12.5 kPa (see Table 5).

Unusual patterns in the variation of the sorption properties were observed for a number of NIIC-10 formulations with the composition $Zn_{12}(tdc)_6(Rglycolate)_6(dabco)_3]\cdot \cdot x\,DMF\cdot y\,H_2O$ [where H_2tdc is thiophene-2,5-dicarboxylic acid, Rglycolate is a dianion of $RCH(OH)CH_2OH$ glycols; R = H, Me, Et, Pr, CH_2OH].[73] The structure of these MOF contains long channels built of dodecanuclear macrocycles $\{Zn_{12}(tdc)_6(Rglycolate)_6\}$ whose inner surface is decorated with substituents R of the glycolate ions. The largest channel diameter (5 Å) was found for R = H, and the same MOF showed the best sorption selectivity for benzene over cyclohexane, namely 92 : 1 and 20 : 1 for the sorption from a 1 : 1 mixture in the liquid and vapour phase, respectively. Moreover, elongation of the alkyl substituent R increases the cyclohexane sorption, despite the narrowing of the channel aperture, and even selectivity reversal was observed for R = Et and Pr^n. To understand the nature of the interaction of benzene molecules with the framework,

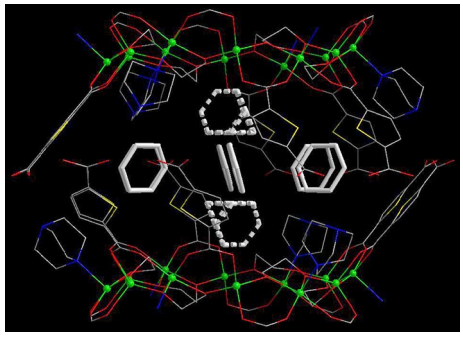


Figure 21. Localization of benzene molecules in the channels of the NIIC-10-Et structure according to XRD data.[73] Carbon atoms are shown in grey, oxygen atoms in red, nitrogen atoms in blue, zinc atoms in green, and sulfur atoms in yellow. The image is published with permission from the American Chemical Society.

single-crystal X-ray diffraction study of MOF with incorporated sorbate molecules was performed. Two crystallographically independent positions of benzene molecules were found on the third-order axis at the centre of the channel and near the thiophene moieties (Fig. 21). Three benzene molecules are included in one formula unit $\{Zn_{12}\}$, with no specific interactions identified between them and the framework.

A recent work [142] demonstrated a high sorption capacity of the MOF with the $(Me_2NH_2)_2[Dy_6(\mu_3\text{-}OH)_8(ftzb)_6(H_2O)_6]$ composition [where H_2ftzb is 4-(1*H*-tetrazol-5-yl)-2-fluorobenzoic acid] for benzene that amounted to 109.5 $cm^3\ g^{-1}$, while the selectivity factor with respect to cyclohexane according to IAST was ~2.8. Simulation of the interaction of benzene molecules with the framework by the molecular dynamics method showed the presence of two main adsorption sites where the benzene molecules are bound by CH···F hydrogen bonds and owing to π···π-stacking (Fig. 22).

In all the examples considered above, MOF exhibited selectivity of benzene sorption over cyclohexane, which is necessary in practice for the separation of the benzene admixture from cyclohexane. On the other hand, studies where inverse selectivity is observed are of great interest. For example, as mentioned above, an increase in

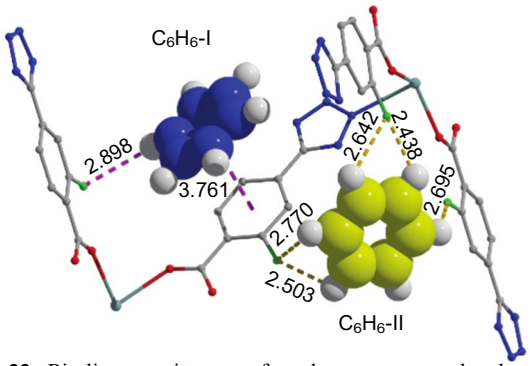


Figure 22. Binding sites of benzene molecules in $(Me_2NH_2)_2[Dy_6(\mu_3\text{-}OH)_8(ftzb)_6(H_2O)_6]$ according to molecular dynamics simulations.[142] Carbon atoms are shown in grey, oxygen atoms in red, nitrogen atoms in dark blue, and dysprosium atoms in green; different types of sorbed benzene molecules are shown in dark blue and yellow-green. The distances are given in angstroms. The image is published with permission from the Royal Society of Chemistry.

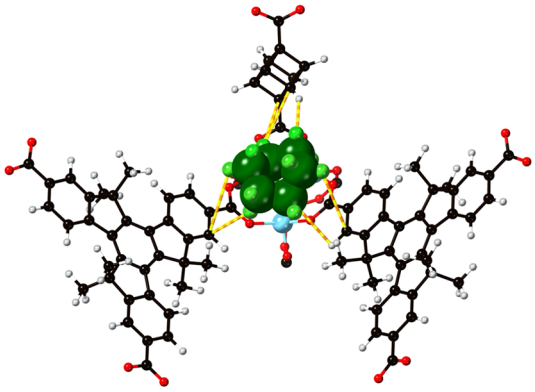


Figure 23. Interaction of cyclohexane molecules with CUB-30 according to DFT calculations.[144] Carbon atoms are shown in black, oxygen atoms in red, zinc atoms in blue; the bound cyclohexane molecule is shown in green. The figure is published with the permission from John Wiley and Sons.

the substituent length in the MOF of the NIIC-10 series with dodecanuclear building blocks $[Zn_{12}(tdc)_6(Rglycolate)_6(dabco)_3]$ with R = Pe (where PeH_2 is pentane-1,2-diol) decreases the selectivity with respect to benzene, then selectivity is reversed to reach 5 : 1 in the sorption from a cyclohexane – benzene vapour mixture with 1 : 1 composition.[73]

Apparently, MOF-5 is the simplest MOF with preferential cyclohexane sorption. Its sorption capacity for cyclohexane exceeds that for benzene.[138]

The synthesis of four-component metal-organic frameworks MUF-77 with the composition $[Zn_4O(hmtt)_{4/3}(bpdc)_{1/2}(bdc)_{1/2}]$ and CUB-30 with the composition $[Zn_4O(hmtt)_{4/3}(bpdc)_{1/2}(cdc)_{1/2}]$ (where H_3hmtt is 5,5,10,10,15,15-hexamethyltruxene-2,7,12-tricarboxylic acid, H_2bpdc is biphenyl-4,4′-dicarboxylic acid) was reported.[144] These MOFs are isostructural and differ in only one linker, *i.e.* there is terephthalic acid in MUF-77 and cubane-1,4-dicarboxylic acid in CUB-30. Both MOFs demonstrated selectivity for cyclohexane sorption over benzene at low partial pressures, while selectivity reversal occurred at pressures > 1 kPa (298 K). The binding energy of cyclohexane in CUB-30 determined by quantumchemical calculations was 12 kJ mol^{-1} larger than that of benzene. The preferential sorption of cyclohexane is due to the conformational mobility of its molecules, which allows them to form multiple contacts with the truxene and cubane moieties in the framework walls (Fig. 23).[144]

Mukherjee *et al.*[146] summarized literature data on 22 MOFs that manifest selectivity in benzene sorption, determined the binding sites of sorbate molecules by DFT method, built theoretical breakthrough curves, and calculated the selectivity factors for comparable conditions.

5. Separation of isomeric xylenes

Each of the xylene isomers serves as a raw material in basic organic synthesis. *p*-Xylene, which is oxidized into terephthalic acid, a monomer for polyesters (polyethylene terephthalate, polybutylene terephthalate) and polyamides (poly-*p*-phenylene terephthalamide), is the most important one.[147] Phthalic anhydride and subsequently phthalic acid esters — plasticizers for polymers — are synthesized from *o*-xylene. Oxidation of *m*-xylene gives isophthalic acid, a monomer for the synthesis of polyamides and polybenzimidazole.[148] Mixtures of isomeric xylenes (along with ethylbenzene) are obtained by catalytic reforming of oil. Their production in 2020 was 58 million tons and grows by 2 – 6% every year.[149] Refinement of the process for the separation of xylenes is regarded as one of the seven separation tasks that can 'change the world'.[19] This task is complicated by the similarity of the physical and chemical properties of xylenes (see Table 1). The boiling point difference of 5 °C allows *o*-xylene to be separated by distillation, but this requires columns with more than 150 theoretical plates that would require very significant energy consumption.[150] A larger melting point difference opens up the possibility of using fractional crystallization to separate the isomers, but the need to perform the process below −48 °C and the isolation of as little as 60 – 70% *p*-xylene increases the separation costs.[151]

The major portion of xylenes is currently separated by adsorption methods with a pseudo-moving sorbent bed,[152] using HZSM-5,[153] ZSM-5,[154] SMZ-100,[155] and FAU [156, 157] zeolites as the sorbents. However, the separation process is performed at 180 °C and a pressure of 9 bar, which increases the capital and operating costs. Therefore, the search for new sorbents capable of efficient separation of isomeric xylenes under milder conditions and with high productivity continues. Macrocyclic compounds — cavitands [158, 159] and porous covalent organic frameworks [160, 161] were suggested as alternatives to zeolites. Data on the sorption of xylenes on MOFs that show selectivity to particular isomers are presented in Table 6.

The results of the first study on the selective sorption of one of the isomeric xylenes from their mixture using MOFs were published in 2004.[176] In the synthesis of the MOF with the composition $[Zn_2(2,6\text{-ndc})_2(dmf)_2]$ (where 2,6-H_2ndc is naphthalene-2,6-dicarboxylic acid) in the presence of various xylenes, inclusion compound $[Zn_2(2,6\text{-ndc})_2(dmf)_2]\ C_8H_{10}$ was formed only in the case of *p*-xylene. The structure of this compound was determined by single crystal XRD (Fig. 24). A possible explanation for the selectivity of *p*-xylene inclusion in the framework pores based on quantum chemical calculations was suggested. The binding energy of the *para*-isomer was found to be larger than that of the *meta*-isomer due to the more significant framework rearrangement required for the inclusion of *m*-xylene.

Single crystal XRD of the inclusion compounds formed by each of the three isomers in MOF pores was performed [177] for the three-dimensional framework $[Cd(ClO_4)_2(abptr)_2]$ {where Habptr is 4-amino-3,5-bis[3-(4-pyridyl)phenyl]-1,2,4-triazole} (Fig. 25). The CH – π-interactions involving the aromatic ligand rings are the main type of identified interactions between the sorbate and the framework. The sorption selectivity was estimated for an equimolar mixture of isomers. As a result, the inclusion compound was obtained with almost equivalent amounts of *ortho*- and *meta*-isomers, whereas the *para*-isomer was not sorbed at all.

The selectivity of *para*-isomer sorption by MIL-47(V) was observed by Alaerts *et al.*,[162] who pointed out that the selectivity is due to the effects of molecule packing inside the pores rather than to the differences in the binding energies of sorbates (the changes in sorption enthalpy are almost equal for the three isomeric xylenes). Steric effects were confirmed by structure studies that showed that the *p*-xylene molecules in the pores of MIL-47(V) are arranged practi-

Table 6. Sorption properties of MOFs that show selectivity to xylene isomers.

MOF	Capacity for xylene, *o*/*m*/*p*, mmol g^{-1}	*S*	Ref.
	Selective to p-xylene		
MIL-47(V)	3.3/2.7/3.6	14 (*p*/*m*), hexane	162
MAF-X8	0.5/1.0/2.1	5.2 (*p*/{*o*+*m*+*p*}), v	163
MFM-300(Fe)	–	18 (*p*/*m*), pentane	164
MFM-300(V)	–	15 (*p*/*m*), pentane	164
$[Cd_2(dcba)(H_2O)_3]\cdot 2\,DEF$	3.8	8.5 (*p*/*m*), v	165
DUT-8(Cu)	4.8/4.9/5.5, v	8.3 (*p*/*o*), l; 12.5 (*p*/*m*), l	166
MAF-36	–	51 (*p*/{*o*+*m*+*p*})	167
$[Zn_4O(L)_3(dmf)_2]$	0.05/0.22/2.85, l	56 (*p*/*o*), l	168
[Cu(cdc)]	1.1/5.8/12.7, v	10 (*p*/*o*); 7 (*p*/*m*), mesitylene	169
	Selective to m-xylene		
NIIC-30(Ph)	–/26.5/26.5	3.03 (*m*/*o*), l	143
	Selective to o-xylene		
Cr-MIL-101	–	1.86 (*o*/*m*), DCM; 1.44 (*m*/*p*), DCM	170
$[Co_2(dobdc)]$	3.6/3.4/3.3, v, $P/P_0 = 0.007$	3.9 (*o*/*p*), heptane	171
$[Cu(4\text{-pmntd})_2(NO_3)_2]$	4.0/1.2/1.9, v	–	172
CD-MOF-1	2.8/0.7/0.2	13.5 (*o*/*p*), hexane	173
MIL-53(Cr)	0.22/0.08/0.05	6.27 (*o*/*p*); 3.89 (*m*/*p*), l	174
MIL-101(Cr)	1.1/1.2/1.2	1.2 (*o*/*p*), v	175

Notes. The sorption capacities are given for $P/P_0 = 1$, unless specified otherwise. The *S* values are given for sorption from liquid phase (designated as 'l') or from vapour phase (designated as 'v') or from solution (the corresponding solvent is specified).

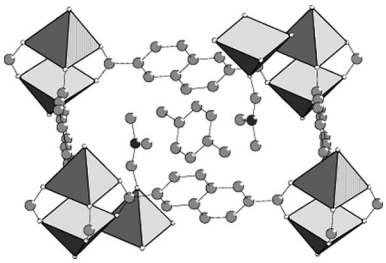


Figure 24. A fragment of the crystal structure of $[Zn_2(2,6\text{-ndc})_2(dmf)_2]$ with incorporated *p*-xylene molecules.[176] Carbon atoms are shown in grey and nitrogen atoms, in black; zinc tetrahedra are shown in dark grey. The image is published with permission from the American Chemical Society.

cally parallel to each other, thus a strong π–π-interaction between them is provided. At the same time, the distance between the *p*-xylene molecules and the terephthalate linkers of the framework is quite large, so the interaction of the sorbate with the framework is very weak. The arrangement of *o*- and *p*-xylene molecules is generally similar, but the π–π-interaction is less efficient because of the violation of the parallel orientation of the aromatic rings. The greatest steric hindrance was observed for *m*-xylene due to the

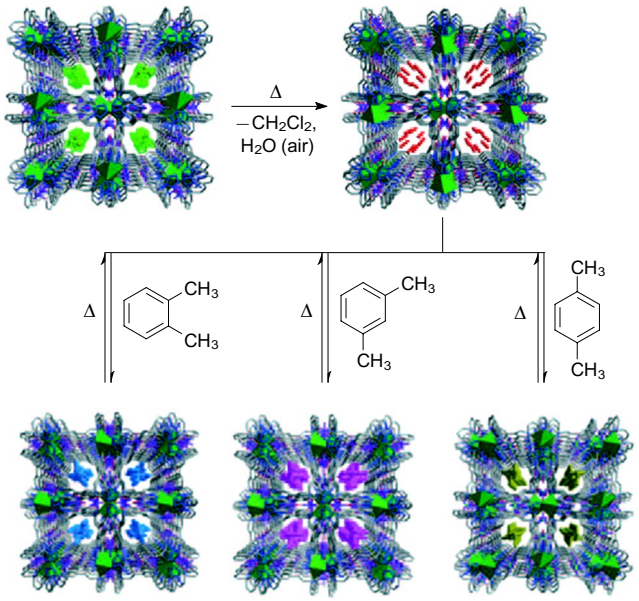


Figure 25. Models of the crystal structures of $[Cd(ClO_4)_2L_2]$ with included molecules of isomeric xylenes according to single crystal XRD data.[177] Carbon atoms are shown in grey, oxygen atoms in red, nitrogen atoms in dark blue; *o*-xylene molecules are shown in dark blue, *m*-xylene molecules in purple, and *p*-xylene molecules in green. The figure is published with the permission from John Wiley and Sons.

repulsion of the methyl groups in the sorbed molecules. The work in question was the first one where the practical separation of isomers was studied: breakthrough curves were built for a binary mixture of *p*- and *m*-xylenes at a flow rate of 0.5 mL min^{-1}, from which the selectivity factor was estimated to be 2.5.

The chromatographic separation of xylenes using another framework of the same family, Cr-MIL-101, but with selectivity for *o*-xylene was implemented.[170] The selectivity factors for the *ortho*/*meta* and *meta*/*para* isomer pairs were 1.86 and 1.44, respectively.

The metal-azolate framework MAF-X8 with the composition [Zn(mpba)] [where H_2mpba is 4-(3,5-dimethyl-1*H*-pyrazol-4-yl)benzoic acid] is one of the best frameworks in terms of parameters of xylene separation. It is almost not inferior in the selectivity of *p*-xylene sorption to the BaX zeolite used in industrial processes but significantly exceeds the latter in the sorption capacity, which prolongs the sorbent operation cycle and reduces the number of regenerations.[163] It was noted that the reason for its selectivity to *p*-xylene is that its molecule size matches the channel geometry in the MAF-X8 structure almost completely, as molecular modelling confirmed.

The sorption of xylenes by the Co-MOF-74 metal-organic framework with the composition $[Co_2(dobdc)]$ in one- and multicomponent systems with high selectivity to the *ortho*-isomer was studied.[171] The sorption capacity for xylenes was also rather high, 3.1–3.6 mmol g^{-1} (at 7 mbar). This value corresponds to one molecule of xylene per formula unit of MOF. It should be noted that Co-MOF-74 is superior to the NaY zeolite used industrially for xylene separation in terms of sorption capacity per unit volume of the sorbent. The feasibility of separating xylenes in a wide range of their concentrations in pentane (0.040–6.8 mol L^{-1}) is of great importance for the prac-

tical application of Co-MOF-74. Moreover, the upper limit of this range is close to the concentrations in a mixture of the isomers without a solvent. The binding sites of xylene molecules in the framework pores were determined by single-crystal X-ray diffraction analysis. After incorporation of *o*-xylene into the framework, three of four framework pores expand, with four *o*-xylene molecules entering each distorted pore and three *o*-xylene molecules entering the undistorted pore. Isomeric xylenes are involved in π–π-stacking with aromatic linkers. The distances between the ring centres of gravity are close for all the three isomers, *i.e.* this type of intermolecular interaction does not play a determining role in the sorption selectivity. In contrast, *o*- and *m*-xylene molecules are involved in short contacts with cobalt(II) ions, whereas the least bound *p*-xylene interacts with only one Co^{2+} coordination site (Fig. 26).

The synthesis of compound [$Ag(PF_6)$(btmtin)] based on silver ions and tridentate ligand L [where btmtin is benzene-1,3-5-triyltris(4-methyloxybenzyl)triisonicotinate], which is a one-dimensional coordination polymer built of 60-membered metal rings, was reported.[178] As polymer chains are packed into a crystal, open channels with 11.0×3.2 Å dimension are formed, which allows isomeric xylene molecules to be incorporated. The MOF crystals were stable enough to allow the exchange of guest molecules in the channels to occur during the single crystal–single crystal conversion. It is interesting that *o*-xylene did not enter the channels under all the conditions studied, whereas inclusion compounds with *m*- and *p*-xylenes were obtained and their structures were determined (Fig. 27). The authors noted that the substantial differentiation between *o*- and

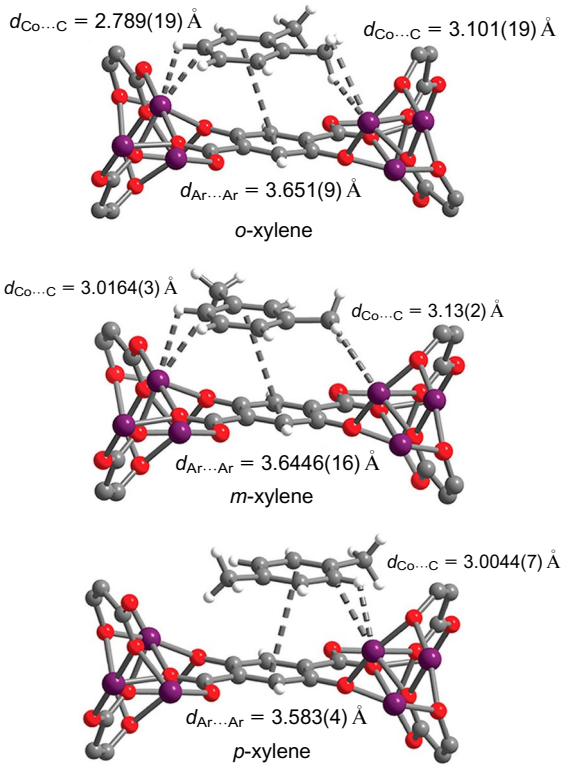


Figure 26. Interaction of xylene molecules with the surface of the Co-MOF-74 framework according to XRD data.[171] Carbon atoms are given in grey, hydrogen atoms in white, oxygen atoms in red, cobalt atoms in purple. The image is published with permission from the American Chemical Society.

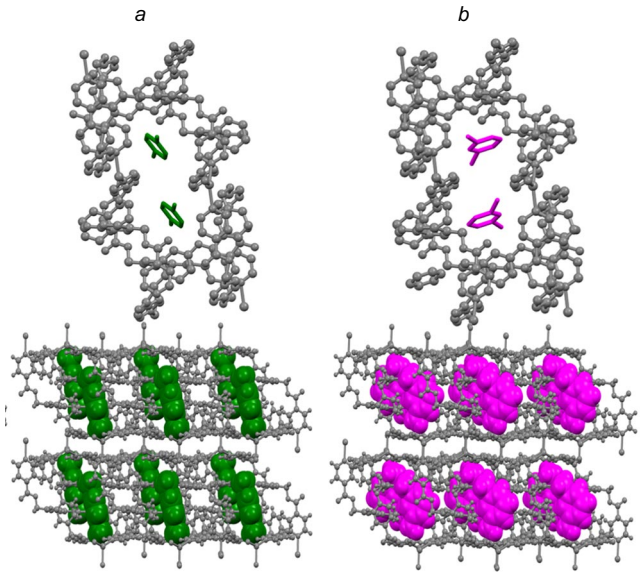


Figure 27. Crystal structure of [$Ag(PF_6)$L] with included *p*- (*a*) and *m*-xylene molecules (*b*) according to XRD data.[178] All the carbon atoms in MOF are shown in grey; *p*-xylene molecules are shown in green, and *m*-xylene molecules are in purple. The image is published with permission from the American Chemical Society.

m-xylenes is the first example of this kind. In the case of a mixture of *m*- and *p*-xylenes (1 : 1), selective incorporation of *p*-xylene into the channels was observed.

The majority of MOFs studied for the separation of isomeric xylenes showed selectivity in a certain isomer pair [*e.g.*, *p*- and *m*-xylene for MIL-47(V)], whereas for other pairs (*e.g.*, *p*- and *o*-xylene) selectivity was low or was not observed at all. Therefore, the separation of the three isomers using a single sorbent was not possible. The applicability of the MOF of the MFM-300 family with the [$M_2(OH)_2$(bptc)] composition (M = In^{3+}, V^{3+}, Fe^{3+}, Al^{3+}) for complete separation of ternary xylene mixtures was shown.[164] *p*-Xylene, which is the most important isomer from the practical point of view, is eluted first upon chromatographic separation, which is beneficial for the performance of the separation process. The MFM-300(M) isostructural adsorbents have one-dimensional channels with a square cross-section whose size varies depending on the metal ion radius from 7.4 Å for In^{3+} to 6. 5 Å for Al^{3+}, while the size of the channels for M = In, V, Fe is sufficient for incorporating any of the xylenes, whereas the channels with M = Al are narrower than the *m*- and *o*-xylene molecules. As a result, in the separation of an equimolar mixture of the three xylene isomers by high-performance liquid chromatography, adsorbents such as MFM-300(V) and MFM-300(Fe) showed extremely high separation ratios of chromatographic peaks $\alpha_{m,p}$ that amounted to 15 and 18, respectively, while MFM-300(Al) failed to separate the isomers.

High selectivity factors were also obtained in the separation by the frontal method. The binding sites of isomeric xylenes in the pores of MFM-300 were studied by powder X-ray diffraction using synchrotron radiation. In the channels of MFM-300(In), the *p*-xylene molecules and the planes of the aromatic linkers are located at an angle to each other, so there are no significant π–π-interactions between them (Fig. 28 *a*). The molecules of *o*- and *m*-xylene are involved in π–π-stacking with the phenyl rings of the linkers with a

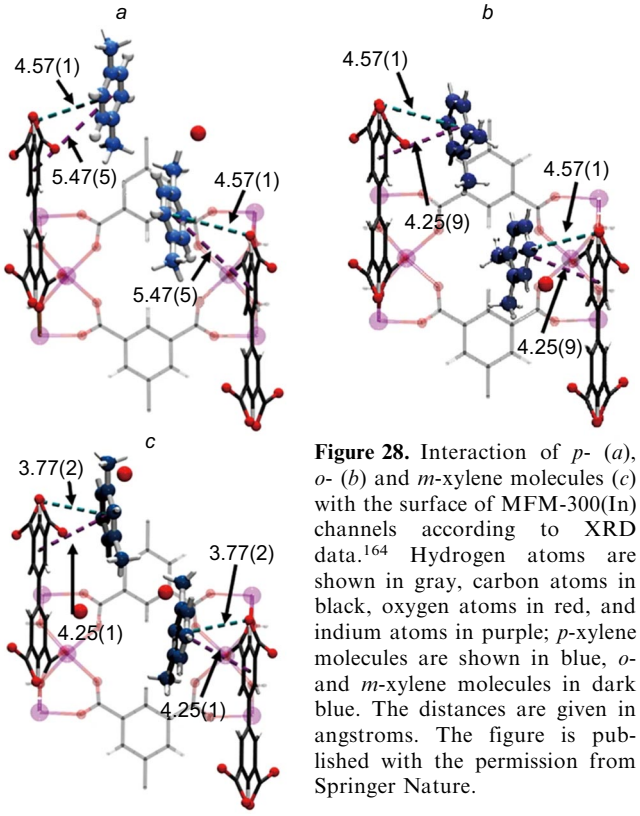


Figure 28. Interaction of *p*- (*a*), *o*- (*b*) and *m*-xylene molecules (*c*) with the surface of MFM-300(In) channels according to XRD data.[164] Hydrogen atoms are shown in gray, carbon atoms in black, oxygen atoms in red, and indium atoms in purple; *p*-xylene molecules are shown in blue, *o*- and *m*-xylene molecules in dark blue. The distances are given in angstroms. The figure is published with the permission from Springer Nature.

distance of ~4.25 Å (Fig. 28 *b*,*c*). For *m*-xylene, additional short contacts with carboxylate oxygen atoms exist, with interatomic distances of 3.77 Å (Fig. 28 *c*). The identified structural features match the high selectivity of the framework for *m*-xylene observed experimentally.

A structural confirmation that only *m*-xylene molecules are selectively incorporated into the framework cavities was obtained.[179] The three-dimensional PSP-CMERI-2 framework with the composition [Zn(oba)(bpd)] {where H_2oba is 4,4′-oxydibenzoic acid, bpd is 4,4′-bis[1-(4-pyridyl)ethylidene]hydrazine} has two types of pores with sizes of 8.3 × 8.4 and 18.5 × 15.2 Å. The *m*-xylene molecules incorporated in the pores are involved in π–π-interactions with

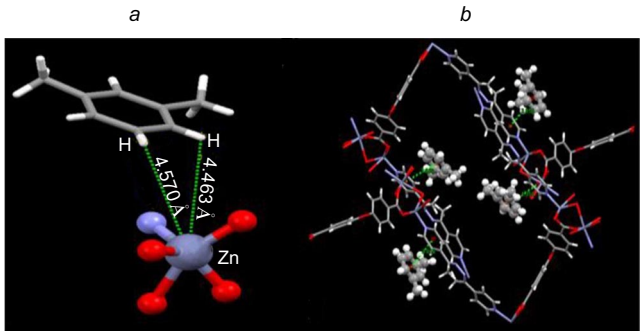


Figure 29. C–H-Interactions of *m*-xylene molecules with open Zn^{II} sites (*a*) and π–π-interactions of guest molecules with aromatic rings in the structure of [Zn(oba)(bpd)] according to XRD data (*b*).[179] Hydrogen atoms are shown in grey, carbon atoms in black, oxygen atoms in red, zinc atoms in purple The figure is published with the permission from the American Chemical Society.

the aromatic rings of the bpd ligands and with coordinatively unsaturated (CN = 5) zinc ions (Fig. 29).

The selectivity of benzene sorption compared to cyclohexane by MOF such as NIIC-30(Ph) with the composition $[Li_2Zn_2(bpy)(ndc)_3]$ was considered above.[143] The same coordination polymer shows extremely high selectivity in the sorption of xylenes. Experiments on the separation of equimolar binary and ternary mixtures of xylenes were performed both in the liquid phase and in saturated vapours. The highest selectivity factor (3.03) was obtained for the *m*- and *o*-xylene pair. In terms of this parameter, NIIC-30(Ph) surpasses all the MOFs reported to date. The sorption capacity for *m*-xylene is also rather high (~25 mass %). Based on the combination of capacity and selectivity, NIIC-30(Ph) became a new standard for comparing sorbents in terms of the separation of *m*- and *o*-xylenes. A sufficiently high, though not record-high, selectivity of sorption with $S = 2.94$ was observed for the *p*- and *m*-xylene pair of isomers. Taking into account the high sorption capacity of NIIC-30(Ph), it can be considered as a competitive material for the separation of this pair of isomers, too. The selectivity factors also retained their values on transition from binary to ternary xylene mixtures. To study the nature of the sorption selectivity of *m*- and *p*-xylenes compared to the *ortho*-isomer, the crystal structure of the inclusion compounds of each xylene in NIIC-30(Ph) was determined. It was found that as saturation is reached, approximately two xylene molecules are sorbed per formula unit of the framework. The *o*-xylene molecules in the framework channels are stabilized by the CH···π-interactions with the aromatic rings of naphthalene-1,4-dicarboxylic acid (3.51 Å) and 4,4′-bipyridine (3.56 Å) (Fig. 30). The type of contacts is similar for the *meta*- and

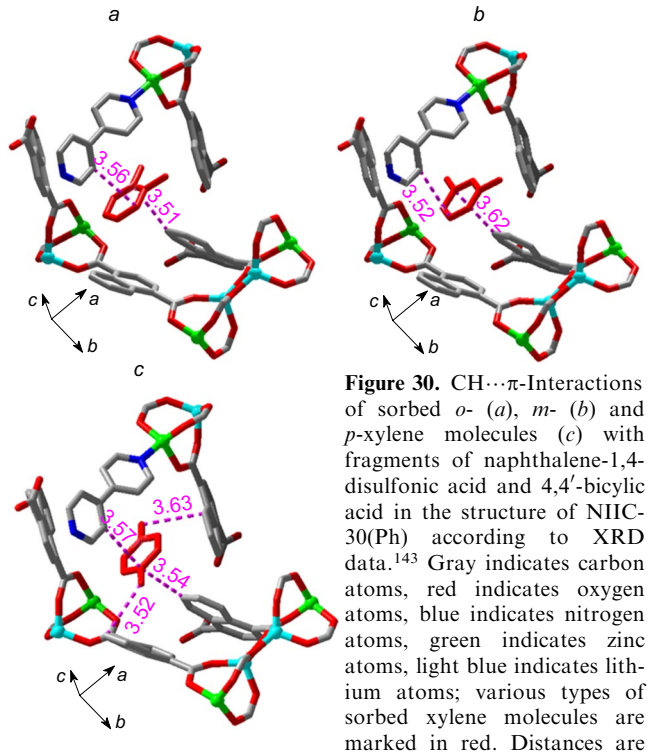


Figure 30. CH···π-Interactions of sorbed *o*- (*a*), *m*- (*b*) and *p*-xylene molecules (*c*) with fragments of naphthalene-1,4-disulfonic acid and 4,4′-bicylic acid in the structure of NIIC-30(Ph) according to XRD data.[143] Gray indicates carbon atoms, red indicates oxygen atoms, blue indicates nitrogen atoms, green indicates zinc atoms, light blue indicates lithium atoms; various types of sorbed xylene molecules are marked in red. Distances are given in angstroms. The figure is published with the permission from the American Chemical Society.

para-isomers, but the total number of stabilizing contacts differs: for *m*-xylene there are two specific interactions in one binding site, five such interactions in two binding sites were detected for *p*-xylene, while for *o*-xylene there are only three contacts in two binding sites. Incorporation of *o*-xylene causes the greatest rearrangement of the framework structure as the channel sizes change from 2.9×9.6 to 4.0×9.6 Å after sorption. Thus, the combination of two factors, a weaker host–guest interaction and the need for a significant structural rearrangement, determines the low susceptibility of NIIC-30(Ph) to the sorption of *o*-xylene.

A two-dimensional MOF with the composition $[Cd_2(dcba)(H_2O)_3] \cdot 2\,DEF$ {where H_4dcba is 4″,6′-diamino-5′,5″-bis(4-carboxyphenyl)-[1,1′:3′,1″:3″,1‴-quaterphenyl]-4,4‴-dicarboxylic acid; DEF is diethylformamide], whose layers are packed into a porous structure, was synthesized.[165] A study of the adsorption of vapours of isomeric xylenes showed the selectivity of *p*-xylene sorption with a capacity of 85 $cm^3\ g^{-1}$; moreover, the adsorption isotherm contains a jump near $P/P_0 = 0.3$ characteristic of the sorbent's gate opening effect.

Zhou *et al.*[180] demonstrated the molecular sieve effect with adsorption of sorbates that have molecules of intermediate size. The metal-organic framework MAF-41 with the composition $[Cu_2(fbdim)]$ {where H_2fbdim is 2,6-bis(trifluoromethyl)-1.7-dihydrobenzo[1,2-*d*;4,5-*d*]diimidazole} has $4.2 \times 9.8 \times 10.1$ Å pores that incorporate *p*-xylene molecules (Fig. 31). Benzene and toluene, though their molecules are smaller, were not incorporated in the framework pores. This effect was attributed to the unique dynamic behaviour of the framework during adsorption.

The selective sorption of *o*-xylene from vapours by the two-dimensional coordination polymer $[Cu(4\text{-pmntd})_2(NO_3)_2]$ [where 4-pmntd is *N*,*N*′-bis(4-pyridimethyl)naphthalene-1,4,5,8-carbodiimide], whose layers form rhombic 6.8×6.8 Å channels upon packing, was studied.[172] According to the adsorption isotherms, as the pressure increases, the capacity for *o*-xylene increases rapidly and reaches saturation at $P/P_0 \approx 0.15$, which corresponds to 0.5 molecules of *o*-xylene per formula unit. At the same time, the sorption of *m*- and *p*-xylenes was insignificant in the entire pressure range. Unfortunately, the sorption selectivity factors were not reported.

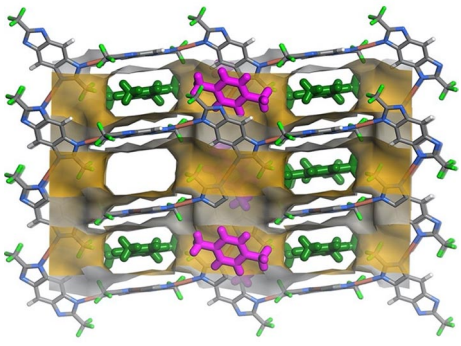


Figure 31. A fragment of the crystal structure of the MAF-41 framework with incorporated *p*-xylene molecules according to XRD data.[180] Grey indicates carbon atoms, dark blue indicates nitrogen atoms, light green indicates fluorine atoms, orange indicates zinc atoms, green and purple indicate various types of sorbed *p*-xylene molecules. Framework channels are marked by grey-orange surfaces. The figure is published with the permission from Springer Nature.

Kim *et al.*[166] studied the sorption of xylenes on the three-dimensional coordination polymer DUT-8(Cu) with the composition $[Cu(2,6\text{-ndc})(dabco)_{0.5}]$ (where $2,6\text{-}H_2ndc$ is naphthalene-2,6-dicarboxylic acid). The framework has one-dimensional channels with a square cross-section (9.8×9.6 Å) and a high specific surface area of 2685 $m^2\ g^{-1}$ according to BET. Sorption from a ternary mixture of xylenes in vapor state showed selectivity for the *p*-isomer with a coefficient of ~2. Sorption from a liquid mixture of isomeric xylenes gave even greater selectivity factors for *p*-xylene, 8.3 for the *p*- and *o*-xylene pair and 12.5 for the *p*- and *m*-xylene pair. These values are among the highest of all the values reported in literature. An explanation for the high selectivity of *p*-xylene sorption based on quantumchemical calculations was suggested. Molecular dynamics simulations showed that *p*-xylene molecules are arranged parallel to the axes of DUT-8(Cu) channels and are localized near the dabco linkers, while the molecules of the *meta*- and *ortho*-isomers fill the channels irregularly (Fig. 32). DFT calculations of the binding energies of the isomers also gave the highest selectivity value for the *para*-isomer.

An exceptionally high selectivity for *p*-xylene was achieved by Yang *et al.*,[167] who reported a synthesis of a metal-organic framework MAF-36 with the composition $[Cu_2(pypz)_2] \cdot 0.5\,p\text{-xyl}$ [where Hpypz is 4(1*H*-pyrazol-4-yl)pyridine; *p*-xyl is *p*-xylene] that had channels filled with *p*-xylene molecules. Removal of the guest molecules in the temperature range of 30–150 °C resulted in a structural rearrangement accompanied by compression of the unit cell and deformation of the layers of the α-$[Cu_2(pypz)_2]$ coordi-

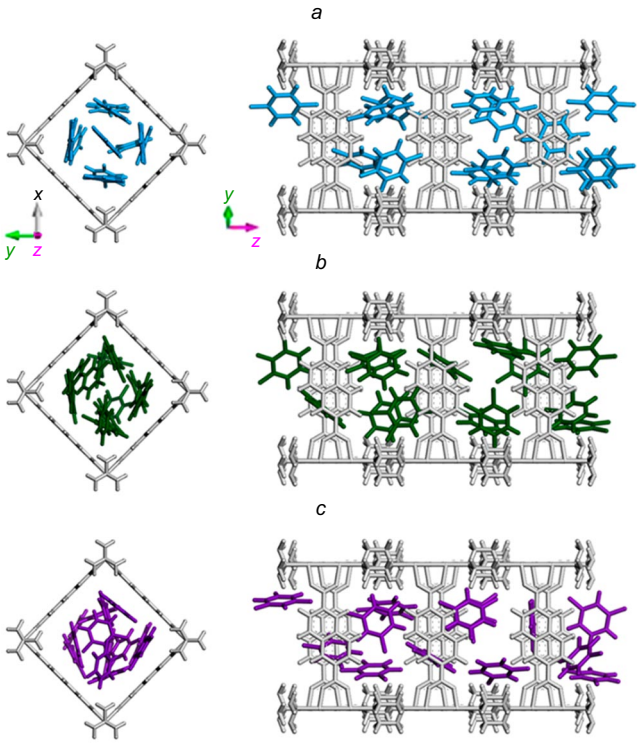


Figure 32. Arrangement of *p*- (*a*), *o*- (*b*), and *m*-xylene molecules (*c*) in the channels of the DUT-8(Cu) framework based on DFT calculations.[166] All framework atoms are shown in grey, *p*-xylene molecules in blue, *o*-xylene molecules in dark green, and *m*-xylene molecules in purple. The figure is published with the permission from the American Chemical Society.

nation polymer. On further heating, a phase transition to give a three-dimensional MOF with the composition β-$[Cu_2(pypz)_2]$ occurred. Both forms of MAF-36 from which the guests had been removed showed exceptionally high selectivity of *p*-xylene sorption from an equimolar liquid mixture of the three isomers: the selectivity factor was 16 for α-$[Cu_2(pypz)_2]$ and 51 for β-$[Cu_2(pypz)_2]$. Despite the lower selectivity, α-$[Cu_2(pypz)_2]$ had the following significant advantage related to the sorption kinetics: the sorption equilibrium on it was reached in 2 min, whereas it took hours on β-$[Cu_2(pypz)_2]$ and on the majority of the known MOFs. Thus, this study [167] demonstrated the effect of molecular imprinting, in which the sorption selectivity of a particular compound was preset at the stage of MOF synthesis, which is very important for the design of highly efficient sorbents.

Mukherjee *et al.*[168] reported a synthesis of the $[Zn_4O(tbpdb)_3(DMF)_2]$ coordination polymer {where H_2tbpdb is 4,4′-[(4-*tert*-butyl-1,2-phenylene)bis(oxy)]dibenzoic acid}, which after activation showed high selectivity of *p*-xylene sorption from vapours. The sorption capacity for *p*-xylene was 64 $cm^3\ g^{-1}$, whereas it was as small as 5 and 1.15 $cm^3\ g^{-1}$ for the *meta*- and *ortho*-isomers, respectively. The crystal structure of this MOF with *p*-xylene molecules incorporated in the channels was determined by XRD (Fig. 33).

The separation of xylenes on the metal-organic framework CD-MOF-1 with the composition $[K_2(CD)(OH)_2]_2$ based on γ-cyclodextrin (CD), a readily available natural compound, was studied.[173] The framework exhibited selectivity towards *o*-xylene, which was attributed to the similarity of the kinetic diameter of its molecule (7.4 Å) and the pore size in the MOF structure (9 Å). The practical feasibility of separation was demonstrated by frontal liquid chromatography of ternary equimolar isomer mixtures: the dynamic capacity for *o*-xylene was 63.0 mg g^{-1}, while the highest selectivity factor of 13.5 was observed for the *o*-/*p*-xylene pair.

A detailed study on the separation of xylenes on MIL-53(Cr) with the composition [Cr(OH)(bdc)] was performed.[174] In the sorption from a ternary liquid mixture of isomers, MIL-53(Cr) exhibited selectivity for *o*-xylene compared to the *para*- and *meta*-isomers with selectivity factors of 6.27 and 3.89, respectively. The kinetic and thermodynamic parameters of the process that are important for engineering calculations were also studied. The sorption of xylenes can be described by pseudo-second order kinetic equations, and equilibrium is reached in 0.5 h, which is faster than in the case of zeolite X (1.5 h) used in industrial separation processes with a pseudo-moving sorbent bed. The changes in the adsorption enthalpy and entropy observed for *o*-xylene were negative and the smallest in modulus, which can be explained by denser packing of its molecules in the sorbent pores. As it can be seen, the sorption selectivity is determined by a combined effect of the enthalpy and entropy factors. The feasibility of complete separation of isomeric xylenes was proved in frontal chromatography experiments, while the sorbent stability was confirmed by the fact that the decrease in the capacity in five separation cycles was insignificant.

Adsorption from vapors on the mesoporous polymer MIL-101(Cr) with the composition $[Cr_3O(OH)(H_2O)_2(bdc)_3]$ showed selectivity to *o*-xylene over the other two isomers, with the selectivity factors in the range of 1.2–1.3.[175] The high sorption capacities of MIL-101(Cr) of up to 1200 mg g^{-1} for all the three xylene isomers [181] should also be noted. In a recent work,[182] MIL-100(Cr) was used to obtain a composite sorbent SiO_2@MIL-101(Cr) used in high performance liquid chromatography, which is capable of separating all the three isomers.

The selective sorption of *p*-xylene on MOF with the composition [Cu(chdc)] was reported.[169] The sorption capacity for *p*-xylene was ~12 wt%. The selectivity factors in sorption from solutions containing all the three isomers were ~10 and ~7, respectively, for the *para*-/*ortho*- and *para*-/*meta*- pairs of xylene isomers. Rietveld refinement of the crystal structure of [Cu(chdc)] with included *p*-xylene molecules showed that the guest molecules are located at the centre of the framework channels whose sizes match exactly the sizes of the sorbate molecules (Fig. 34).

EPR monitoring of the dynamic behaviour of the ZIF-8 coordination polymer with the composition [Zn(mim)] (where Hmim is 2-methylimidazole) by introducing a spin label, the (2,2,6,6-tetramethylpiperidin-1-yl)oxyl (TEMPO) radical, into the framework pores allowed the optimal conditions for selective sorption of xylene *para*- and *meta*-

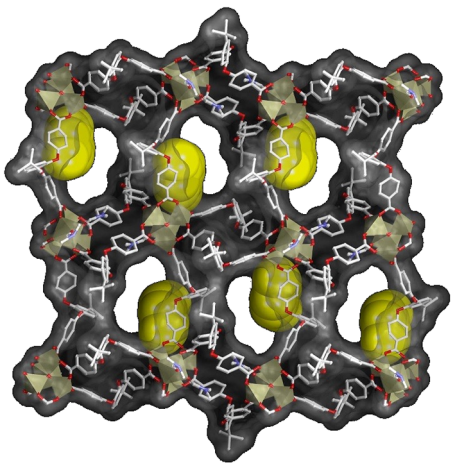


Figure 33. A fragment of the crystal structure of $[Zn_4O(L)_3(dmf)_2]$ {H_2L = 4,4′-[(4-(*tert*-butyl)-1,2-phenylene)bis(oxy)]dibenzoic acid} with incorporated *p*-xylene molecules according to XRD data.[168] Carbon atoms are shown in light grey, nitrogen atoms in dark blue, and oxygen atoms in red; *p*-xylene molecules are shown in yellow, and the surface of the framework channels is shown in dark grey. The figure is published with the permission from Springer Nature.

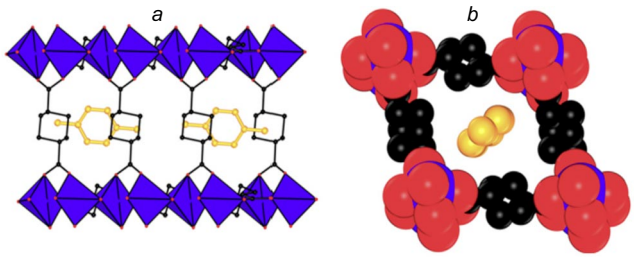
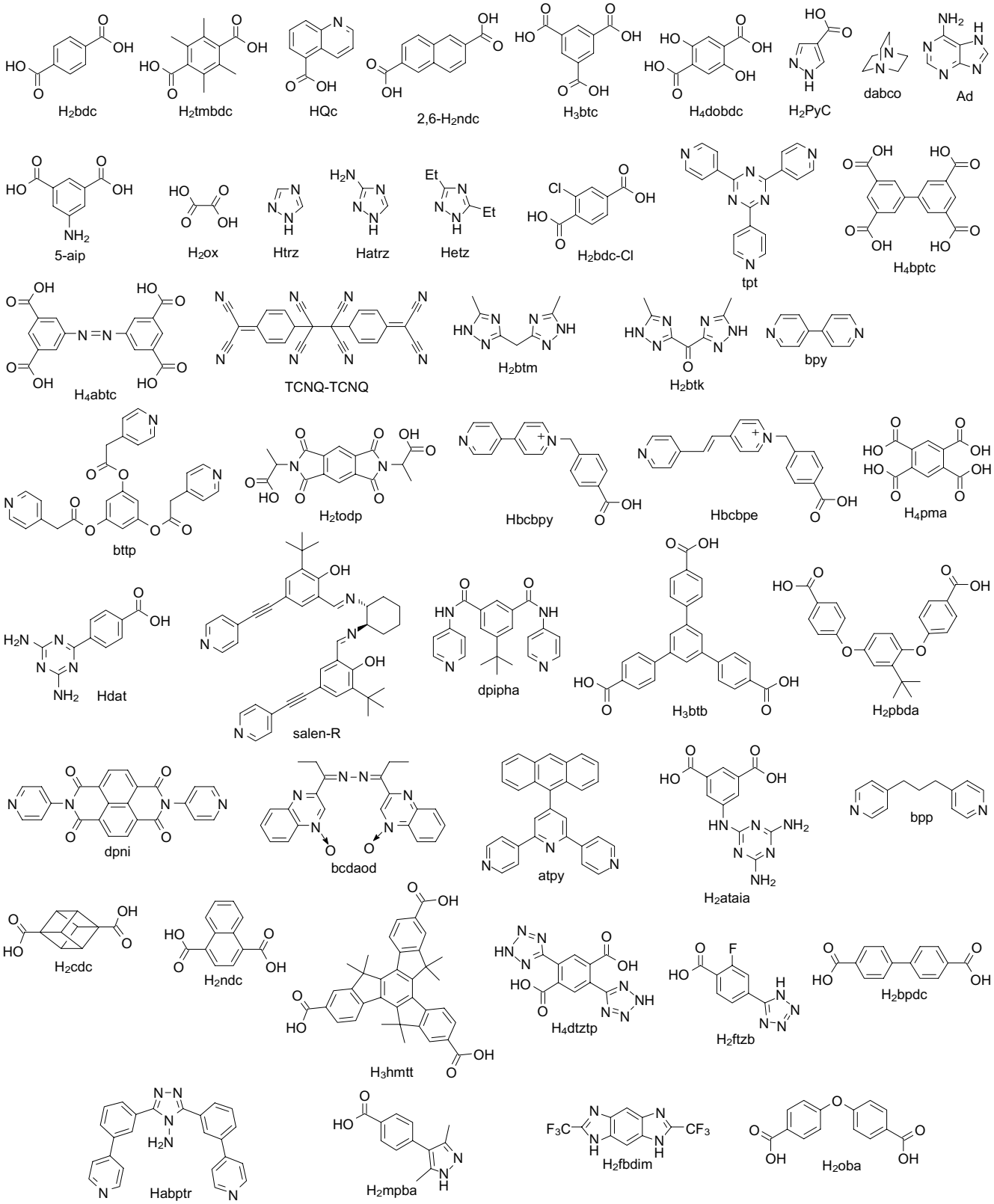
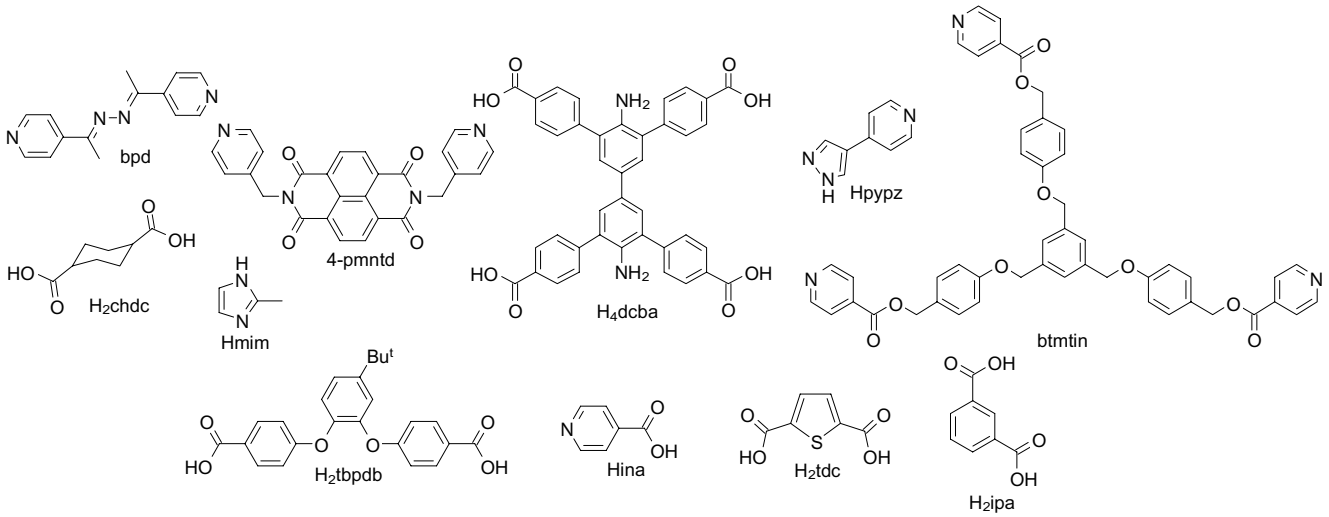


Figure 34. Arrangement of *p*-xylene molecules in the channels of the [Cu(chdc)] structure according to XRD data.[169] (*a*) View along axis *b* (ball-and-stick model); (*b*) view along axis *a* (van der Waals ball model).[69] Black indicates carbon atoms, red indicates oxygen atoms, dark blue tetrahedra and spheres indicate zinc atoms, and orange indicates *p*-xylene molecules. The figure is published with the permission from Elsevier.

isomers to be found.[183] The gate aperture of 3.6 Å in ZIF-8 is smaller than the molecule size of any benzene derivative, but the effective aperture increases with an increase in temperature, *i.e.*, size-selective sorption can be controlled by varying the process temperature. Observing the incorporation of xylene molecules into ZIF-8 pores by measuring the variation in the EPR signal of the TEMPO radical indicated that only *p*-xylene was sorbed with 93% selectivity over *m*-xylene at 298 K, whereas at 333 K the separation of *meta*- and *ortho*-isomers with 92% efficiency was possible.[183]

6. The structural formulas of the organic compounds mentioned in the review





7. Conclusion

Metal-organic coordination polymers are not just new porous materials. They are valuable sorbents capable of competing with the modern adsorption materials. Combining inorganic building blocks with organic linkers makes it possible to control the geometric parameters of the pores and create such a coordination environment in the pores that would provide highly selective guest – host interactions and record-high selectivity values. The large (and in some cases record-large) specific surface areas of MOFs determine their high sorption capacity for a number of substrates. The scientific breakthrough in improving the efficiency of porous materials based on metal-organic frameworks for the separation of hydrocarbons is based on the deep understanding of the nature of adsorption sites in such structures, the specifics of interatomic interactions between the sorbent walls and a particular substrate, and the structural response of a framework (host) as it is filled with guest molecules. Metal-organic frameworks have very important advantages over many other porous materials. For example, they readily form single crystals, so guest – host systems can be studied by direct structural methods. The wide application of X-ray diffraction methods, especially that using synchrotron radiation sources and neutronography, provides the richest information and allows the visualization of results on the characterization of inclusion compounds based on MOFs. Theoretical methods play an increasing role in understanding the nature of host – guest interactions and the reasons for the high selectivity of separation on MOFs.

As shown by the literature data provided in the review, porous coordination polymers synthesized and studied to date are superior to the industrially used sorbents in terms of capacity and selective sorption, as well as separation of commercially important hydrocarbon mixtures such as ethane/ethylene, propane/propylene, benzene/cyclohexane and xylene isomers. At the same time, some challenges remain to be solved in order to start a widespread application of MOFs in industrial separation processes of large-tonnage products. The main challenges are:

— confirming the practical feasibility and scalability of the separation process; most publications presented only data on the sorption capacity and sorption selectivity, and just a few researchers performed laboratory separation by frontal chromatography; in none of the papers published by the time this review was written, scaling of the separation process was performed, while the flow rates were limited to a few millilitres per minute, which is incomparable with the productivity required by industry, namely, hundreds and thousands of tons per day;

— reproducibility and scalability of MOF synthesis; nearly all studies were performed using samples of 1 g or less; the problem of reproducibility of synthesizing an MOF with a given structure, which is determined by many factors, is also relevant;

— synthesizing MOFs that are not inferior to industrial sorbents in terms of stability; only a few studies confirmed the preservation of sorption properties in sorption – desorption cycles, but even then it is usually just a few cycles, whereas the expected lifetime of a sorbent for industrial applications should amount to years.

The achievements in the study of porous metal-organic frameworks give a reason to assume with certainty that these problems will be solved, and materials based on MOFs will be used in the future for highly efficient industrial separation of hydrocarbon mixtures.

This review was prepared with financial support from the Russian Foundation for Basic Research (Project No. 20-13-50158) and the Ministry of Science and Higher Education of the Russian Federation (Project No. 121031700321-3).

8. List of abbreviations and symbols

Ade — adenine,
5-aip — 5-aminoisophthalic acid,
atpy — 4′-(9-anthryl)-4,2′:6′,4″-terpyridine,
bcdaod — 3,6-bis(quinoxalin-1-oxido-3-yl)-4,5-diaza-octa-3,5-diene, or *N*,*N*′-bis[1-(quinoxalin-1-oxido-3-yl)propylidene]hydrazine,
bpd — *N*,*N*′-bis[1-(4-pyridyl)ethylidene]hydrazine,
bpp — 1,3-di(4-pyridyl)propane,
bpy — 4,4′-bipyridine,
btmtin — {[(benzene-1,3,5-triyltris(methylene)tris-(oxy)]tris(benzene-4,1-diyl)}tris(methylene)triisonicotinate, or benzene-1,3.5-triyltris(4-methyloxybenzyl)triisonicotinate,
bttp — benzene-1,3,5-triyltriisonicotinate, or 1,3,5-tris(4-pyridylacetoxy)benzene,
CD — γ-cyclodextrin,
dabco — 1,4-diazabicyclo[2.2.2]octane,

DCM — dichloromethane,
DEF — diethylformamide,
DMA — dimethylacetamide,
dpipha — 5-*tert*-butyl-*N*,*N*′-di(4-pyridyl)isophthaldiamide,
dpni — *N*,*N*′-di(4-pyridyl)naphthalene-1,4,5,8-tetracarboxydiimide,
H_2bdc — benzene-1,4-dicarboxylic (terephthalic) acid,
H_2tmbdc — 2,3,5,6-tetramethylterephthalic acid,
HQc — quinoline-5-carboxylic acid,
2,6-H_2ndc — naphthalene-2,6-dicarboxylic acid,
H_3btc — benzene-1,3,5-tricarboxylic (trimesic) acid,
H_4dobdc — 2,5-dihydroxyterephthalic acid,
H_2PyC — pyrazole-4-carboxylic acid,
H_2ox — oxalic acid,
Htrz — 1,2,4-triazole,
Hatrz — 3-amino-1*H*-1,2,4-triazole,
Hetz — 3,5-diethyl-1*H*-1,2,4-triazole,
H_2bdc-Cl — 2-chlorobenzene-1,4-dicarboxylic acid,
H_4bptc — biphenyl-3,3′,5,5′-tetracarboxylic acid,
H_4abtc — azobenzene-3,3′,5,5′-tetracarboxylic acid,
H_2btm — bis(5-methyl-1*H*-1,2,4-triazole-3-yl)methane,
H_2btk — bis(5-methyl-1*H*-1,2,4-triazole-3-yl)methanone,
H_2todp — 2,2′-(1,3,5,7-tetraoxo-5,7-dihydropyrrolo[3,4-f]isoindole-2,6(1*H*,3*H*)-diyl)dipropionic acid, or pyromellitic acid *N*,*N*′-bis(1-carboxyethyl)diimide,
Hbcbpy — 1-(4-carboxybenzyl)-4,4′-bipyridinium,
Hbcbpe — 1-(4-carboxybenzyl)-4-[2-(4-pyridyl)vinyl]-pyridinium,
H_4pma — benzene-1,2,4,5-tetracarboxylic (pyromellitic) acid,
Hdat — 4,6-diamino-2-(4-carboxyphenyl)triazine,
H_2salen — *trans*-*N*,*N*′-bis[3-*tert*-butyl-5-(4-pyridyl-ethynyl)salicylidene]-cyclohexane-1,2-diamine,
H_3btb — 4,4′,4″-benzene-1,3,5-triyltribenzoic acid, or 1,3,5-tris(4-carboxyphenyl)benzene
H_2pbda — 4,4′-[2-*tert*-butyl-1,4-phenylene)bis(oxy)]dibenzoic acid, or 2-*tert*-butyl-1,4-bis(4-carboxyphenoxy)benzene,
H_2ataia — 5-[(4,6-diamino-1,3,5-triazine-2-yl)amino]-isophthalic acid,
H_2cdc — cubane-1,4-dicarboxylic acid,
H_2ndc — naphthalene-1,4-dicarboxylic acid,
H_3hmtt — 5,5,10,10,15,15-hexamethyltruxene-2,7,12-tricarboxylic acid,
H_4dtztp — 2,5-di(2*H*-tetrazol-5-yl)terephthalic acid,
H_2ftzb — 4-(1*H*-tetrazol-5-yl)-2-fluorobenzoic acid,
H_2bpdc — biphenyl-4,4′-dicarboxylic acid,
Habptr — 4-amino-3,5-bis[3-(4-pyridyl)phenyl]-1,2,4-triazole,
H_2mpba — 4-(3,5-dimethyl-1*H*-pyrazole-4-yl)benzoic acid,
H_2fbdim — 2,6-bis(trifluoromethyl)-1,7-dihydrobenzo-[1,2-*d*:4,5-*d*′]diimidazole,
H_2oba — 4,4′-oxydibenzoic acid,
H_2chdc — *trans*-cyclohexane-1,4-dicarboxylic acid,
Hmim — 2-methylimidazole,
H_4dcba — 4″,6′-diamino-5′,5″-bis(4-carboxyphenyl)-[1,1′:3′,1″:3″,1‴-quaterphenyl]-4,4‴-dicarboxylic acid,
Hpypz — 4-(1*H*-pyrazol-4-yl)pyridine,
H_2tbpdb — 4,4′-[(4-*tert*-butyl-1,2-phenylene)bis(oxy)]-dibenzoic acid, or 4-*tert*-butyl-1,2-bis(4-carboxyphenyloxy)benzene,
Hina — isonicotinic acid,
H_2tdc — thiophene-2,5-dicarboxylic acid,
H_2ipa — isophthalic acid,
NMP — *N*-methyl-2- pyrrolidone,
OTf — trifluoromethylsulfonate,
PeH_2 — pentane-1,2-diol,
4-pmntd — *N*,*N*′-bis(4-pyridylmethyl)naphthalene-1,4,5,8-carbodiimide,
pyr — pyrazine,
TCNQ-TCNQ — 7,7,8,8-tetracyano-*p*-quinodimethane dimer,
tpt — 2,4,6-tri(4-pyridyl)-1,3,5-triazine,
o-xyl — *o*-xylene,
m-xyl — *m*-xylene,
p-xyl — *p*-xylene.

9. References

1. H.Furukawa, K.E.Cordova, M.O'Keeffe, O.M.Yaghi. *Science*, **341**, 1230444 (2013)
2. H.-C.Zhou, S.Kitagawa. *Chem. Soc. Rev.*, **43**, 5415 (2014)
3. A.U.Czaja, N.Trukhan, U.Müller. *Chem. Soc. Rev.*, **38**, 1284 (2009)
4. Y.Cui, B.Li, H.He, W.Zhou, B.Chen, G.Qian. *Acc. Chem. Res.*, **49**, 483 (2016)
5. H.Furukawa, N.Ko, Y.B.Go, N.Aratani, S.B.Choi, E.Choi, A.O.Yazaydin, R.Q.Snurr, M.O'Keeffe, J.Kim, O.M.Yaghi. *Science*, **329**, 424 (2010)
6. A.Corma, H.Garcia, F.X.L.i Xamena. *Chem. Rev.*, **110**, 4606 (2010)
7. A.Wang, J.Li, T.Zhang. *Nat. Rev. Chem.*, **2**, 65 (2018)
8. J.-R.Li, J.Sculley, H.-C.Zhou. *Chem. Rev.*, **112**, 869 (2012)
9. M.P.Suh, H.J.Park, T.K.Prasad, D.-W.Lim. *Chem. Rev.*, **112**, 782 (2012)
10. K.Sumida, D.L.Rogow, J.A.Mason, T.M.McDonald, E.D.Bloch, Z.R.Herm, T.-H.Bae, J.R.Long. *Chem. Rev.*, **112**, 724 (2012)
11. Y.He, W.Zhou, G.Qian, B.Chen. *Chem. Soc. Rev.*, **43**, 5657 (2014)
12. V.V.Arslanov, M.A.Kalinina, E.V.Ermakova, O.A.Raitman, Y.G.Gorbunova, O.E.Aksyutin, A.G.Ishkov, V.A.Grachev, A.Y.Tsivadze. *Russ. Chem. Rev.*, **88**, 775 (2019)
13. A.Y.Tsivadze, O.E.Aksyutin, A.G.Ishkov, M.K.Knyazeva, O.V.Solovtsova, I.E.Men'shchikov, A.A.Fomkin, A.V.Shkolin, E.V.Khozina, V.A.Grachev. *Russ. Chem. Rev.*, **88**, 925 (2019)
14. L.E.Kreno, K.Leong, O.K.Farha, M.Allendorf, R.P.V.Duyne, J.T.Hupp. *Chem. Rev.*, **112**, 1105 (2012)
15. V.G.Ponomareva, K.A.Kovalenko, A.P.Chupakhin, D.N.Dybtsev, E.S.Shutova, V. P.Fedin. *J. Am. Chem. Soc.*, **134**, 15640 (2012)
16. D.-W. Lim, H. Kitagawa. *Chem. Soc. Rev.*, **50**, 6349 (2021)
17. J.Yan, Q.Wang, T.Wei, Z. Fan. *Adv. Energy Mater.*, **4**, 1300816 (2013)
18. P.Horcajada, R.Gref, T.Baati, P.K.Allan, G.Maurin, P.Couvreur, G.Férey, R.E.Morris, C.Serre. *Chem. Rev.*, **112**, 1232 (2012)
19. D.S.Sholl, R.P.Lively. *Nature (London)*, **532**, 435 (2016)
20. Z.R.Herm, E.D.Bloch, J.R.Long. *Chem. Mater.*, **26**, 323 (2013)
21. Z.Bao, G.Chang, H.Xing, R.Krishna, Q.Ren, B.Chen. *Energy Env. Sci.*, **9**, 3612 (2016)
22. S.Zhang, M.Taylor, L.Jiang, H.Ren, G.Zhu. *Chem. – Eur. J.*, **26**, 3205 (2020)
23. R.T.Yang. *Adsorbents: Fundamentals and Applications*. (Hoboken, NJ: Wiley-Interscience, 2003)
24. S.Mukherjee, D.Sensharma, K.-J.Chen, M.Zaworotko. *Chem. Commun.*, **56**, 10419 (2020)
25. B.Barnett, M.Gonzalez, J. Long. *Trends Chem.*, **1**, 159 (2019)
26. J.Pei, K.Shao, L.Zhang, H.-M.Wen, B.Li, G. Qian. *Top. Curr. Chem.*, **377**, 33 (2019)

27. T.Lan, L.Li, Y.Chen, X.Wang, J.Yang, J.Li. *Mater. Chem. Front.*, **4**, 1954 (2020)
28. Y.He, R.Krishna, B.Chen. *Energy Env. Sci.*, **5**, 9107 (2012)
29. S.J.Geier, J.A.Mason, E.D.Bloch, W.L.Queen, M.R.Hudson, C.M.Brown, J.R.Long. *Chem. Sci.*, **4**, 2054 (2013)
30. S.Yang, A.J.Ramirez-Cuesta, R.Newby, V.Garcia-Sakai, P.Manuel, S.K.Callear, S.I.Campbell, C.C.Tang, M.Schröder. *Nat. Chem.*, **7**, 121 (2014)
31. G.Chang, M.Huang, Y.Su, H.Xing, B.Su, Z.Zhang, Q.Yang, Y.Yang, Q.Ren, Z.Bao, B.Chen. *Chem. Commun.*, **51**, 2859 (2015)
32. Y.Zhang, B.Li, R.Krishna, Z.Wu, D.Ma, Z.Shi, T.Pham, K.Forrest, B.Space, S.Ma. *Chem. Commun.*, **51**, 2714 (2015)
33. R.-B.Lin, L.Li, H.-L.Zhou, H.Wu, C.He, S.Li, R.Krishna, J.Li, W.Zhou, B.Chen. *Nat. Mater.*, **17**, 1128 (2018)
34. M.H.Mohamed, Y.Yang, L.Li, S.Zhang, J.P.Ruffley, A.G.Jarvi, S.Saxena, G.Veser, J.K.Johnson, N.L.Rosi. *J. Am. Chem. Soc.*, **141**, 13003 (2019)
35. L.Zhang, L.Li, E.Hu, L.Yang, K.Shao, L.Yao, K.Jiang, Y.Cui, Y.Yang, B.Li, B.Chen, G.Qian. *Adv. Sci.*, **7**, 1901918 (2020)
36. C.Gu, N.Hosono, J.-J.Zheng, Y.Sato, S.Kusaka, S.Sakaki, S.Kitagawa. *Science*, **363**, 387 (2019)
37. H.Zeng, X.-J.Xie, M.Xie, Y.-L.Huang, D.Luo, T.Wang, Y.Zhao, W.Lu, D.Li. *J. Am. Chem. Soc.*, **141**, 20390 (2019)
38. P.-Q.Liao, W.-X.Zhang, J.-P.Zhang, X.-M.Chen. *Nat. Commun.*, **6**, 8697 (2015)
39. Y.Chen, H.Wu, D.Lv, R.Shi, Y.Chen, Q.Xia, Z.Li. *Ind. Eng. Chem. Res.*, **57**, 4063 (2018)
40. C.Altintas, S.Keskin. *Chem. Eng. Sci.*, **139**, 49 (2016)
41. J.Kim, L.C.Lin, R.L.Martin, J.A.Swisher, M.Haranczyk, B.Smit. *Langmuir*, **28**, 11923 (2012)
42. C.Altintas, S.Keskin. *RSC Adv.*, **7**, 52283 (2017)
43. H.Tang, J. Jiang. *AIChE J.*, **67**, e17025 (2020)
44. P.Halder, J.Singh. *Energy Fuels*, **34**, 14591 (2020)
45. C.Gücüyener, J.van den Bergh, J.Gascon, F.Kapteijn. *J. Am. Chem. Soc.*, **132**, 17704 (2010)
46. U.Böhme, B.Barth, C.Paula, A.Kuhnt, W.Schwieger, A.Mundstock, J.Caro, M.Hartmann. *Langmuir*, **29**, 8592 (2013)
47. J.Pires, M.L.Pinto, V.K.Saini. *ACS Appl. Mater. Interfaces*, **6**, 12093 (2014)
48. R.Pillai, M.Pinto, J.Pires, M.Jorge, J.Gomes. *ACS Appl. Mater. Interfaces*, **7**, 624 (2015)
49. M.Hartmann, U.Böhme, M.Hovestadt, C.Paula. *Langmuir*, **31**, 12382 (2015)
50. W.Liang, F.Xu, X.Zhou, J.Xiao, Q.Xia, Y.Li, Z.Li. *Chem. Eng. Sci.*, **148**, 275 (2016)
51. X.Wang, Z.Niu, A.Al-Enizi, A.Nafady, Y.Wu, B.Aguila, G.Verma, L.Wojtas, Y.-S.Chen, Z. Li, S.Ma. *J. Mater. Chem., A*, **7**, 13585 (2019)
52. H.Xiang, A.Ameen, P.Gorgojo, F.Siperstein, S.Holmes, X.Fan. *Microporous Mesoporous Mater.*, **292**, 109724 (2020)
53. D.Lv, R.Shi, Y.Chen, Y.Wu, H.Wu, H.Xi, Q.Xia, Z.Li. *ACS Appl. Mater. Interfaces*, **10**, 8366 (2018)
54. W.Yuan, X.Zhang, L.Li. *J. Solid State Chem.*, **251**, 198 (2017)
55. J.Cai, J.Yu, H.Xu, Y.He, X.Duan, Y.Cui, C.Wu, B.Chen, G.Qian. *Cryst. Growth Des.*, **13**, 2094 (2013)
56. L.Li, R.-B.Lin, R.Krishna, H.Li, S.Xiang, H.Wu, J.Li, W.Zhou, B.Chen. *Science*, **362**, 443 (2018)
57. Y.Chen, Z.Qiao, H.Wu, D.Lv, R.Shi, Q.Xia, J.Zhou, Z.Li. *Chem. Eng. Sci.*, **175**, 110 (2018)
58. O.Qazvini, R.Babarao, Z.-L.Shi, Y.-B.Zhang, S.Telfer. *J. Am. Chem. Soc.*, **141**, 5014 (2019)
59. R.-B.Lin, H.Wu, L.Li, X.-L.Tang, Z.Li, J.Gao, H.Cui, W.Zhou, B.Chen. *J. Am. Chem. Soc.*, **140**, 12940 (2018)
60. Y.Tang, S.Wang, X.Zhou, Y.Wu, S.Xian, Z.Li. *Chem. Eng. Sci.*, **213**, 115355 (2020)
61. J.Pires, J.Fernandes, K.Dedecker, J.Gomes, G.Pérez-Sánchez, F.Nouar, C.Serre, M.Pinto. *ACS Appl. Mater. Interfaces*, **11**, 27410 (2019)
62. H.Wu, Y.Chen, W.Yang, D.Lv, Y.Yuan, Z.Qiao, H.Liang, Z.Li, Q.Xia. *Ind. Eng. Chem. Res.*, **58**, 10516 (2019)
63. J.Peng, Y.Sun, Y.Wu, Z.Lv, Z.Li. *Ind. Eng. Chem. Res.*, **58**, 8290 (2019)
64. H.Wu, Y.Chen, D.Lv, R.Shi, Y.Chen, Z.Li, Q.Xia. *Sep. Purif. Technol.*, **212**, 51 (2019)
65. F.-Z.Sun, S.-Q.Yang, R.Krishna, Y.-H.Zhang, Y.-P.Xia, T.-L.Hu. *ACS Appl. Mater. Interfaces*, **12**, 6105 (2020)
66. L.Yang, Y.Wang, Y.Chen, J.Yang, X.Wang, L.Li, J. Li. *Chem. Eng. J.*, **387**, 124137 (2020)
67. C.He, Y.Wang, Y.Chen, X.Wang, J.Yang, L.Li, J.Li. *Ind. Eng. Chem. Res.*, **59**, 6123 (2020)
68. J.Pei, J.-X.Wang, K.Shao, Y.Yang, Y.Cui, H.Wu, W.Zhou, B.Li, G.Qian. *J. Mater. Chem. A*, **8**, 3613 (2020)
69. H.Yang, Y.Wang, R.Krishna, X.Jia, Y.Wang, A.Hong, C.Dang, H.Castillo, X.Bu, P.Feng. *J. Am. Chem. Soc.*, **142**, 2222 (2020)
70. X.-W.Lei, H.Yang, Y.Wang, Y.Wang, X.Chen, Y.Xiao, X.Bu, P.Feng. *Small*, **17**, 2003167 (2020)
71. K.Cho, J.Yoon, J.Lee, J.Kim, K.Kim, U.-H.Lee, S.Kwak, J.-S.Chang. *Microporous Mesoporous Mater.*, **307**, 110473 (2020)
72. Z.Xu, X.Xiong, J.Xiong, R.Krishna, L.Li, Y.Fan, F.Luo, B.Chen. *Nat. Commun.*, **11**, 3163 (2020)
73. A.A.Lysova, D.G.Samsonenko, P.V.Dorovatovskii, V.A.Lazarenko, V.N.Khrustalev, K.A.Kovalenko, D.N.Dybtsev, V.P.Fedin. *J. Am. Chem. Soc.*, **141**, 17260 (2019)
74. A.Lysova, D.Samsonenko, K.Kovalenko, A.Nizovtsev, D.Dybtsev, V.Fedin. *Angew. Chem., Int. Ed.*, **59**, 20561 (2020)
75. H.Thakkar, Q.Al-Naddaf, N.Legion, M.Hovis, A.Krishnamurthy, A.Rownaghi, F.Rezaei. *ACS Sustainable Chem. Eng.*, **6**, 15228 (2018)
76. N.Dvoyashkina, D.Freude, S.Arzumanov, A.Stepanov. *J. Phys. Chem. C*, **121**, 25372 (2017)
77. O.Qazvini, L.Macreadie, S.Telfer. *Chem. Mater.*, **32**, 6744 (2020)
78. B.Liang, X.Zhang, Y.Xie, R.-B.Lin, R.Krishna, H.Cui, Z.Li, Y.Shi, H.Wu, W.Zhou, B.Chen. *J. Am. Chem. Soc.*, **142**, 17795 (2020)
79. H.Jarvelin, J.R.Fair. *Ind. Eng. Chem. Res.*, **32**, 2201 (1993)
80. N.Lamia, M.Jorge, M.Granato, F.Almeida Paz, H.Chevreau, A.Rodrigues. *Chem. Eng. Sci.*, **64**, 3246 (2009)
81. J.Yoon, I.Jang, K.-Y.Lee, Y.Hwang, J.-S.Chang. *Bull. Korean Chem. Soc.*, **31**, 220 (2010)
82. Z.Bao, S.Alnemrat, L.Yu, I.Vasiliev, Q.Ren, X.Lu, S.Deng. *Langmuir*, **27**, 13554 (2011)
83. D.-L.Chen, H.Shang, W.Zhu, R.Krishna. *Chem. Eng. Sci.*, **117**, 407 (2014)
84. H.Abedini, A.Shariati, M.Khosravi-Nikou. *Chem. Eng. Res. Des.*, **153**, 96 (2020)
85. S.-Y.Kim, T.-U.Yoon, J.Kang, A.-R.Kim, T.-H.Kim, S.-I.Kim, W.Park, K.Kim, Y.-S.Bae. *ACS Appl. Mater. Interfaces*, **10**, 27521 (2018)
86. D.-X.Xue, A.Cadiau, Ł.Weseliński, H.Jiang, P.Bhatt, A.Shkurenko, L.Wojtas, C.Zhijie, Y.Belmabkhout, K.Adil, M.Eddaoudi. *Chem. Commun.*, **54**, 6404 (2018)
87. Y.Chen, H.Wu, D.Lv, N.Yuan, Q.Xia, Z.Li. *Sep. Purif. Technol.*, **204**, 75 (2018)
88. Z.Chang, R.-B.Lin, Y.Ye, C.Duan, B.Chen. *J. Mater. Chem., A*, **7**, 25567 (2019)
89. L.Li, R.-B.Lin, X.Wang, W.Zhou, L.Jia, J.Li, B.Chen. *Chem. Eng. J.*, **354**, 977 (2018)
90. J.Peng, H.Wang, D.Olson, Z.Li, J.Li. *Chem. Commun.*, **53**, 9332 (2017)

91. A.Cadiau, K.Adil, P.Bhatt, Y.Belmabkhout, M.Eddaoudi. *Science*, **353**, 137 (2016)
92. Z.Zhang, Q.Ding, X.Cui, X.-M.Jiang, H.Xing. *ACS Appl. Mater. Interfaces*, **12**, 40229 (2020)
93. Y.Wang, N.-Y.Huang, X.-W.Zhang, H.He, R.-K.Huang, Z.-M.Ye, Y.Li, D.-D.Zhou, P.-Q.Liao, X.-M.Chen, J.-P.Zhang. *Angew. Chem., Int. Ed.*, **58**, 7692 (2019)
94. H.Wang, X.Dong, V.Colombo, Q.Wang, Y.Liu, W.Liu, X.-L.Wang, X.-Y.Huang, D.M.Proserpio, A.Sironi, Y.Han, J.Li. *Adv. Mater.*, **30**, 1805088 (2018)
95. J.van den Bergh, C.Gücüyener, E.A.Pidko, E.J.M.Hensen, J.Gascon, F. Kapteijn. *Chem. – Eur. J.*, **17**, 8832 (2011)
96. Y.Chen, Z.Qiao, D.Lv, C.Duan, X.Sun, H.Wu, R.Shi, Q.Xia, Z.Li. *Chem. Eng. J.*, **328**, 360 (2017)
97. X.Wang, R.Krishna, L.Li, B.Wang, T.He, Y.-Z.Zhang, J.-R.Li, J.Li. *Chem. Eng. J.*, **346**, 489 (2018)
98. T.Liu, H.Cui, X.Zhang, Z.-Y.Zhang, R.-B.Lin, B.Liang, J.Zhang, D.Li, B.Chen. *ACS Appl. Mater. Interfaces*, **12**, 48712 (2020)
99. M.Jorge, N.Lamia, A.Rodrigues. *Colloids Surf., A*, **357**, 27 (2010).
100. S.Ernst, A.Wagener. In *Proceedings of the 19th World Petroleum Congress 2008: A World in Transition: Delivering Energy for Sustainable Growth 2 : 947*. (Madrid, 2008). P. 947
101. A.Ferreira, J.Santos, M.Plaza, N.Lamia, J.Loureiro, A.Rodrigues. *Chem. Eng. J.*, **167**, 1 (2011)
102. M.Fischer, J.Gomes, M.Fröba, M.Jorge. *Langmuir*, **28**, 8537 (2012)
103. M.Plaza, A.Ferreira, J.Santos, A.Ribeiro, U.Müller, N.Trukhan, J.Loureiro, A.Rodrigues. *Microporous Mesoporous Mater.*, **157**, 101 (2012)
104. M.Plaza, A.Ribeiro, A.Ferreira, J.Santos, U.-H.Lee, J.-S.Chang, J.Loureiro, A.Rodrigues. *Sep. Purif. Technol.*, **90**, 109 (2012)
105. M.Rubes, A.Wiersum, P.Llewellyn, L.Grajciar, O.Bludský, P.Nachtigall. *J. Phys. Chem. C*, **117**, 11159 (2013)
106. M.Gholami, S.Yeganegi. *Adsorption*, **23**, 507 (2017)
107. K.Kim, C.Lee, D.Fairen-Jimenez, S.Nguyen, J.Hupp, R.Snurr. *J. Phys. Chem. C*, **118**, 9086 (2014)
108. K.Li, D.H.Olson, J.Seidel, T.J.Emge, H.Gong, H.Zeng, J.Li. *J. Am. Chem. Soc.*, **131**, 10368 (2009)
109. F.Rashidi, J.Leisen, S.-J.Kim, A.Rownaghi, C.Jones, S.Nair. *Angew. Chem., Int. Ed.*, **58**, 236 (2019)
110. B.Zheng, G. Maurin. *Angew. Chem. Int. Ed.*, **58**, 13734 (2019)
111. K.Eum, S.Yang, B.Min, C.Ma, J.Drese, Y.Tamhankar, S.Nair. *ACS Appl. Mater. Interfaces*, **12**, 27368 (2020)
112. J.James, L.Lang, L.Meng, J. Lin. *ACS Appl. Mater. Interfaces*, **12**, 3893 (2020)
113. Y.Zhao, Y.Wei, L.Lyu, Q.Hou, J.Caro, H.Wang. *J. Am. Chem. Soc.*, **142**, 20915 (2020)
114. H.Lyu, S.Li, C.Cui, X.Yu, J.Sun. *Sep. Purif. Technol.*, **257**, 117907 (2021)
115. X.Wang, C.Ma, J.Xiao, Q.Xia, J.Wu, Z.Li. *Chem. Eng. J.*, **335**, 970 (2018)
116. X.Shen, R.Ou, Y.Lu, A.Yuan, J.Liu, J.Gu, X.Hu, Z.Yang, F.Yang. *Environ. Int.*, **143**, 105774 (2020)
117. F.Temel, S.Kutluay. *New J. Chem.*, **44**, 12949 (2020)
118. H.Yao, Y.-M.Wang, M.Quan, M.U.Farooq, L.-P.Yang, W.Jiang. *Angew. Chem., Int. Ed.*, **59**, 19945 (2020)
119. Y.Ding, L.O.Alimi, B.Moosa, C.Maaliki, J.Jacquemin, F.Huang, N.M.Khashab. *Chem. Sci.*, **12**, 5315 (2021)
120. S.Shimomura, S.Horike, R.Matsuda, S.Kitagawa. *J. Am. Chem. Soc.*, **129**, 10990 (2007)
121. J.-P.Zhang, X.-M.Chen. *J. Am. Chem. Soc.*, **130**, 6010 (2008)
122. G.Li, C.Zhu, X.Xi, Y.Cui. *Chem. Commun.*, 2118 (2009)
123. J.-B.Lin, J.-P.Zhang, W.-X.Zhang, W.Xue, D.-X.Xue, X.-M.Chen. *Inorg. Chem.*, **48**, 6652 (2009)
124. S.Shimomura, R.Matsuda, S.Kitagawa. *Chem. Mater.*, **22**, 4129 (2010)
125. R.Yang, L.Li, Y.Xiong, J.-R.Li, H.-C.Zhou, C.-Y.Su. *Chem. – Asian J.*, **5**, 2358 (2010)
126. G.Ren, S.Liu, F.Ma, F.Wei, Q.Tang, Y.Yang, D.Liang, S Li, Y.Chen. *J. Mater. Chem.*, **21**, 15909 (2011)
127. Y.Hijikata, S.Horike, M.Sugimoto, H.Sato, R.Matsuda, S.Kitagawa. *Chem. – Eur. J.*, **17**, 5138 (2011)
128. B.Joarder, S.Mukherjee, A.K.Chaudhari, A.V.Desai, B.Manna, S.K.Ghosh. *Chem. – Eur. J.*, **20**, 15303 (2014)
129. C.-X.Ren, L.-X.Cai, C.Chen, B.Tan, Y.-J.Zhang, J.Zhang. *J. Mater. Chem., A*, **2**, 9015 (2014)
130. B.Manna, S.Mukherjee, A.V.Desai, S.Sharma, R.Krishna, S.K.Ghosh. *Chem. Commun.*, **51**, 15386 (2015)
131. A.Karmakar, A.V.Desai, B.Manna, B.Joarder, S.K.Ghosh. *Chem. – Eur. J.*, **21**, 7071 (2015)
132. S.Mukherjee, B.Manna, A.V.Desai, Y.Yin, R.Krishna, R.Babarao, S.K.Ghosh. *Chem. Commun.*, **52**, 8215 (2016)
133. L.Zhang, W.Yang, X.-Y.Wu, C.-Z.Lu, W.-Z.Chen. *Chem. – Eur. J.*, **22**, 11283 (2016)
134. S.Mukherjee, R.Babarao, A.V.Desai, B.Manna, S.K.Ghosh. *Cryst. Growth Des.*, **17**, 3581 (2017)
135. A.Santra, M.Francis, S.Parshamoni, S.Konar. *ChemistrySelect*, **2**, 3200 (2017)
136. A.Kondo, T.Suzuki, R.Kotani, K.Maeda. *Dalton Trans.*, **46**, 6762 (2017)
137. P.Das, S.K.Mandal. *ACS Appl. Maer. Interfaces*, **10**, 25360 (2018)
138. L.K.Macreadie, E.J.Mensforth, R.Babarao, K.Konstas, S.G.Telfer, C.M.Doherty, J.Tsanaktsidis, S.R.Batten, M.R.Hill. *J. Am. Chem. Soc.*, **141**, 3828 (2019)
139. A.A.Sapianik, K.A.Kovalenko, D.G.Samsonenko, M.O.Barsukova, D.N.Dybtsev, V.P.Fedin. *Chem. Commun.*, **56**, 8241 (2020)
140. G.-D.Wang, Y.-Z.Li, W.-J.Shi, L.Hou, Z.Zhu, Y.-Y.Wang. *Inorg. Chem. Front.*, **7**, 1957 (2020)
141. P.A.Demakov, A.S.Poryvaev, K.A.Kovalenko, D.G.Samsonenko, M.V.Fedin, V.P.Fedin, D.N.Dybtsev. *Inorg. Chem.*, **59**, 15724 (2020)
142. Y.-Z.Li, H.-H.Wang, G.-D.Wang, L.Hou, Y.-Y.Wang, Z.Zhu. *Inorg. Chem. Front.*, **8**, 376 (2021)
143. A.A.Sapianik, E.R.Dudko, K.A.Kovalenko, M.O.Barsukova, D.G.Samsonenko, D.N.Dybtsev, V.P.Fedin. *ACS Appl. Mater. Interfaces*, **13**, 14768 (2021)
144. L.K.Macreadie, R.Babarao, C.J.Setter, S.J.Lee, O.T.Qazvini, A.J.Seeber, J.Tsanaktsidis, S.G.Telfer, S.R.Batten, M.R.Hill. *Angew. Chem., Int. Ed.*, **59**, 6090 (2020)
145. J.-Y.Cheng, P.Wang, J.-P.Ma, Q.-K.Liu, Y.-B.Dong. *Chem. Commun.*, **50**, 13672 (2014)
146. S.Mukherjee, D.Sensharma, O.T.Qazvini, S.Dutta, L.K.Macreadie, S.K.Ghosh, R.Babarao. *Coord. Chem. Rev.*, **437**, 213852 (2021)
147. Y.Yang, P.Bai, X.Guo. *Ind. Eng. Chem. Res.*, **56**, 14725 (2017)
148. P.M.Lorz, F.K.Towae, W.Enke, R.Jäckh, N.Bhargava, W.Hillesheim. In *Phthalic Acid and Derivatives. Ullmann's Encyclopedia of Industrial Chemistry*. (Hoboden, NJ: John Wiley and Son, 2005)
149. J.Wang, J.Jiang, Y.Sun, X.Meng, X.Wang, R.Ruan, A.J.Ragauskas, D.C.Tsang. *J. Hazard. Mater.*, **414**, 125418 (2021)
150. C.H.Seo, Y.H.Kim. *Sep. Purif. Technol.*, **209**, 1 (2019)
151. L.-D.Shiau. *Sep. Purif. Technol.*, **255**, 117688 (2021)
152. M.Minceva, A.E.Rodrigues. *AIChE J.*, **53**, 138 (2006)
153. C.Wang, L.Zhang, X.Huang, Y.Zhu, G.K. Li, Q.Gu, J.Chen, L.Ma, X.Li, Q.He, J.Xu, Q.Sun, C.Song, M.Peng, J.Sun, D.Ma. *Nat. Commun.*, **10**, 4348 (2019)
154. A.A.Alomair, Y.Alqaheem. *ACS Omega*, **4**, 19005 (2019)
155. E.F.Eydi, A. Shariati, M.R.Khosravi-Nikou. *J. Dispers. Sci. Technol.*, **40**, 453 (2018)
156. M.Rasouli, N.Yaghobi, S.Chitsazan, M.H.Sayyar. *Microporous Mesoporous Mater.*, **152**, 141 (2012)

157. M.Rasouli, N.Yaghobi, F.Allahgholipour, H.Atashi. *Chem. Eng. Res. Des.*, **92**, 1192 (2014)
158. M.du Plessis, V.I.Nikolayenko, L.J.Barbour. *J. Am. Chem. Soc.*, **142**, 4529 (2020)
159. G.Zhang, B.Hua, A.Dey, M.Ghosh, B.A.Moosa, N.M.Khashab. *Acc. Chem. Res.*, **54**, 155 (2020)
160. J.Huang, X.Han, S.Yang, Y.Cao, C.Yuan, Y.Liu, J.Wang, Y.Cui. *J. Am. Chem. Soc.*, **141**, 8996 (2019)
161. E.Jackson, M.Miklitz, Q.Song, G.A.Tribello, K.E.Jelfs. *J. Phys. Chem. C*, **123**, 21011 (2019)
162. L.Alaerts, C.Kirschhock, M.Maes, M.van der Veen, V.Finsy, A.Depla, J.Martens, G.Baron, P.Jacobs, J.Denayer, D.De Vos. *Angew. Chem., Int. Ed.*, **46**, 4293 (2007)
163. A.Torres-Knoop, R.Krishna, D.Dubbeldam. *Angew. Chem., Int. Ed.*, **53**, 7774 (2014)
164. X.Li, J.Wang, N.Bai, X.Zhang, X.Han, I.da Silva, C.G.Morris, S.Xu, D.M.Wilary, Y.Sun, Y.Cheng, C.A.Murray, C.C.Tang, M.D.Frogley, G.Cinque, T.Lowe, H.Zhang, A.J.Ramirez-Cuesta, K.M.Thomas, L.W.Bolton, S.Yang, M.Schröder. *Nat. Commun.*, **11**, 4280 (2020)
165. R.Yuan, H.Chen, Q.-Q.Zhu, H.He. *J. Solid State Chem.*, **297**, 122036 (2021)
166. S.-I.Kim, S.Lee, Y.G.Chung, Y.-S.Bae. *ACS Appl. Mater. Interfaces*, **11**, 31227 (2019)
167. X.Yang, H.-L.Zhou, C.-T.He, Z.-W.Mo, J.-W.Ye, X.-M.Chen, J.-P.Zhang. *Research*, **2019**, 1 (2019)
168. S.Mukherjee, B.Joarder, B.Manna, A.V.Desai, A.K.Chaudhari, S.K.Ghosh. *Sci. Rep.*, **4**, 5761 (2014)
169. J.Lannoeye, B.V.de Voorde, B.Bozbiyik, H.Reinsch, J.Denayer, D.D.Vos. *Microporous Mesoporous Mater.*, **226**, 292 (2016)
170. C.-X.Yang, X.-P.Yan. *Anal. Chem.*, **83**, 7144 (2011)
171. M.I.Gonzalez, M.T.Kapelewski, E.D.Bloch, P.J.Milner, D.A.Reed, M.R.Hudson, J.A.Mason, G.Barin, C.M.Brown, J.R.Long. *J. Am. Chem. Soc.*, **140**, 3412 (2018)
172. G.Li, J.Chen, B.Song, S.Wang, R.Pan, L.Pei, S.Liu, Q.-Y.Yang. *Sep. Purif. Technol.*, **256**, 117781 (2021)
173. L.Chen, D.-D.Zhu, G.-J.Ji, S.Yuan, J.-F.Qian, M.-Y.He, Q.Chen, Z.-H.Zhang. *J. Chem. Technol. Biotechnol.*, **93**, 2898 (2018)
174. Z.He, Y.Yang, P.Bai, X.Guo. *J. Ind. Eng. Chem.*, **77**, 262 (2019)
175. H.Belarbi, L.Boudjema, C.Shepherd, N.Ramsahye, G.Toquer, J.-S.Chang, P.Trens. *Colloids Surf., A*, **520**, 46 (2017)
176. R.N.Devi, M.Edgar, J.Gonzalez, A.M.Z.Slawin, D.P.Tunstall, P.Grewal, P.A.Cox, P.A.Wright. *J. Phys. Chem. B*, **108**, 535 (2004)
177. Q.-K.Liu, J.-P.Ma, Y.-B.Dong. *Chem. – Eur. J.*, **15**, 10364 (2009)
178. S.Lee, D.Kim, J.Kim, O.-S.Jung. *Cryst. Growth Des.*, **20**, 3601 (2020)
179. S.Bej, R.Das, N.C.Murmu, P.Banerjee. *Inorg. Chem.*, **59**, 4366 (2020)
180. D.-D.Zhou, P.Chen, C.Wang, S.-S.Wang, Y.Du, H.Yan, Z.-M.Ye, C.-T.He, R.-K.Huang, Z.-W.Mo, N.-Y.Huang, J.-P.Zhang. *Nat. Mater.*, **18**, 994 (2019)
181. P.Trens, H.Belarbi, C.Shepherd, P.Gonzalez, N.A.Ramsahye, U.-H.Lee, Y.-K.Seo, J.-S.Chang. *Microporous Mesoporous Mater.*, **183**, 17 (2014)
182. X.Wu, Y. Shao, B.Hu, J.Wang, X.Hou. *Microchim. Acta*, **187**, 471 (2020)
183. D.M.Polyukhov, A.S.Poryvaev, S.A.Gromilov, M.V.Fedin. *Nano Lett.*, **19**, 6506 (2019)